U.S. DEPARTMENT OF COMMERCE
National Technical Information Service

PB-291 688

Water Movement in Uranium Mill Tailings Profiles

Science and Education Administration, Fort Collins, CO

Prepared for

Office of Radiation Programs, Las Vegas, NV

Sep 78

TECHNICAL REPORT DATA
(Please read Instructions on the reverse before completing)

1. REPORT NO. ORP/LV 78-8	2.	3. RECIPIENT'S ACCESSION NO. PB291688
4. TITLE AND SUBTITLE: Water Movement in Uranium Mill Tailings Profiles		5. REPORT DATE: September 1978 6. PERFORMING ORGANIZATION CODE
7. AUTHOR(S): A. Klute, D. F. Heermann		8. PERFORMING ORGANIZATION REPORT NO.
9. PERFORMING ORGANIZATION NAME AND ADDRESS: U.S. Department of Agriculture, Science and Education Administration, Agricultural Research, Fort Collins, CO 80523		10. PROGRAM ELEMENT NO. 11. ~~CONTRACT/GRANT NO.~~ Interagency Agreement IAG - DG - H026
12. SPONSORING AGENCY NAME AND ADDRESS: Office of Radiation Programs, U.S. Environmental Protection Agency, P. O. Box 15027, Las Vegas, NV 89114		13. TYPE OF REPORT AND PERIOD COVERED: Final April 1976-Sept. 1978 14. SPONSORING AGENCY CODE: U.S. EPA
15. SUPPLEMENTARY NOTES		

16. ABSTRACT

This study characterizes the behavior of water in profiles of uranium mill tailings through (1) measurement of the water retention and transmission properties of selected tailings materials, (2) numerical simulation of water flow in selected profiles of tailings subjected to specific boundary conditions, and (3) analysis and interpretation of the simulation results within the framework of unsaturated soil water flow theory. The sequence of flow events in a tailings profile without vegetation and with a water table at a given depth is: (1) an initial drainage from saturation, with evaporation at the surface, (2) infiltration of varying amounts of rain at irregular intervals, (3) and periods of evaporation and drainage from the profile, with redistribution within the profile, between infiltration events. The water flow regime in the upper 90 cm, particularly the upper 10-20 cm is transient and dynamic. Infiltrated water, which has penetrated to depths more than about 10 cm, continues to flow downward within the profile. The lower part of the profile, below about 70-90 cm, tends to have a quasi-steady downward flow condition.

17. KEY WORDS AND DOCUMENT ANALYSIS

a. DESCRIPTORS	b. IDENTIFIERS/OPEN ENDED TERMS	c. COSATI Field/Group
soil physics, soil profiles, soil properties, soil water, water pollution, simulation, tailings, radioactive wastes, ground water recharge	Uranium mill tailings Salt Lake City	0808 0813 1201

18. DISTRIBUTION STATEMENT: Release unlimited	19. SECURITY CLASS *(This Report)*: unclassified	21. NO. OF PAGES: 98
	20. SECURITY CLASS *(This page)*: unclassified	22. PRICE: A05 - A01

EPA Form 2220-1 (Rev. 4-77) PREVIOUS EDITION IS OBSOLETE

United States
Environmental Protection
Agency

Office of Radiation Programs
Las Vegas Facility
P.O. Box 15027
Las Vegas NV 89114

Technical Note
ORP/LV-78-8
September 1978

PB 291688

Radiation

EPA

Water Movement in Uranium Mill Tailings Profiles

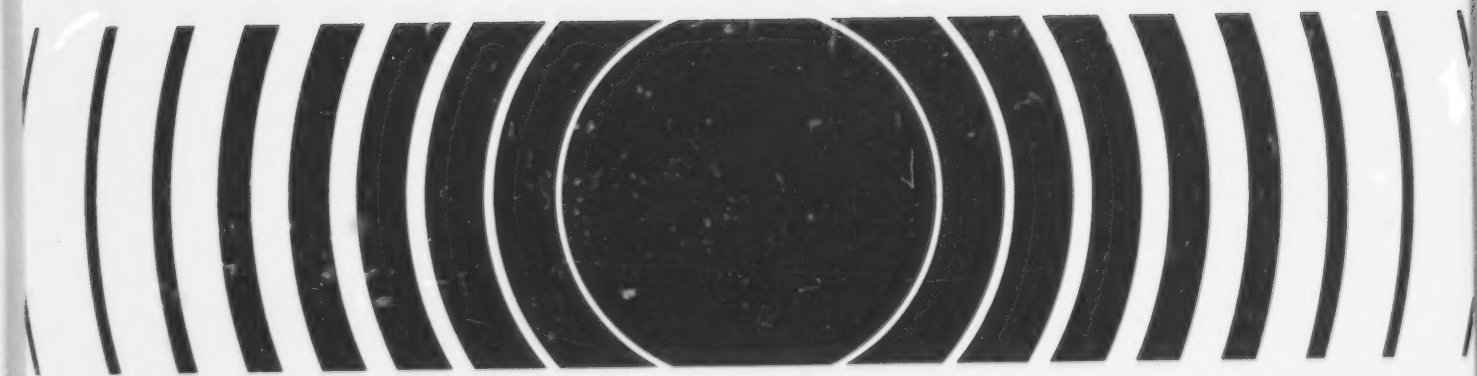

REPRODUCED BY
NATIONAL TECHNICAL
INFORMATION SERVICE
U. S. DEPARTMENT OF COMMERCE
SPRINGFIELD, VA. 22161

Technical Note
ORP/LV-78-8

WATER MOVEMENT IN URANIUM MILL TAILINGS PROFILES

by

A. Klute and D. F. Heermann
U. S. Department of Agriculture
Science and Education Administration
Agricultural Research
Fort Collins, CO 80523

A report of research conducted
under IAG - DG - H026
between USDA - SEA and the
U.S. Environmental Protection Agency

Project Officer
Robert F. Kaufmann
Field Studies Branch
Office of Radiation Programs-Las Vegas Facility
U.S. Environmental Protection Agency
Las Vegas, Nevada 89114

DISCLAIMER

This report has been reviewed by the Office of Radiation Programs - Las Vegas Facility, U.S. Environmental Protection Agency, and approved for publication. Approval does not signify that the contents necessarily reflect the views and policies of the EPA. Mention of trade names or commercial products does not constitute endorsement or recommendation for their use. Neither the United States nor the EPA makes any warranty, expressed or implied, or assume any legal liability or responsibility for any information, apparatus, product or process disclosed, or present that its use could not infringe on privately owned rights.

FOREWORD

The Office of Radiation Programs of the U.S. Environmental Protection Agency carries out a national program designed to evaluate population exposure to ionizing and non-ionizing radiation, and promote the development of controls to protect the public health and safety.

This report was prepared as an integral element of the overall program to control radiation from uranium mill tailings piles situated in the western United States. Such piles are composed of materials containing concentrations of radium-226 two to three orders of magnitude more than background rock and soil. Radon-222, the noble gas progeny of radium-226, is produced within the pile and diffuses to the atmosphere as a continuing long-term source resulting in radiation exposure of the surrounding populace.

Pathways of exposure from uranium mill tailing piles include airborne particulates and contamination of surface or ground water. This report assists in understanding the impact of normal precipitation cycles on recharge of shallow ground water with contaminated leachate from tailings piles. Knowledge of the vertical distribution of soil moisture also assists in evaluating the magnitude of radon diffusion from a tailings pile.

This study represents what we believe is the first application of digital modeling techniques to simulate the unsaturated or soil moisture regime in a uranium tailings pile under average and extreme precipitation and evaporation cycles typified by a climatologic setting in Salt Lake City, Utah. Beginning with initial gravity drainage of the saturated pile, long-term soil moisture variations as a function of time, depth, and tailings lithology are simulated. The results clearly indicate that long-term recharge to underlying ground water can occur and that the upper 10 to 20 centimeters of the profiles tend to dry out rapidly. The presence of vegetation would increase the rate and probably the depth of dewatering. Clearly then, there is a tradeoff at least qualitatively identified between management/stabilization schemes calling for minimal recharge to ground water and reduction of radon diffusion by maintenance of relatively high water content in the very near surface tailings. Future studies will be needed for identification and analysis of the tradeoffs. This was well beyond the scope of the present study.

Readers of this report are encouraged to inform the Office of Radiation Programs - Las Vegas Facility of any omissions or errors. Requests for further information or comments concerning this report are also welcome.

Donald W. Hendricks

Donald W. Hendricks
Director, Office of
Radiation Programs, LVF

ABSTRACT

The general objective of this study was to characterize the behavior of water in profiles of uranium mill tailings. The approach taken consisted of (1) measurement of the water retention and transmission properties of selected tailings materials, (2) numerical simulation of water flow in selected profiles of tailings subjected to specific boundary conditions, and (3) analysis and interpretation of the simulation results within the framework of unsaturated soil water flow theory.

The sequence of flow events in a tailings profile without vegetation and with a water table at a given depth is: (1) an initial drainage from saturation, with evaporation at the surface, (2) infiltration of varying amounts of rain at irregular intervals, (3) and periods of evaporation and drainage from the profile, with redistribution within the profile, between infiltration events. The water flow regime in the upper 90 cm, particularly the upper 10-20 cm is transient and dynamic. Rainfall events produce wetting, which lasts only a few days, in the upper portion of the profile. The wetted zone is dried by evaporation to depths of about 10-15 cm in evaporation periods lasting 15 to 30 days. Infiltrated water, which has penetrated to depths more than about 10 cm, continues to flow downward within the profile while evaporation is occurring from the surface.

The lower part of the profile, below about 70-90 cm, tends to behave in a quasi-steady downward flow condition. The average flow rate in this portion of the profile is determined by the fraction of the rainfall trapped in the profile and not re-evaporated during the time interval of averaging. The water content of the profile at depths below 70-90 cm and at distances more than 50-70 cm above the water table is that corresponding to a hydraulic conductivity equal to the magnitude of the downward flux.

CONTENTS

	Page
FOREWORD	iii
ABSTRACT	v
FIGURES	viii
TABLES	xii
SYMBOLS	xiii
ACKNOWLEDGMENT	xiv
1. INTRODUCTION	1
2. CONCLUSIONS	2
3. RECOMMENDATIONS	4
4. SOIL WATER FLOW CONCEPTS AND TERMINOLOGY	5
5. DETERMINATION OF THE HYDRAULIC PROPERTIES OF TAILINGS	12
Sampling and Basic Physical Characteristics	12
Water Retention Characteristics	13
Sample Preparation	15
Method for Determination of Hysteresis	15
Hydraulic Conductivity-Water Relationships	20
6. SIMULATION OF WATER FLOW IN TAILINGS PROFILES	28
The Numerical Solution Process	28
7. ANALYSIS OF WATER FLOW IN TAILINGS PROFILES	34
The Sequence of Flow Events	34
Drainage of Initially Saturated Profiles	34
Drainage Without Evaporation	35
Drainage With Evaporation	40
Drainage of Layered Profiles with Evaporation	45

Page

Infiltration Events 51

Infiltration into a Uniform Coarse Profile 51
Infiltration into the M/F/M Profile 55

Evaporation Following a Rain 60

Uniform Coarse Profile 60
Evaporation from the M/F/M Profile 61

Discussion of the Flow in the Tailings Profile 70

The Development of the Quasi-Steady State Profile . . 72

REFERENCES 77

GLOSSARY 79

FIGURES

Number		Page
1	A diagram of the relationships between hydraulic head, H, pressure head, h, and gravitational head, z	6
2	Diagram of the hysteresis in the water content-pressure head relation, $\theta(h)$	9
3	Diagram of the pressure chamber apparatus used to determine the water retention characteristics of the tailings materials	14
4	Water retention functions for the Coarse tailings	17
5	Water retention functions for the Medium tailings	18
6	Water retention functions for the Fine tailings	19
7	Hydraulic conductivity-water content function for Coarse tailings	25
8	Hydraulic conductivity-water content function for Medium tailings	26
9	Hydraulic conductivity-water content function for Fine tailings	27
10	Diagram showing the division of the space-time domain into increments and the numbering of the nodes	29
11	Expanded view of the nodes about the general node n, m showing the identification of the nodal values of pressure head	31
12	Water content profiles at several times during the drainage, without evaporation, of a uniform Coarse tailings profile . .	36
13	Water content profiles at several times during the drainage, without evaporation, of a uniform Fine tailings profile . . .	36
14	Water content versus time at several depths in a uniform Coarse tailings profile draining without evaporation at the top	37

Number		Page
15	Water content versus time at several depths in a uniform Fine tailings profile draining without evaporation at the top	37
16	Flux across the water table (0 to 1 day) from uniform profiles of Coarse, Medium and Fine tailings, draining without evaporation at the upper end	38
17	Flux across the water table (0 to 30 days) from uniform profiles of Coarse, Medium and Fine tailings, draining without evaporation at the upper end	38
18	Water content profiles at several times in a uniform Coarse tailings profile draining with a 1 cm/day potential evaporation rate at the top	41
19	Water content profiles at several times in a uniform Medium tailings profile draining with a 1 cm/day potential evaporation rate at the top	41
20	Water content versus time at several depths in the uniform Coarse tailings profile of Fig. 18	42
21	Water content versus time at several depths in the uniform Medium tailings profile of Fig. 19	42
22	Flux versus depth in the upper 30 cm of the uniform Coarse profile of Fig. 18	44
23	Flux versus depth in the upper 30 cm of the uniform Medium profile of Fig. 19	44
24	Flux across the surface (actual evaporation rate) of the uniform Coarse and Medium profiles of Fig. 18, and 19	45
25	Water content profiles at various times in a two-layer, Coarse over Medium, profile draining with a potential evaporation rate of 1 cm/day	46
26	Pressure head distributions for the profile of Fig. 25	46
27	Flux across the water table (0 to 1 day) for draining profiles of uniform Coarse (Fig. 18), Coarse over Medium (Fig. 25), and Coarse over Fine (Fig. 29)	48
28	Same as Fig. 27, except 0 to 15 days	48
29	Water content profiles at several times in a two-layer, Coarse over Fine profile, draining with evaporation	50

Number		Page
30	Pressure head distributions for the profile of Fig. 29	50
31	Flux across the surface (negative of the rainfall rate) of the uniform Coarse profile	52
32	Water content distributions in the uniform Coarse profile subjected to a 2.3 cm rainfall	53
33	Detail of water content distributions in the upper 30 cm of the profile of Fig. 32	54
34	Pressure head profiles corresponding to the water content profiles of Fig. 33	54
35	Flux versus depth in the upper 30 cm of the profile of Fig. 32	55
36	Flux across the surface (negative of the rainfall rate) of the layered M/F/M tailings profile	57
37	Water content distributions in a layered (M/F/M) profile at several times during a 12 cm rain	58
38	Flux versus depth at various times in the upper 90 cm of the M/F/M profile of Fig. 37	58
39	Detail of water content distributions in the upper 90 cm of the M/F/M profile of Fig. 37	59
40	Water content distributions in a uniform Coarse tailings profile subjected to a potential evaporation rate of 0.5 cm/day after a 2.3 cm rain	62
41	Detail of water content distributions in the upper 30 cm of the uniform Coarse profile of Fig. 40	62
42	Flux versus depth at various times during the evaporation from the profile of Fig. 40	63
43	Flux across the surface during evaporation from the uniform Coarse profile (Fig. 40), M/F/M profile, 12 cm rain (Fig. 44), and M/F/M profile, 6 cm rain (Fig. 47)	64
44	Water content distributions in the M/F/M profile subjected to a 0.5 cm/day potential following a 12 cm rain	65
45	Detail of water content distributions in the upper 90 cm of the M/F/M profile of Fig. 44	65

Number		Page
46	Flux versus depth at several times during evaporation from the M/F/M profile of Fig. 44	67
47	Water content distribution in the M/F/M profile with a 0.5 cm/day potential evaporation rate following a 6 cm rain	69
48	Detail of the upper 90 cm of the M/F/M profile of Fig. 47 . . .	69
49	Flux versus depth in the upper 90 cm of the M/F/M profile of Fig. 47	71
50	Water content distributions for two states of steady flow in a uniform Medium tailings profile	74
51	Water content distributions for two states of steady flow in a profile of Medium tailings with a Fine layer at 30 to 60 cm depth	75
52	Water content distributions for two states of steady flow in a profile composed of alternating 30 cm layers of Medium and Fine tailings	75

TABLES

Number		Page
1	IN SITU BULK DENSITY AND PARTICLE DENSITY OF THE SELECTED FRACTIONS OF MILL TAILINGS, VITRO MILL SITE	12
2	PARTICLE SIZE DISTRIBUTION OF THE MILL TAILINGS FRACTIONS	13
3	PARAMETERS OF THE EMPIRICAL $\theta(h)$ AND $K(\theta)$ FUNCTIONS OF THE COARSE TAILINGS	21
4	PARAMETERS OF THE EMPIRICAL $\theta(h)$ AND $K(\theta)$ FUNCTIONS OF THE MEDIUM TAILINGS	21
5	PARAMETERS OF THE EMPIRICAL FUNCTIONS OF THE FINE TAILINGS	22
6	SUMMARY OF CONDITIONS FOR SIMULATIONS OF DRAINAGE WITHOUT EVAPORATION	39
7	SUMMARY OF CONDITIONS FOR SIMULATIONS OF DRAINAGE WITH EVAPORATION AT THE SURFACE	40
8	SUMMARY OF CONDITIONS FOR SIMULATION OF DRAINAGE WITH EVAPORATION OF A TWO-LAYER, COARSE OVER MEDIUM PROFILE	47
9	SUMMARY OF CONDITIONS FOR SIMULATION OF DRAINAGE WITH EVAPORATION OF A TWO-LAYER COARSE OVER FINE PROFILE	49
10	SUMMARY OF CONDITIONS FOR SIMULATION OF THE FILTRATION INTO A UNIFORM COARSE PROFILE	52
11	SUMMARY OF CONDITIONS FOR SIMULATION OF INFILTRATION OF 6 AND 12 CM RAINFALL INTO THE M/F/M PROFILE	56
12	SUMMARY OF CONDITIONS FOR SIMULATION OF EVAPORATION FOLLOWING A RAIN ON A UNIFORM COARSE TAILINGS PROFILE	60
13	SUMMARY OF CONDITIONS FOR SIMULATION OF EVAPORATION FOLLOWING A 12 CM RAIN ON THE M/F/M PROFILE	64
14	SUMMARY OF CONDITIONS FOR SIMULATION OF EVAPORATION FOLLOWING A 6 CM RAIN ON THE M/F/M PROFILE	68

LIST OF SYMBOLS

Symbol	Definition	Units
A	Empirical curve fitting parameter in the hydraulic conductivity function, $K(\theta) = A\exp(B\theta)$, Eq. (18).	L/T, cm/day
B	Empirical curve fitting parameter in the hydraulic conductivity function, See A, above.	None
a	Empirical curve fitting parameter in the relation $\theta(h) = (h/d)^a$, Eq. (11).	None
d	Ditto.	L, cm
C	Water capacity, $d\theta/dh$	L^{-1}, cm^{-1}
h	Pressure head of the soil water	L, cm
h_o	Empirical curve fitting parameter in the water retention function, Eqs. (8), (9) and (10)	L, cm
b	Ditto.	None
θ	Volumetric water content	None
θ_o	Empirical curve fitting parameter in the water retention function, Eqs. (8), (9) and (10). The water content at zero pressure head.	None
θ_r	Ditto. The water content limit as $h \to -\infty$.	None
θ_i	Volumetric water content at the intersection of the empirical $\theta(h)$ functions, Eq. (8) and Eq. (11).	None
h_i	Pressure head at the intersection of the empirical $\theta(h)$ functions, Eq. (8) and Eq. (11).	cm
K	Hydraulic conductivity	L/T, cm/day

ACKNOWLEDGMENTS

The United States Department of Agriculture, Science and Education Administration, Agricultural Research, and Colorado State University, carry out research on problems of mutual interest under a broad form cooperative agreement. The cooperation of the Department of Agronomy, Colorado State University, in this investigation is gratefully acknowledged.

SECTION 1

INTRODUCTION

The tailings materials which result from the extraction of uranium from ore are deposited in piles formed from a slurry containing up to 80-90% water. The piles consist of interbedded layers of materials ranging from clay to coarse sand in texture. The radionuclides in the tailings are a potential source of airborne, waterborne, and direct gamma radiation exposure to people. Radon-222, a noble gas daughter of radium-226 is formed within the pile and transported to the surface.[1/] A primary variable affecting the diffusion of radon to the surface of a pile is the distribution of the water content of the tailings as a function of time and depth. It was the general objective of the study reported here to develop background information on the behavior of water in profiles of tailings materials.

The specific objectives of this project were:

1. Characterize the movement and storage of water in tailings profiles consisting of clay, silt and sand-sized particles.

2. Estimate future moisture conditions under typical (average) and extreme precipitation, and evaporative conditions.

A simulation approach to the objectives was taken, which involved: (1) the determination of the hydraulic conductivity and water retention functions for each tailings material of interest. (2) selection and mathematical description of the appropriate boundary and initial conditions to characterize specific flow problems, and (3) numerical solution of the equation of water movement. The numerical solutions gave the water content, and soil water flux distributions within the tailings profile subjected to specific boundary and initial conditions. The results from the numerical simulations were then interpreted and analyzed in the framework of the concepts of unsaturated flow theory.

1/ Radon, in turn, decays by alpha emission to several daughters most notably lead-210 and polonium-210, both of which are particulates. Inhalation of radon and its daughters, therefore, results in exposure to alpha particles and is related to an increase in cancer incidence.

SECTION 2

CONCLUSIONS

In a profile of tailings without vegetation and with a water table at a given depth, the sequence of water flow events may be described as:

1. An initial period of drainage from saturation, with evaporation at the surface.

2. Infiltration of varying amounts of rain at irregular intervals.

3. Periods of evaporation and drainage from the profile, and redistribution of water within the profile, between rainfall events.

The initial drainage from saturation, if not disturbed by rainfall events, could last for several years. However, rain events will prevent the profile from attaining a steady state condition in the upper profile. The water flow regime in the upper profile (depths to about 90 cms) will be one of dynamic, transient fluctuations in water content and flux. The lower part of the profile will tend toward a quasi-steady state downward flow condition.

Rainfall infiltration events will wet the upper profile to volumetric water contents, θ, on the order of 0.25 to 0.4 in the coarser fractions of tailings and to about 0.6 in the finer fractions. These levels of θ will be maintained for only a short time (a fraction of a day) during and just after a rainfall. Infiltration produces a "wetting front" which moves downward into the profile. Above the front, the general level of θ will be about as given above. Below the front the water content will not be affected during the period of infiltration. Wetting front penetration increases with the magnitude of the rainfall event and the initial level of water content in the profile. An approximation of the depth of wetting, d, can be obtained from $d = r/(\theta_u - \theta_i)$, where θ_u is the water content in the wetted zone, θ_i is the initial water content of the profile, and r is the depth of rainfall applied. This relation holds only if θ_u and θ_i are constant with depth, and normally they are not. The level of water content reached in the wetted zone during a rain event will depend on the intensity of the rain — the higher the intensity, the higher the water content.

In the simulations conducted in this study a rainfall of 2.3 cm penetrated 20 cm into coarse tailings (c.f. Fig. 33) and a rain of 5.5 cm penetrated about 18 cm into medium tailings. The initial water content of the latter was lower than that of the coarse tailings. In view of the characteristics of the rainfall at a location such as the Vitro Mill site, Salt Lake City, Utah, where rains of greater than 2 cm occur several times a year,

and rains of 5 cm or more very infrequently, the depth of wetting during rainfall infiltration will usually be less than 20 cm.

Layers of finer textured material at depths greater than about 30 cm will have no appreciable effect on the dynamic transient behavior of the water content profile above that depth.

Evaporation at the surface of a profile following a rain event will dry only the upper 5 to 10 cm of the profile even when the evaporation period extends to 15 or more days. If the preceding rain has penetrated beyond this depth the water in the wetted zone will continue to move downward and eventually moves to the water table.

The long term (e.g. annual) average flux in the lower part of the profile, which is in the quasi-steady state condition, will be downward and its magnitude will be between zero and $R/\Delta t$, where R is the amount of rainfall in the averaging time interval Δt.

The water content distribution in the lower part of the profile when it is in quasi-steady state will be determined by the texture of the material in that region, the magnitude of the average downward flux, and the proximity to the water table. At depths below approximately 70-90 cm and at distances more than 50-70 cm above a water table the water content of such a profile approximates that corresponding to a hydraulic conductivity equal to the magnitude of the downward flux. For example, for a downward average flow rate of .05 cm/day (about 10 cm/year), the water content of coarse tailings would be about 0.3, that of the fine tailings about 0.5 to 0.6.

Under limited rainfall conditions, such as at the Vitro Mill site in Salt Lake City, any significant vegetative cover on the tailings pile would use all the available precipitation, leaving little or no water to flow below the root zone to greater depths.

SECTION 3

RECOMMENDATIONS

Many aspects of water movement in tailings profiles could not be adequately explored within the scope of the project. The simulations and analyses should be extended to include a series of rainfall and evaporation events with a fuller exploration of the effects of various rainfall intensities and magnitudes on water flow within the profile. The extraction of water by plant root systems should be included in the simulations and its effect on the behavior of water in the profile determined. A more extensive and systematic examination should be made of the effect of profile layering on the water content distribution in the upper 30 to 60 cm of the tailings profile. Another factor that should be explored is the effect of water table depth on the flow in the profile, including the case of a water table at great depth or the "no water table" case.

A logical extension of the present work on simulation of water flow in tailings profiles would be the combination of a model for radon transport in the profile with the water transport model. Such a combination could provide a method of systematic examination of the effect of various profile layering sequences on radon transport to the pile surface. Also, a combination of the soil water flow model with a model for transport of dissolved chemical species would seem to be a possible method of examining transport of contaminants to the ground water.

SECTION 4

SOIL WATER FLOW CONCEPTS AND TERMINOLOGY

The salient features of the theory of flow of water in unsaturated porous materials, such as soils, will be outlined in order to provide the reader, who may be unfamiliar with this subject, with the essential concepts and definitions of terms required for the subsequent discussion and analysis of flow systems. For further, more detailed, background on the subject the reader is referred to the cited literature (Childs 1969, Klute 1973, Swartzendruber 1969). Selected terms used in this report are defined in the Glossary of this report.

Water movement in soil can occur in the liquid phase or the gas phase. In each phase water may be transported by convective motion or by diffusion processes. The convective motion of a phase is driven by mechanical forces such as gravity and pressure gradients. Movement by diffusion within a phase occurs in response to gradients of the thermodynamic chemical potential of the water within the phase. In many cases diffusion may be considered to be driven by the concentration gradients of the water.

In a water saturated medium the water transport is of necessity solely in the liquid phase and is dominantly a process of convective transport driven by mechanical forces. These forces are given by the negative gradient of a potential function. A commonly used potential function is the energy per unit weight of soil water or the hydraulic head, H. The hydraulic head is made up of two components, the gravitational head and the pressure head. The gravitational head of the soil water at a point in the soil is the elevation of that point above an arbitrarily chosen reference and is a measure of the gravitational potential energy per unit weight of the soil water at a given point in the gravity force field of the earth. In saturated soils the pressure head, h, is related to the pressure in the soil water by the relation:

$$h = \frac{P_w - P_{atm}}{d\ g} \qquad (1)$$

where d is the soil water density, g is the acceleration of gravity, P_w is the pressure of the soil water and P_{atm} is atmospheric pressure. The hydraulic head and its components may be measured in those cases where $P_w > P_{atm}$ with a piezometer, which is a cased well, usually of small diameter, terminated at the point in the soil at which the head is to be measured. Fig. 1 shows a piezometer, and the interpretation from it, of the hydraulic head and its components. In reference to a piezometer, the hydraulic head is defined as the elevation of the free water surface in the piezometer tube relative to an arbitrarily chosen reference elevation.

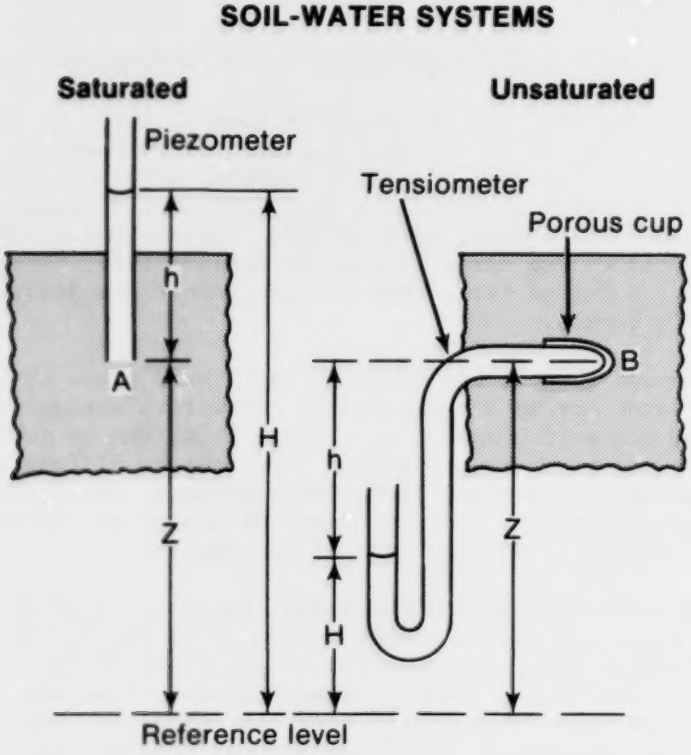

Fig. 1. A diagram of the relationships between hydraulic head, H, pressure head, h, and gravitational head, Z. The pressure head is measured from the level of termination of the piezometer or tensiometer in the soil to the water level in the manometer and is negative in the unsaturated soil.

In unsaturated soils the pressure in the liquid phase P_w is usually less than atmospheric, and the piezometer cannot be used to measure the hydraulic head. A tensiometer, which consists of a porous permeable membrane or cup connected to a manometer or other pressure measuring device (See Fig. 1), is used to extend the measurement of hydraulic head to unsaturated soils. The pressure of the water inside the "cup" when the water in the tensiometer is in equilibrium with the soil water is then used in equation (1) to obtain the pressure head. The pressure that must be applied to the tensiometer water to establish equilibrium between it and the soil water is determined by the water content of the soil which in turn is related to factors such as the curvature and surface tension of the air water interface within the soil water system, and the magnitude and extent of the adsorptive forces between the soil solid matrix and the soil water.

The equation of soil water transport, which was used in the simulations and analyses described in this report, is developed by combining a mass balance for the soil water with a flux equation. The mass balance equation relates the time rate of change of water content of a differential volume element of soil to the excess of inflow over outflow from the element and to the time rate of production of soil water within the element. If it is assumed that the soil water is of constant density, the mass balance may be written as a volume balance, which for one dimensional flow becomes:

$$\frac{\partial \theta}{\partial t} = - \frac{\partial Q}{\partial z} + S \qquad (2)$$

In equation (2) θ is the volumetric water content, z is the vertical space coordinate taken as positive upward, t is the time, Q is the soil water flux and S is a source term or the time rate of production of soil water per unit soil volume. The latter may be used to represent the extraction of water from soil by plant roots in which case the production rate is generally negative. Equation (2) expresses the fact that there are two reasons for the change in water content of a differential soil volume element at a point in the flow system, (1) the excess of inflow to the element over outflow from the element, which is mathematically described by $- \partial Q/(\partial z)$, and (2) the production (positive or negative) of water by any processes or reactions in the soil within the element. In the simulations described in this report we have not considered extraction of water by plant roots, and have set the source function S equal to zero.

The soil water flux is assumed to be given by the Darcy equation which is the product of the hydraulic conductivity, k, and a driving force expressed as the negative gradient of the hydraulic head. For a saturated soil the hydraulic conductivity is a maximum for the given soil. As the water content of the soil decreases from saturation the ability of the soil to transmit water, which is measured by the hydraulic conductivity, decreases very strongly. The Darcy equation has been extended to unsaturated soils by considering the conductivity to be a function of the water content. The primary reasons for the decrease of K as θ decreases are (1) the decrease in effective cross section of the soil which is available for liquid flow, (2) the drainage of water from the largest pores, which contribute strongly to the conductivity, and a decrease in the average size of the liquid-filled flow

channels and, (3) the increase in tortuosity (crookedness) of the liquid flow path.

In one dimension the Darcy equation or flux equation may be written as:

$$Q = - K(\theta)\frac{\partial H}{\partial z} \tag{3}$$

where $K(\theta)$ is the hydraulic conductivity water content function. The conductivity is a positive quantity, and since the hydraulic gradient may in a given case be either positive or negative, the flux Q may be either positive or negative. The algebraic sign of the flux indicates the direction of the flow with respect to the chosen coordinate axis, a positive flux being in the positive z axis direction, and vice versa for a negative flux. Since the hydraulic head is the sum of the pressure and gravitational heads, equation (3) may be written:

$$Q = - K\ (\theta)(\frac{\partial h}{\partial z} + 1) \tag{4}$$

where $\partial h/\partial z$ is the pressure head gradient. Combining equation (4) with (2) with $S = 0$ yields:

$$\frac{\partial \theta}{\partial t} = \frac{\partial}{\partial z}\ (K\ (\theta)(\frac{\partial h}{\partial z} + 1)\ ) \tag{5}$$

Equation (5) is a partial differential equation in two dependent variables, θ and h. In order to obtain an equation for water flow in one dependent variable, another relation between θ and h is required. This relationship is the water retention function, $\theta(h)$. The schematic form of this function is shown in Fig. 2. In general, the water content decreases as the pressure head decreases (becomes more negative). The retention function displays a phenomenon called *hysteresis*, i.e., the water content at a given pressure head depends on the historical sequence of pressure heads which has been imposed on the soil. If the flow process is entirely one of drainage from saturation or of wetting from a given initial water content, the relation between θ and h is single valued and non-hysteretic. If, however, the flow process involves sequences of wetting and drying the water content-pressure head relation is multi-valued and hysteretic. There is an infinite number of possible $\theta(h)$ relationships or scanning curves lying between the initial drainage curve and the main wetting curve (See Fig. 2). The scanning curve to be applied at any time and place in a flow process depends on the sequence of reversal points that have occurred at that place. A reversal point is described by the paired values of pressure head and water content (such as h_1, θ_1 or h_2, θ_2 in Fig. 2) at which a reversal in the time-trend of water content change has taken place. In non-hysteretic flow simulation the function $\theta(h)$ is single valued and may easily be represented empirically. In hysteretic flow simulation the $\theta(h)$ relation is much more complicated because some method must be devised to keep account of the necessary reversal points and select the appropriate scanning curve. We have devised procedures to treat the hysteresis in the $\theta(h)$ relation that can be used in the numerical solution process for the flow equation to be described in another section of this report.

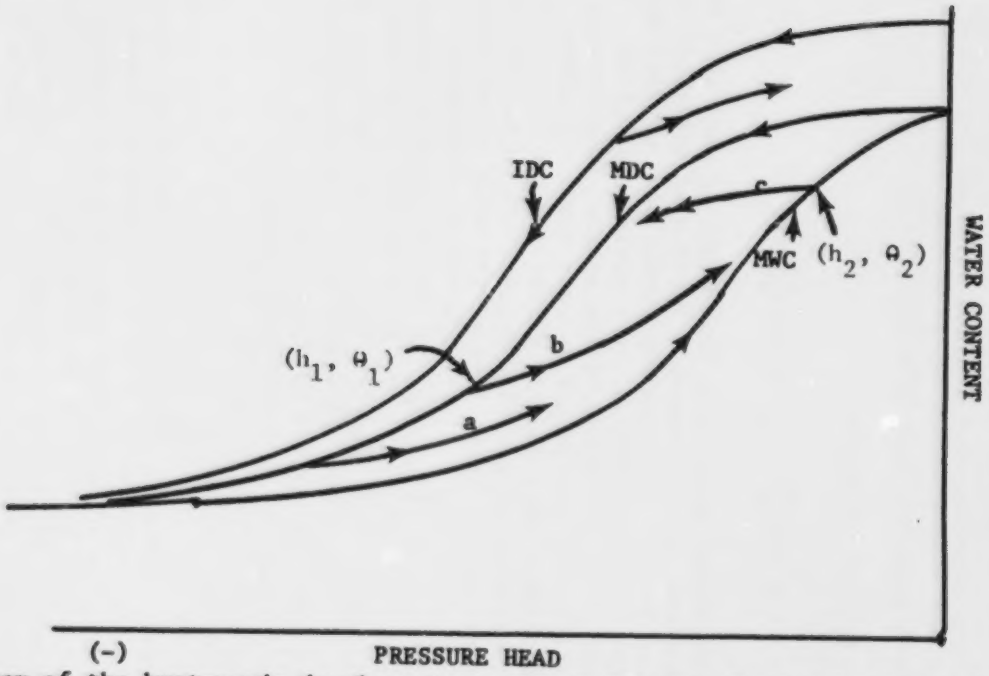

Fig. 2. Diagram of the hysteresis in the water content-pressure head relation, $\theta(h)$. IDC - initial drainage curve. MDC - main drainage curve. MWC- main wetting curve. a and b - primary wetting scanning curves. c - primary drying scanning curve. Higher order (e.g., secondary, etc.) are possible and reverse from lower order scanning curves.

Assuming that proper mathematical description of the $\theta(h)$ relation and its hysteresis is available, the time derivative term in equation (5) can be transformed to

$$\frac{\partial \theta}{\partial t} = \frac{d\theta}{dh} \frac{\partial h}{\partial t} = C \frac{\partial h}{\partial t} \tag{6}$$

In equation (6) the water capacity function, C, is the rate of change of water content with pressure head, $d\theta/dh$, and is the derivative of the appropriate applicable drying or wetting scanning curve of the $\theta(h)$ relationship. The water capacity is a function of the water content. It may be seen from the general shape of the $\theta(h)$ function (Fig. 2) that the water capacity will have a maximum at some pressure head less than zero.

Using equation (6) in (5) yields

$$C\ (\theta) \frac{\partial h}{\partial t} = \frac{\partial}{\partial z} \left(K\ (\theta)\left(\frac{\partial h}{\partial z} + 1\right)\right) \tag{7}$$

which is the one-dimensional soil water flow equation used as a basis for the simulations described in this report. Particular solutions of equation (7), subject to given initial and boundary conditions, predict and describe the dependence of the pressure head, h, upon position and time. An initial condition is a mathematical statement of the spatial distribution of pressure head at the time arbitrarily designated as zero time. Boundary conditions are mathematical statements that specify either the pressure head or the soil water flux at the boundaries of the flow region. The functions $C(\theta)$ and $K(\theta)$ are the hydraulic functions or properties of the soil in the region of flow, and are the avenue by which the soil affects the flow behavior. A solution of equation (7), viz, the function $h(z, t)$, may be used to obtain the water content position-time function, $\theta(z, t)$, by using the water retention function $\theta(h)$. The soil water flux distribution, $Q(z, t)$, may also be obtained by using $h(z, t)$ in the Darcy law, equation (4). The assumptions implicit in equation (7) have been summarized by Klute (1973). One of these assumptions is that the air phase is at atmospheric pressure, and has essentially a zero pressure gradient. This assumption is sometimes not well satisfied in practice. For various reasons it is not possible to give a complete assessment of the errors introduced by this assumption. Some qualitative statements may be made, however. Air pressure build up may occur during rapid infiltration from ponded water into a soil profile bounded at its lower end by a water table or a soil layer of low air permeability. The qualitative effect in this case is to decrease the rate of infiltration and the extent of penetration of the infiltrating water. Conversely, drainage of a layered soil profile, when air access to the soil layers is restricted, will not occur as rapidly as would be predicted from theory based on the assumption of constant atmospheric pressure within the gas phase. In general, a more correct approach to water flow in unsaturated soils would involve a two-phase flow treatment, and a flow equation for each phase (gas and water) would have to be solved. Such an approach is inherently more complex than the one-phase approach used in this study. We do not feel that the errors introduced in the analyses described herein due to neglect of the air phase flow are extremely significant. In the infiltration cases that were studied herein, no ponding occurred on the soil surface, hence, the situation of a

pressure build-up in a gas phase trapped between a water table and overlying ponded water could not occur. Simulations of drainage of an initially saturated layered soil column may be significantly in error when a fine textured layer overlies a coarser textured layer and air must enter the coarse layer through the overlying wetter fine material, which may have a low air permeability. The error would be greatest during the initial (first one or two days) rapid drainage of the layered profile. The water content of a coarse layer under a finer textured layer would be higher than predicted by the method of simulation used in this study. However, after a few days, there is an increased probability of leakage or access of air to the buried coarse layers, and furthermore, the rate of flow and drainage would be decreasing. Both of these factors suggest that the error due to neglect of air flow would decrease in significance with time of drainage.

The conductivity water content relationship $K(\theta)$ has been found not to be very much hysteretic. In many cases the hysteresis in $K(\theta)$ if it exists is hidden within the uncertainty of determination of the relationship. For the purpose of the analyses described in this report, it was assumed that $K(\theta)$ is not hysteretic. However, the $K(h)$ function will be hysteretic because of the hysteresis in the $\theta(h)$ function.

SECTION 5

DETERMINATION OF THE HYDRAULIC PROPERTIES OF TAILINGS

SAMPLING AND BASIC PHYSICAL CHARACTERISTICS

Upon consultation with representatives of the Office of Radiation Programs, U. S. Environmental Protection Agency, Las Vegas, Nevada, the tailings pile at the Vitro Mill site in Salt Lake City, Utah was selected as a test area. A visit to the site was made in April, 1976, to become familiar with the general features and characteristics of tailings materials. Three size fractions of tailings material were selected for characterization. These are hereafter designated as Coarse, Medium and Fine. A second trip to the site was made in June, 1976, to collect bulk samples of these fractions. Due to the generally single-grain structure of the tailings material in situ, it was decided to use core samples which were packed in the laboratory from bulk material for the determination of hydraulic properties. A limited number of core samples was taken at the site for the purpose of establishing the general level of in situ bulk density of the selected tailings fractions. These results are summarized in Table 1.

TABLE 1. IN SITU BULK DENSITY AND PARTICLE DENSITY OF THE SELECTED FRACTIONS OF MILL TAILINGS, VITRO MILL SITE

Fraction	Bulk Density	Particle Density
	g/cm^3	g/cm^3
Coarse	1.48 to 1.57	2.70
Medium	1.28 to 1.50	2.71
Fine	0.9 to 1.1	2.89

The bulk samples were packed in drums, with plastic liners, and transported to the laboratory. Particle size distributions were determined by sieving and by the hydrometer method (Day, 1965). Table 2 lists the summation percentage for each of the fractions. The particle density of each fraction was determined by the picnometer method (Blake, 1965). The results are shown in Table 1.

TABLE 2. PARTICLE SIZE DISTRIBUTION OF MILL TAILINGS FRACTIONS SUMMATION PERCENTAGES[1/]

Particle Diameter	Tailings Fraction		
	Coarse	Medium	Fine
1000 μm	92 %	98 %	-
500	76	95	-
250	41	81	-
125	22	55	100 %
63	15	33	95
48	10	24.4	92
25	7.5	4.2	84
16	5	2.1	80
9	3.4	1.3	57
7	-	-	42
3	-	-	5.9

[1/] Percent of the fraction with particle diameters less than or equal to the indicated diameter.

WATER RETENTION CHARACTERISTICS

The $\theta(h)$ relationship for each fraction was determined using a combination of pressure chamber apparatus or suction apparatus (Rose, 1966; Taylor and Ashcroft, 1972). Fig. 3 illustrates the pressure apparatus. The suction apparatus was similar, except that the chamber enclosing the samples was maintained at atmospheric pressure, and suction was applied to the samples by lowering the water bottle relative to the porous plate to an appropriate distance. Generally, pressure chamber apparatus was used to obtain data in

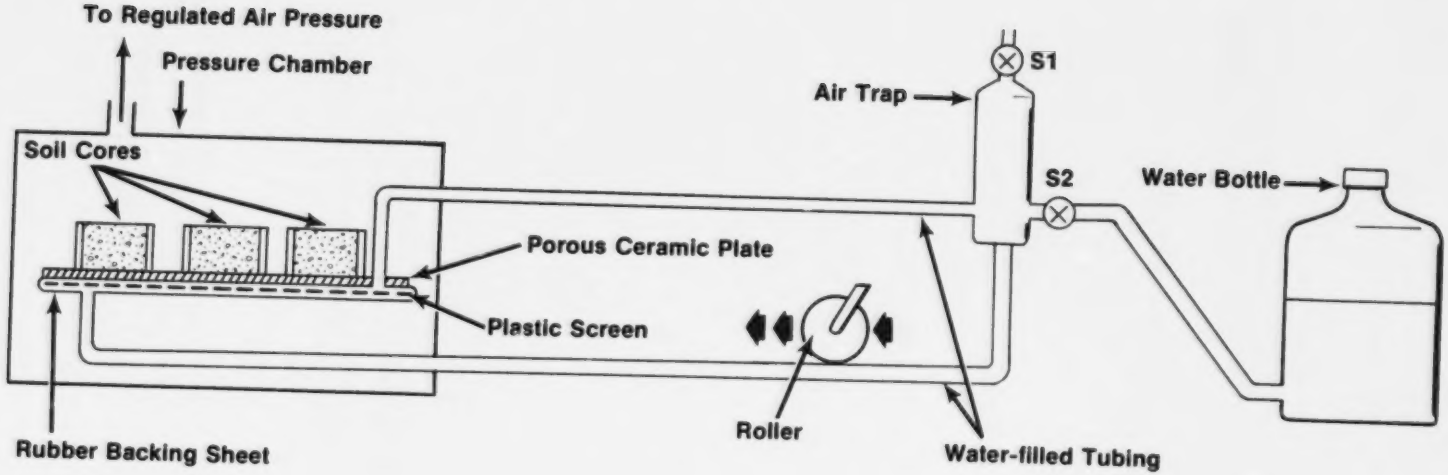

Fig. 3 Diagram of the pressure chamber apparatus used to determine the water retention characteristics of the tailings materials.

the range of pressure heads less than -60 cm of water, and suction apparatus for h > -60 cm.

Sample Preparation

It was desired to pack core samples to the field value of bulk density. The following procedure was used for the Coarse and Medium fractions. A bulk quantity of a given fraction was thoroughly mixed with sufficient water to bring it to a water content of 6 - 10% by weight, and placed in a plastic bag to prevent loss of water. Sub-samples were taken to determine the actual weight percentage of water. The weight of moist material to be packed in a sample ring (volume 48.3 cm^3, height 2.5 cm) to obtain the desired bulk density was calculated. A hydraulic press was used to pack the desired weight of moist tailings material into the sample rings. Cores were packed to bulk densities of 1.53 and 1.47 g/cm^3 for the Coarse and Medium fractions, respectively.

Cores of the Fine fraction were prepared by a filtration procedure, in which a filter cake of the material was formed in the sample ring by suction filtration from a slurry of the Fine material. Cores with bulk densities in the range 0.95 to 0.99 g/cm^3 were obtained by this technique.

After packing the cores, a piece of cheesecloth held in place by a rubber band, was placed over the lower end of the core to prevent loss of material from the core in subsequent handling.

Method for Determination of Hysteresis

In the simulation procedure the main drainage and main wetting curves for each fraction were required. Because any rewet curve of $\theta(h)$ starting at pressure heads less (i.e., more negative) than -7000 cm does not differ much from the rewet curve starting at -7000 cm, it was arbitrarily decided to determine the "main" wetting curve starting at h = -7000 cm and neglect any hysteresis at lower pressure heads. Pressure heads of -2, -7.5, -15, -30, -60, -120, -250, -500, -1000, -3000, and -7000 cms of water were selected as the standard points of measurement on the $\theta(h)$ curves.

To determine the main wetting curve (MWC) beginning at h = -7000 cm, a large number of core samples (30 or more) was packed and soaked in water for at least 24 hours. They were then placed on a porous plate in a pressure chamber at a gas phase pressure of 7000 cm of water (corresponding to h = -7000 cm) and brought to hydraulic equilibrium. Equilibrium was determined by removal of the cores from the porous plate and weighing them. When the weight of the core remained constant (within approximately .05 gm, corresponding to an uncertainty in θ of about 0.001) the cores were distributed to a series of pressure chambers at gas phase pressures of 3000, 1000, 500, 250, and 120 cms of water and to suction plates at pressure heads of -60, -30, -15, -7.5 and -2 cms of water, and allowed to take up water until they were at equilibrium. Gas bubbles tend to accumulate in the water beneath the porous plate and in the connecting tubing to the water bottle. These bubbles may block the flow of water to the ceramic plate and the core samples. Periodically, the gas bubbles were removed to the air trap by closing

stopcock S_2 (See Fig. 3) and circulating the water in the closed loop consisting of the air trap, the space below the ceramic plate and the connecting tubing, using a roller on one of the tubes. This modification of the apparatus allowed us to determine the wetting $\theta(h)$ curve.

After equilibrium was reached the water content of each core was determined by standard gravimetric procedures. The data thus obtained were used to develop the MWC.

The main drying curve MDC was determined by preparing a large number of cores, which were soaked for 24 hours or more, equilibrated in a pressure apparatus at h = -7000 cm, and then on a suction apparatus at h = -2 cm. This sequence was necessary to establish the rewet saturation at h = -2 cm so that the main drainage curve would be properly determined. After equilibration at h = -2 cm, the cores were distributed to a series of suction plates at pressure heads of -7.5, -15, -30, and -60 cms of water, and to a series of pressure chambers at pressure heads of -120, -250, -500, -1000, -3000, and -7000 cms of water. After equilibration the water content of each core was obtained. The data thus obtained were used to develop the MDC.

The water content-pressure head relation for the Coarse and Medium fractions was determined in the range of pressure heads less than -7000 cm water (-7 bars) by a vapor pressure technique (Croney, et al., 1952). Samples of the materials were equilibrated in vacuum dessicators over saturated salt solutions with relative humidities corresponding to water potentials of -71, -145, -290, -900, and -1,568 bars. The weight percentage water contents were determined at equilibrium and converted to the volumetric basis by multiplying by the bulk density of the cores packed for the $\theta(h)$ determination at pressure heads greater than -7 bars. Due to experimental difficulties (e.g. shrinkage at high suction) with the Fine fraction of tailings, it was decided to limit this study to simulations where the Fine fraction would not be exposed at the profile surface, and therefore, retention data at pressure heads less than -7 bars would not be needed for this fraction.

The water retention data obtained from the measurements described above were represented by empirical functions for use in the numerical simulation. In the range of pressure head, $-7000 \text{ cm} \leq h \leq o$, the following function was used (Gillham, et al., 1976):

$$\theta(h) = \theta_o \left[\frac{\cosh \beta - \Gamma}{\cosh \beta + \Gamma}\right] \tag{8}$$

where

$$\beta = (h/h_o)^b \quad b < o \tag{9}$$

$$\Gamma = (\theta_o - \theta_r) \; / \; (\theta_o + \theta_r) \tag{10}$$

This empirical function for $\theta(h)$ has four parameters, h_o, b, θ_o, and θ_r, which were selected to fit the function to the measured main wetting curve (MWC) and main drying curve (MDC) data. These parameters were selected with

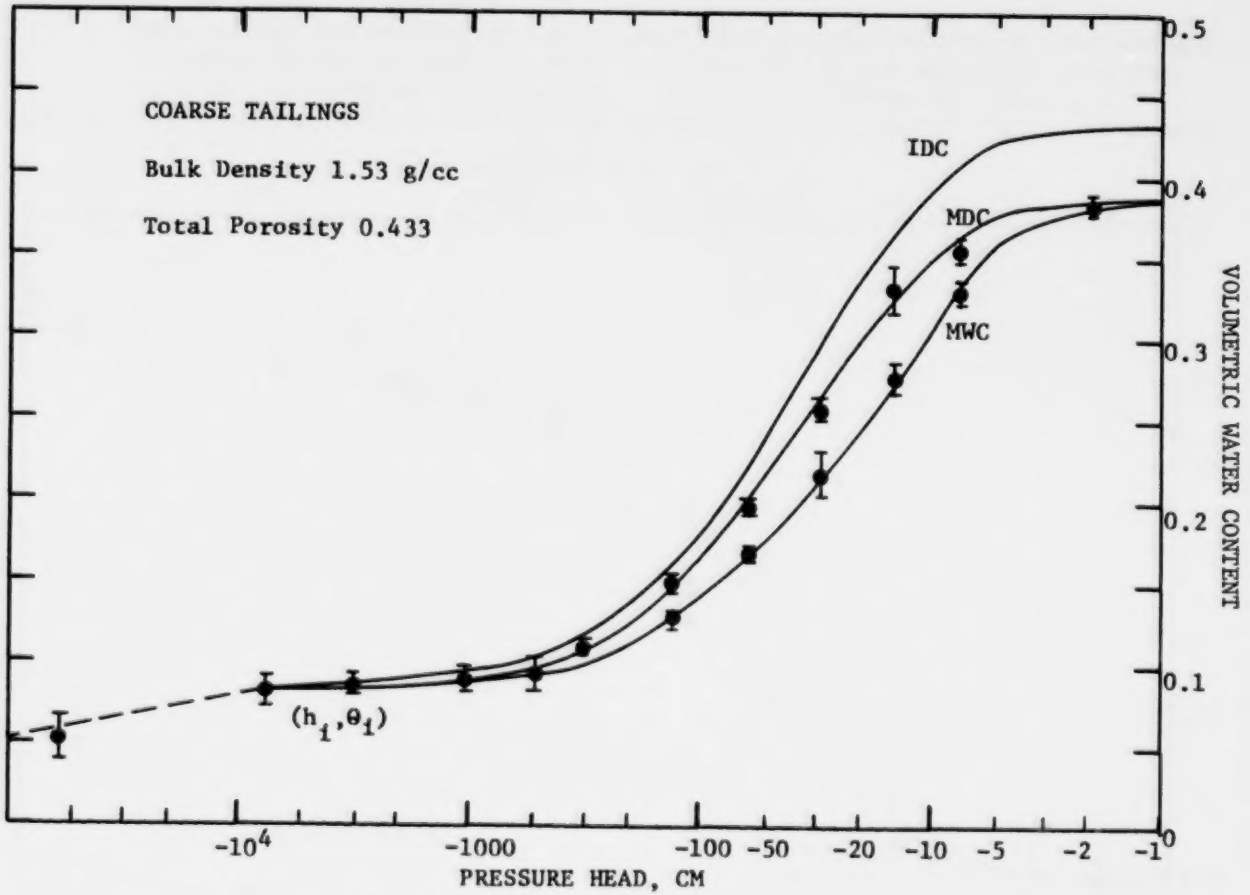

Fig. 4. Water retention functions for the Coarse tailings. Each point is an average of 3 to 15 determinations. The vertical lines represent $\pm$ 1 standard deviation from the mean. The curves are the empirical functions used in the simulations of water flow. The IDC was calculated from the MDC by the theory of Mualem.

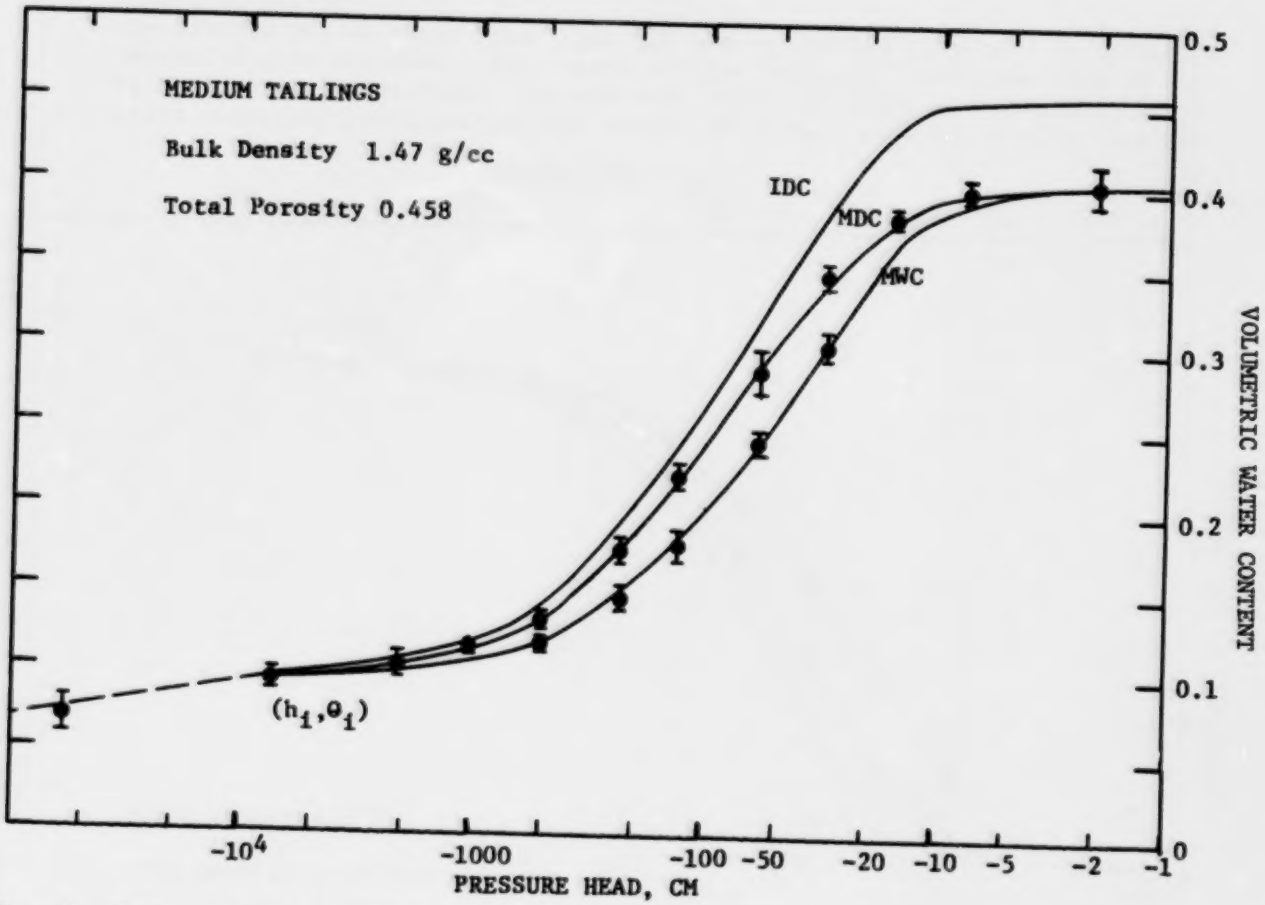

Fig. 5. Water retention functions for the Medium tailings. Each point is an average of 6 to 9 individual measurements. The vertical lines represent $\pm$ 1 standard deviation from the mean. The curves are the empirical functions used in the simulations of water flow. The IDC was calculated from the MDC by the theory of Mualem.

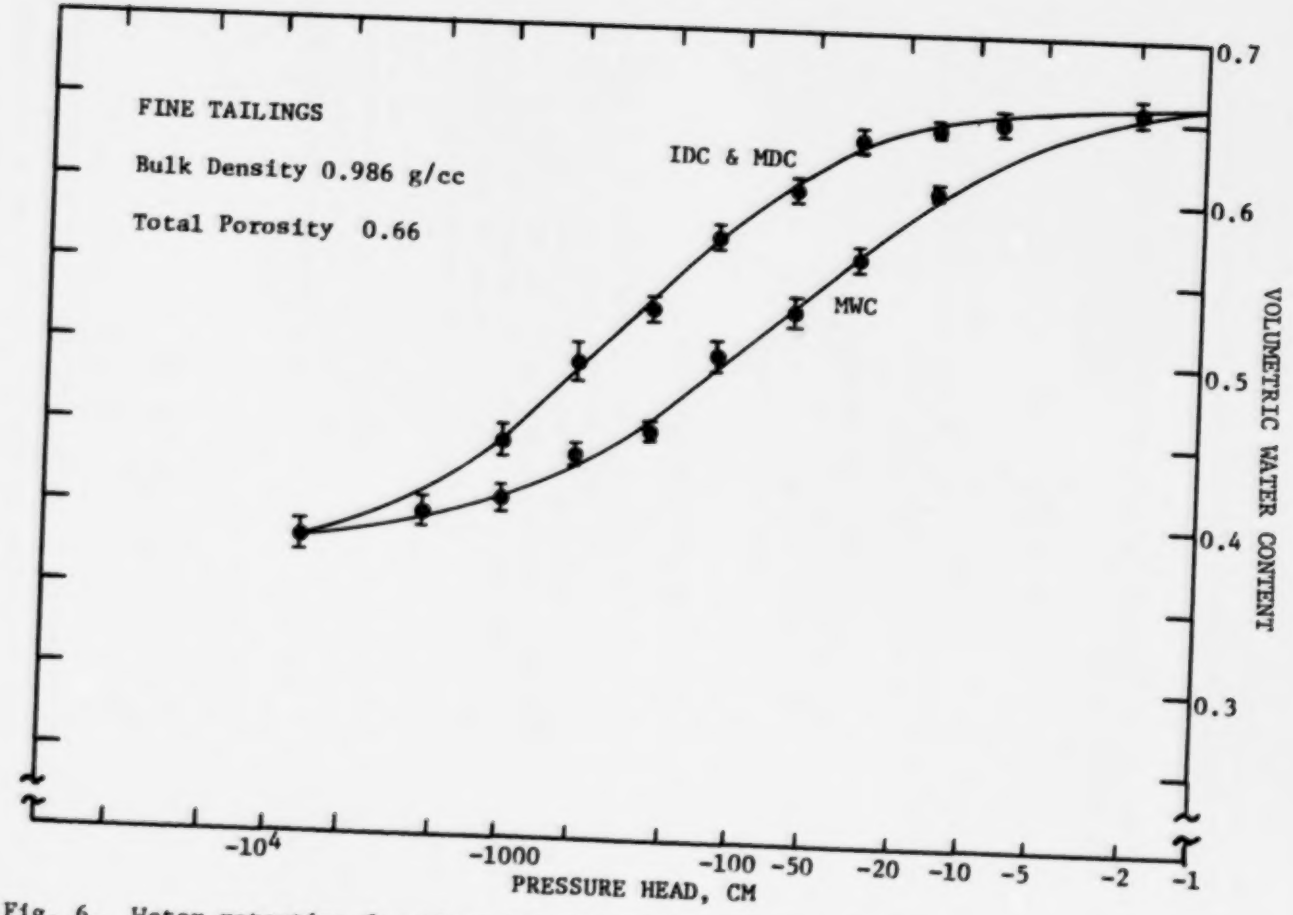

Fig. 6. Water retention functions for the Fine tailings. Each point is an average of 4 to 12 individual determinations. The vertical lines represent $\pm$ 1 standard deviation from the mean. The solid lines are the empirical functions used in the simulations of water flow.

the constraint that the MDC and MWC should intersect at (θ_i, h_i), with h_i about -7000 cm. The empirical functions for the MWC and MDC were used to generate the scanning curves interior to the MWC and MDC. A theory developed and tested by Mualem (1974) was used for this purpose. The initial drainage curve (IDC) was generated by his theory from the MDC. Scanning curves interior to the IDC and MWC were also obtained by his theory. Mualem's theory provides a reasonably accurate method of obtaining scanning curves, which is suited to use in the numerical simulation process, and greatly reduces the necessary amount of experimental measurement required.

At pressure heads more negative than about -7000 cm the $\theta(h)$ data were represented by the empirical form:

$$\theta(h) = \left(\frac{h}{d}\right)^a \tag{11}$$

where a and d are parameters which were selected to fit the data, and with the constraint that the function of Eq. (11) should pass through the intersection point (θ_i, h_i) of the MDC and MWC (see above).

Figs. 4, 5 and 6 show the empirical $\theta(h)$ functions obtained for the Coarse, Medium, and Fine fractions, respectively. The solid curves in these figures are plots of Eq. (8) subject to Eqs. (9) and (10). The dashed line in Figs. 4 and 5 is a plot of Eq. (11). The parameters of the functions are given in Tables 3, 4 and 5.

HYDRAULIC CONDUCTIVITY - WATER CONTENT RELATIONSHIPS

The measurement of the $K(\theta)$ relation may be accomplished by a number of methods (Klute, 1972). All of the available methods require a substantial amount of time and in some cases the methods are rather difficult. Because of these and other difficulties encountered in the direct measurement of the $K(\theta)$ function there has been considerable interest in schemes for the calculation of hydraulic conductivity from pore size distribution data (Jackson, et al., 1965; Kunze, et al., 1968). The latter may be obtained from the water content - pressure head relation.

Lalibertie, et al. (1968) described a method of using water content-pressure head data to calculate the conductivity-water content function. These authors developed an integral equation for the conductivity, which may be written as:

$$K = \frac{\sigma^2}{5\rho g \eta} \left(\frac{\theta - \theta_r}{\theta_s - \theta_r}\right)^2 \int_{\theta_r}^{\theta} \frac{d\theta}{h^2} \tag{12}$$

In Eq. (12), ρ is the density of the soil water, η is its viscosity, σ is its surface tension, g is the acceleration of gravity, and θ_s and θ_r are parameters of the $\theta(h)$ function. To evaluate the integral, and obtain $K(\theta)$, a functional relation between h and θ is needed.

TABLE 3. PARAMETERS OF THE EMPIRICAL HYDRAULIC FUNCTIONS OF THE COARSE TAILINGS

Function and Equation No.	Parameter Symbol	Value		
Water Retention		IDC	MDC	MWC
Eq. (10)	θ_o	0.433	0.385	0.385
	θ_r	0.076	0.0763	0.0776
Eq. (9)	h_o, cm	- 131	- 131	- 67.4
	b	-0.468	-0.468	-0.504
Eq. (11)	d, cm		-1.71×10^{-2}	
	a		-0.1964	
Intersection Point	h_i, cm		-7320	
	θ_i		0.07842	
Hydraulic Conductivity				
Eq. (18)	A, cm/day		5.40×10^{-8}	
	B		54.29	

TABLE 4. PARAMETERS OF THE EMPIRICAL HYDRAULIC FUNCTIONS OF THE MEDIUM TAILINGS

Function and Equation No.	Parameter Symbol	Value		
Water Retention		IDC	MDC	MWC
Eq. (10)	θ_o	0.458	0.401	0.401
	θ_r	0.090	0.0959	0.0939
Eq. (9)	h_o, cm	- 281	- 281	- 166
	b	-0.451	-0.451	-0.503
Eq. (11)	d, cm		-1.102×10^{-2}	
	a		-0.1749	
Intersection Point	h_i, cm		-7121	
	θ_i		-.09589	
Hydraulic Conductivity				
Eq. (18)	A, cm/day		1.99×10^{-8}	
	B		50.0	

TABLE 5. PARAMETERS OF THE EMPIRICAL HYDRAULIC FUNCTIONS FOR THE FINE TAILINGS

Function and Equation No.	Parameter Symbol	Value	
Water Retention		IDC & MDC	MWC
Eq. (10)	θ_o	0.66	0.66
	θ_r	0.31	0.35
Eq. (9)	h_o, cm	-2500	-400
	b	-0.28	-0.28
Eq. (11)	d, cm	--	
	a	--	
Intersection Point	h_i, cm	-6982	
	θ_i	0.3727	
Hydraulic Conductivity			
Eq. (18)	A, cm/day	5.38×10^{-12}	
	B	45.1	

In application of most of the theories which have been developed to calculate $K(\theta)$ from $\theta(h)$, it has been found that the calculated $K(\theta)$ function can be brought into reasonable agreement with measured $K(\theta)$ data by the use of a matching factor. The matching factor M is defined as:

$$M = \left[\frac{K_M}{K_C}\right]_{\theta_1} \tag{13}$$

where K_M is a measured conductivity at some known water content, θ_1, and K_C is the calculated conductivity at that water content. If $K_c(\theta)$ is the calculated conductivity function, the matched, calculated function $K_{mc}(\theta)$ is obtained from

$$K_{mc}(\theta) = M\, K_c(\theta) \tag{14}$$

Nielsen, et al. (1973) conclude that the procedure of calculating $K(\theta)$ from $\theta(h)$, with a matching factor, is a satisfactory method of evaluating the hydraulic conductivity of a field soil, especially when one considers the spatial variability of the hydraulic conductivity.

To avoid the time consuming procedure of determining $K(\theta)$ by one of the available methods of direct measurement (Klute, 1972), and in view of Nielsen's conclusion cited above, as well as the experience of others, I decided to calculate $K(\theta)$ from Eq. (12) and use a matching factor to adjust the calculated function as described above. For this purpose, the $h(\theta)$ function obtained by solving equation (8) (with Eqs. 9 and 10) for h was used in the integral of Eq. (12). The result is:

$$K_c(\theta) = \frac{\sigma^2}{5\rho g \eta} \frac{1}{h_o^2} \left(\frac{\theta-\theta_r}{\theta_o-\theta_r}\right)^2 \int_{\theta_r}^{\theta} \left(\ln\left(y + (y-1)^{\frac{1}{2}}\right)\right)^{-2/b} d\theta \qquad (15)$$

where

$$y = \Gamma \left(\frac{\theta_o + \theta}{\theta_o - \theta_r}\right) \qquad \Gamma = \frac{(\theta_o - \theta_r)}{(\theta_o + \theta_r)}$$

and θ_o, θ_r, h_o and b are the parameters of the empirical $\theta(h)$ function (Eqs. (8), (9) and (10). The integral in Eq. (15) was evaluated numerically.

To obtain the matching factor, the hydraulic conductivity of cores at a known volumetric water content was determined. Core samples of the Coarse and Medium fractions of tailings were packed to the same bulk density and by the same method that was used for the $\theta(h)$ measurements described above. The cores were soaked for at least 24 hours, and the hydraulic conductivity was determined by a standard steady state method (Klute, 1965). After the conductivity measurements were completed, the volumetric water content of the sample was determined. These data provided a value of K_M at $\theta = \theta_1$ for calculating the matching factor from (Eq. 13).

It was not possible to obtain conductivity data for the Fine fraction in the above manner because the driving force for flow of an approximately unit hydraulic gradient as used in the steady-state method produced a flow rate too small to be measured with any reasonable accuracy. Instead, the following procedure was used: a layer of Fine material was deposited by pressure filtration on a ceramic plate which had a bubbling pressure of about 1 bar. The conductivity of the resulting two-layer flow system was then determined by producing a flow through the system with a gas pressure drive in the chamber corresponding to a hydraulic gradient of about 50. The conductance per unit area of the ceramic plate was measured separately, and the conductivity of the Fine material was calculated from:

$$\frac{\ell_f}{K_f} = \frac{\ell}{K_t} - \frac{\ell_p}{K_p}$$

where $(\ell_p/K_p)^{-1}$ is the conductance per unit area of the ceramic plate, $(\ell/K_t)^{-1}$ is the conductance per unit area of the two-layer system, K_f is the conductivity of the Fine material and ℓ_f is the thickness of the deposited Fine material layer.

The planned simulations of water movement involved evaporation from profiles in which the material at the surface was either the Coarse or Medium fractions. The conductivity of these fractions at the low water contents found under evaporative conditions was measured by the following procedure: Columns of each fraction (15 cm dia. x 15 cm high) were packed at an intermediate water content ($\theta \approx 0.15$) and to the same bulk density

used in the $\theta(h)$ determinations. Evaporation from the upper end was allowed to proceed. The bottom end of the column was closed. The water content as a function of depth in each column was measured at a series of times over a 15 to 30 day period, by gamma attenuation (Gardner, 1965). The soil water flux Q as a function of depth and time was calculated from the continuity equation for soil water (Eq. (2)). Integration of the continuity equation, with S = 0, yields:

$$Q(z) = Q(z_o) - \frac{1}{\Delta t}\int_{z_o}^{z} [(\theta(z,t_2) - \theta(z,t_1)]dz \qquad (16)$$

where $Q(z)$ is the average flux at depth z for the time interval $\Delta t = t_2 - t_1$, $Q(z_o)$ is the same for depth z_o, and $\theta(z,t_2)$ and $\theta(z,t_1)$ are the measured water content profiles in the drying column at times t_2 and t_1. The flux at a depth z may be calculated by Eq. (16) if the flux at some depth z_o is known. Since the bottom of the drying column was closed, the flux there is zero, and was chosen as the value of $Q(z_o)$. Repeated application of Eq. (16) was used to develop numerical values of $Q(z,t)$, the flux-depth-time function, for the drying column.

The water content gradient $\partial\theta/(\partial z) = G(z,t)$ as a function of depth and time was also calculated from the measured water content profile data.

The soil water diffusivity $D(\theta)$ (Klute, 1972) was then calculated from the ratio of soil water flux to water content gradient:

$$D(z,t) = -\frac{Q(z,t)}{G(z,t)} \qquad (17)$$

Eq. (17) is derived from Darcy's law, Eq. (3), by assuming a single valued functional relation between θ and h exists (as would be the case in the drying column), and neglecting the gravitational driving force for the flow. The latter is a reasonable approximation at the low water contents involved in the drying column. The diffusivity function $D(z,t)$ obtained from Eq. (17) was converted to a diffusivity water content function, $D(\theta)$, by using the measured $\theta(z,t)$ data.

The conductivity-water content relation was calculated from the soil water diffusivity using the relation $K(\theta) = D(\theta)C(\theta)$. The water capacity function $C(\theta) = d\theta/(dh)$, in the range of water contents found in the drying columns, was calculated from the measurements of $\theta(h)$ as described earlier in this section.

Figs. 7, 8, and 9 show the hydraulic conductivity-water content relation for each of the tailings fractions. The data were represented by an empirical function of the form

$$K = Ae^{B\theta} \qquad (18)$$

where A and B are parameters. The solid lines in these figures are plots of the empirical function for each material. The parameter values are also given in Tables 3, 4 and 5.

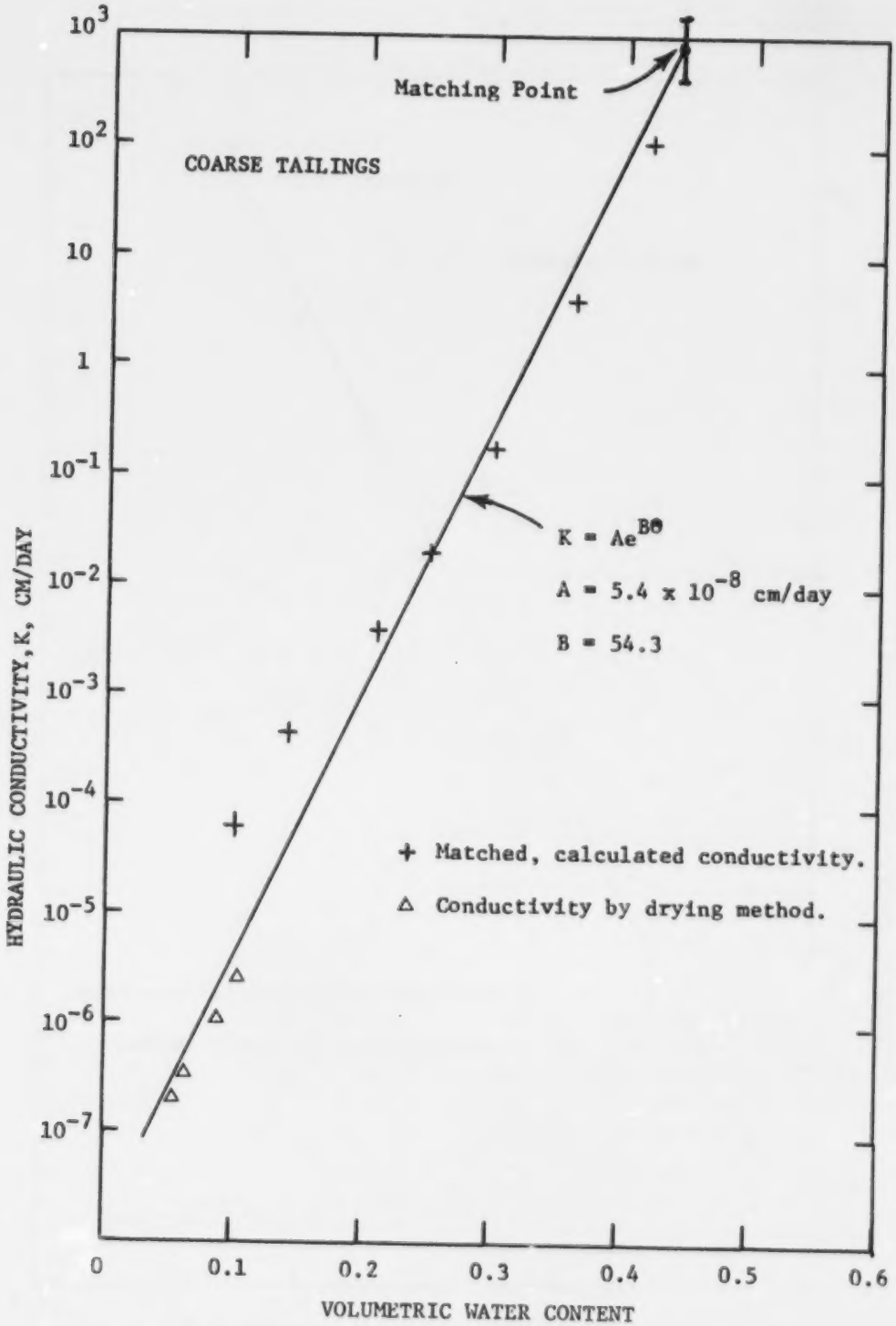

Fig. 7. Hydraulic conductivity - water content function for Coarse tailings.

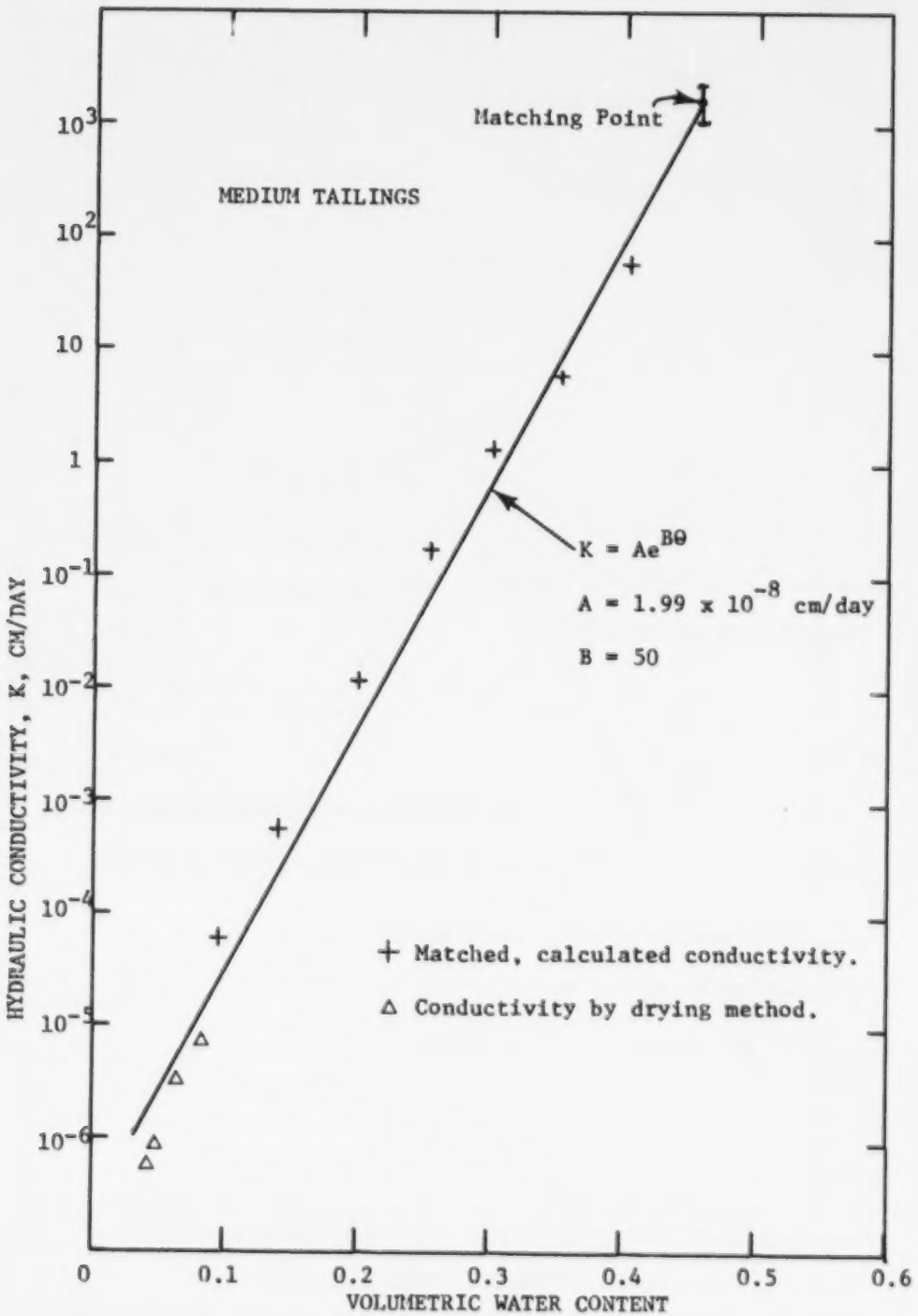

Fig. 8. Hydraulic conductivity - water content function for Medium tailings.

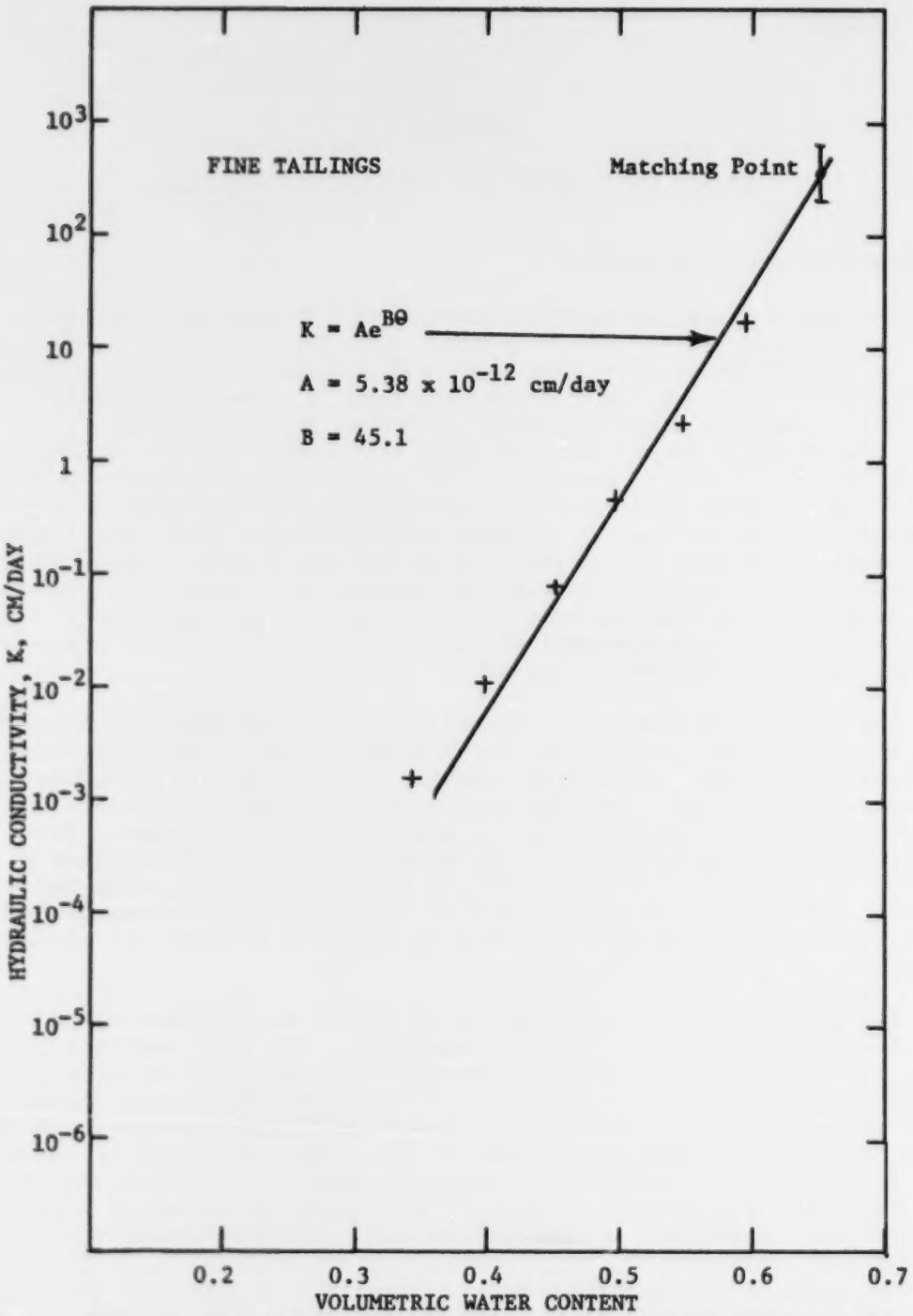

Fig. 9. Hydraulic conductivity - water content function for the Fine tailings.

SECTION 6

SIMULATION OF WATER FLOW IN TAILINGS PROFILES

THE NUMERICAL SOLUTION PROCESS

The flow of water in vertical profiles of tailings is in principle described by solutions of the equation of flow Eq. (7). This equation is a partial differential equation and has an infinite number of solutions. A particular solution which describes the flow in a specific profile is obtained by imposing boundary conditions and an initial condition. In addition, the hydraulic functions K (θ) and C (θ), which characterize a given tailing material, must be specified. If the profile is non-uniform, e.g., is made up of layers, the hydraulic functions appropriate to each layer must be specified. In the case of vertical one-dimensional flow, two boundary conditions are needed, one at each end of the flow region. These conditions are mathematical statements of the time dependence of either the pressure head h, or the flux Q at the ends or boundaries of the flow region. The initial condition is a statement of the spatial distribution of pressure head at the time selected as time zero.

The equation of flow is non-linear due to the dependence of K and C upon θ and hence in turn upon h. Analytic solutions are not available except for idealized situations, such as constant initial pressure head, constant boundary pressure heads, semi infinite regions of flow, non-hysteretic flow, or specific types of conductivity and water retention functions. These idealized conditions are not descriptive of the cases to be examined in this study. We want to deal with non-uniform profiles (layered), time dependent boundary conditions, and hysteretic flow regimes. In such cases the solutions to equation (7) must be obtained by numerical methods, utilizing a computer.

The partial differential equation of flow is solved numerically by replacing it with a set of algebraic equations. The space and time derivatives are approximated by finite difference equations. We desire a solution to equation (7), which is a function $h(z, t)$ for the space-time domain described by $-L < z < o$ and $t > o$. To obtain finite difference approximations to the derivatives in equation (7) the space-time domain of the solution is divided into increments Δt and Δz by imposing a grid on the region (See Fig. 10). The profile of length L is divided into a set of intervals Δz which are, in general, of non-uniform size. The time domain $t > o$ is divided into increments Δt, which are also of non-uniform size. The intersection points of the grid or nodes are identified by indices n and m where n is the space index and m is the time index. The pressure head and other

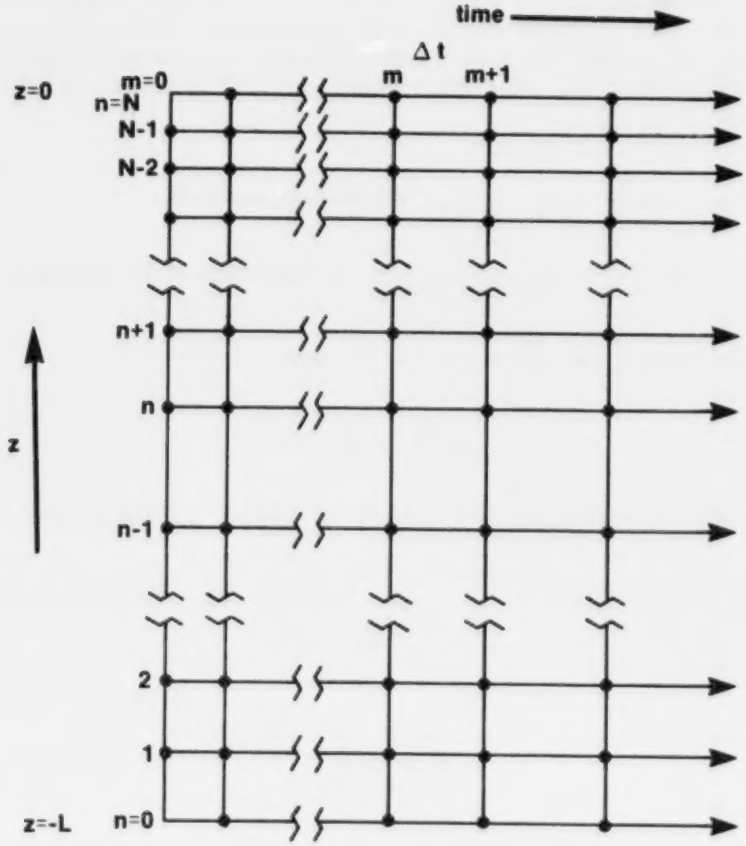

Fig. 10. Diagram showing the division of the space-time domain into increments, and the numbering of the nodes for the identification of variables in the numerical solution process.

quantities at each node are identified by these indices. For example, the pressure head at node n, m is denoted as $h_{n,m}$. The initial condition for a given solution is specified by the set of nodal values of pressure head, $h_{n,o}$, i.e., $m = o$ and $o \leq n \leq N$. Boundary conditions of the pressure head type are specifications of $h_{o,m}$ and $h_{N,m}$, for $m \geq o$. In the Crank-Nicolson finite difference scheme used in this study (von Rosenberg, 1969), six nodal values of pressure head are required. The general case in the interior of the flow region is shown in Fig. 11. The approximation to the time derivative in Eq. (7) is:

$$C \frac{\partial h}{\partial t} \simeq C_{n,\, m+\frac{1}{2}} \frac{h_{n,\, m+1} - h_{n,\, m}}{\Delta t} \tag{19}$$

where $C_{n,\, m+\frac{1}{2}} = (C_{n,\, m} + C_{n,\, m+1})/2$. A function F is defined as:

$F = K(\frac{\partial h}{\partial z} + 1)$ so that $\frac{\partial}{\partial z}(K\ (\frac{\partial h}{\partial z} + 1)\ ) = \frac{\partial F}{\partial z}$ and

$$C \frac{\partial h}{\partial t} = \frac{\partial F}{\partial t} \tag{20}$$

Then the r.h. side of equation (7), which is $\partial F/\partial z$, is approximated by:

$$\frac{\partial F}{\partial z} \simeq \frac{F_{n+\frac{1}{2},\, m+\frac{1}{2}} - (1 - r^2)\, F_{n\, m+\frac{1}{2}} - r^2\, F_{n-\frac{1}{2},\, m+\frac{1}{2}}}{\frac{\Delta z_\ell}{2}\,(r + r^2)} \tag{21}$$

In Eq. (21):

$$r = \Delta z_u / \Delta z_\ell \tag{22}$$

$$F_{n+\frac{1}{2},\, m+\frac{1}{2}} = K_{n+\frac{1}{2},\, m+\frac{1}{2}} \left(\left(\frac{\partial h}{\partial z}\right)_{n+\frac{1}{2},\, m+\frac{1}{2}} + 1 \right) \tag{23}$$

$$F_{n,\, m+\frac{1}{2}} = K_{n,\, m+\frac{1}{2}} \left(\left(\frac{\partial h}{\partial z}\right)_{n,\, m+\frac{1}{2}} + 1 \right) \tag{24}$$

$$F_{n-\frac{1}{2},\, m+\frac{1}{2}} = K_{n-\frac{1}{2},\, m+\frac{1}{2}} \left(\left(\frac{\partial h}{\partial z}\right)_{n-\frac{1}{2},\, m+\frac{1}{2}} + 1 \right) \tag{25}$$

The first spatial derivatives of h in Eqs. (23, 24) and (25) are approximated by:

$$\left(\frac{\partial h}{\partial z}\right)_{n+\frac{1}{2},\, m+\frac{1}{2}} \simeq \frac{1}{2r\Delta z_\ell} \left[(h_{n+1,\, m+1} + h_{n+1,\, m}) - (h_{n,\, m+1} + h_{n,\, m}) \right] \tag{26}$$

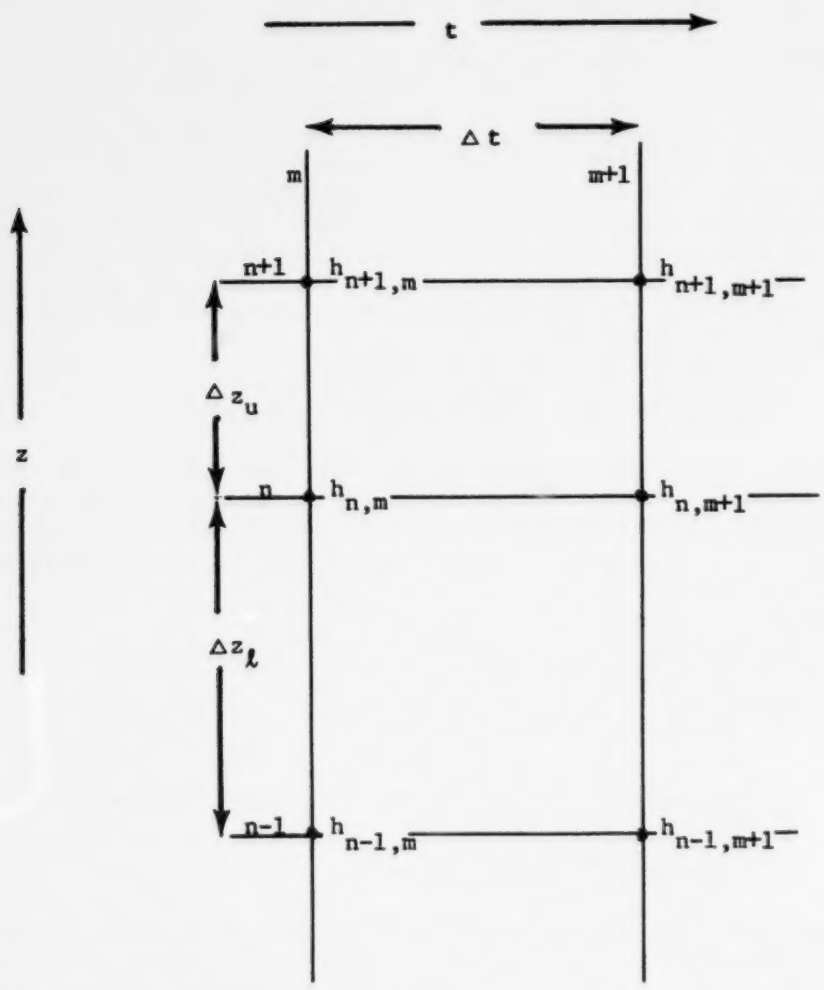

Fig. 11. Expanded view of the nodes about the general node n,m, showing the identification of the nodal values of pressure head. Other variables are subscripted in the same way.

$$\left(\frac{\partial h}{\partial z}\right)_{n,m+\frac{1}{2}} \simeq \frac{1}{2\Delta z_\ell}\left[\frac{(h_{n+1,m+1}+h_{n+1,m})-(1-n^2)(h_{n,m}+h_{n,m+1})-r^2(h_{n-1,m}+h_{n-1,m+1})}{(r+r^2)}\right] \tag{27}$$

$$\left(\frac{\partial h}{\partial z}\right)_{m-\frac{1}{2},m+\frac{1}{2}} \simeq \frac{1}{2\Delta z_\ell}\left[(h_{n,m}+h_{n,m+1})-(h_{n-1,m}+h_{n-1,m+1})\right] \tag{28}$$

To develop the algebraic equations, which replace the partial differential equation (7), Eqs. (26), 27) and (28) are substituted into Eqs. (23), (24) and (25) respectively. The results are then substituted into Eq. (21), and then used to replace the right hand side of Eq. (20). Eq. (19) is used to replace the left hand side of Eq. (20). The terms in the resulting equation are then regrouped so that all pressure heads at the m+1 time level appear on the left side of the equation. The result of all these manipulations is a set of algebraic equations of the form:

$$-A_n\, h_{n+1,m+1} + B_n\, h_{n,m+1} - C_n\, h_{n-1,m+1} = D_n \tag{29}$$

for $o \leq n \leq N$, $0 \leq m$. The unknowns in Eq. (29) are the pressure heads at the m+1 time level. The coefficients A_n, B_n, C_n and D_n are functions of the pressure heads at the m time level, and the average conductivities and average water capacity, $K_{n+\frac{1}{2},m+\frac{1}{2}}$, $K_{n,m+\frac{1}{2}}$, $K_{n-\frac{1}{2},m+\frac{1}{2}}$ and $C_{n,m+\frac{1}{2}}$. These average values were defined as:

$$K_{n+\frac{1}{2},m+\frac{1}{2}} = \tfrac{1}{4}\,(K_{n+1,m} + K_{n+1,m} + K_{n,m} + K_{n,m+1})$$

$$K_{n,m+\frac{1}{2}} = \tfrac{1}{2}\,(K_{n,m} + K_{n,m+1})$$

$$K_{n-\frac{1}{2},m+\frac{1}{2}} = \tfrac{1}{4}\,(K_{n,m} + K_{n,m+1} + K_{n-1,m} + K_{n-1,m+1})$$

$$C_{n,m+\frac{1}{2}} = \tfrac{1}{2}\,(C_{n,m} + C_{n,m+1})$$

In these equations, the conductivities and water capacities at the m+1 time level are functions of the pressure heads at the m+1 level, which are the unknowns in Eq. (29). Consequently, Eq. (29) represents a set of non-linear algebraic equations in the unknowns $h_{n,m+1}$ for $o \leq n \leq N$. The solution process uses the initial condition, $h_{n,o}$, to solve for the set $h_{n,1}$, i.e., the pressure head at the end of the first time step. The set $h_{n,1}$ is then used in turn to solve for $h_{n,2}$. The solution process thus "marches forward" in time by increments Δt. At each time step the set of non-linear algebraic equations represented by Eq. (19) is solved by an iterative process. The solution to the original equation of flow (Eq. (7)) is thus approximated by a set of nodal values of pressure head, $h_{n,m}$ for $o < n < N$, and $o < m$.

The necessary values of conductivity and water capacity were evaluated from the empirical functions that were established for each tailings material fraction (See Section 5). The water content at each node $\theta_{n,m}$ was obtained from $h_{n,m}$ using the empirical water retention function, $\theta(h)$. The flux at

each of the nodes, $Q_{n,m}$, was calculated from a finite difference approximation of the Darcy equation, Eq. (4), in which $h_{n,m}$ and $\theta_{n,m}$ was used.

The computer program for the solution process contains several significant features:

(a) The size of the time step Δt is under program control and is determined by the change in water content across the time step.

(b) The space grid Δz may be of variable size and distributed in an arbitrary manner. This allows the use of a fine grid in those portions of the flow region known to contain steep gradients.

(c) Provision is made to sense the presence of hysteresis (i.e., reversals in the sign of $\partial\theta/\partial t$) and to utilize the appropriate scanning curve in the $\theta(h)$ relationship to determine the water content from the pressure head and to determine the water capacity. All scanning curves are calculated from the main drainage and main wetting curves of the $\theta(h)$ relation, by a theory developed by Y. Mualem (1974). This process also generates scanning curves between the main drying curve and the initial drying curve.

(d) The boundary conditions on the flow may be time dependent, and may be switched from potential to flux type and vice versa during the coarse of the solution process.

(e) The hydraulic properties assigned to each node are arbitrary allowing the representation of non-uniform media.

SECTION 7

ANALYSIS OF WATER FLOW IN TAILINGS PROFILES

THE SEQUENCE OF FLOW EVENTS

Two general types of tailings profile situations may be identified, one with a water table at relatively shallow depth - perhaps less than 4 or 5 meters - and located within the tailings materials, and a second with a water table at great depth and located below the tailings material. The Vitro mill site is an example of the first situation, and in this study we have focused on it. A water table depth of 3 meters was chosen for the simulations.

In a profile of tailings without vegetation, the general sequence of water flow events may be described as follows:

1. An initial period of drainage from complete saturation, with evaporation at the surface.

2. Infiltration of varying amounts of rain at irregular intervals.

3. Periods of evaporation and drainage from the profile and redistribution of water within the profile between rainfall events.

In view of the above sequence, numerical simulations of flow were made (1) for drainage to a water table, with and without evaporation at the surface, (2) for infiltration of rainfall, and (3) for evaporation, drainage and distribution following infiltration events.

DRAINAGE OF INITIALLY SATURATED PROFILES

Although uniform profiles of tailings do not occur, it is desirable to simulate drainage of such profiles for background purposes. The drainage of uniform profiles of each of the tailings fractions, with a water table at 300 cm depth, and with and without evaporation at upper end, was simulated. A water table at the lower end of the profile is represented by a zero pressure head at that boundary.

The surface condition of no evaporation is simulated by an imposed hydraulic gradient of zero at the soil surface. Evaporation at the soil surface was simulated by imposing a constant positive flux upper boundary condition. The constant rate of evaporation was imposed as long as the pressure head at the soil surface was greater than - 15,000 cm (15 bars suction). When the soil surface pressure head decreased to - 15,000 cm, it was subsequently held at that value. This procedure was followed in order to simulate the "energy-limited" and "soil-limited" phases of

evaporation. The evaporation rate from a very wet soil is determined primarily by the energy available for vaporization of the water - the "energy-limited" evaporation regime. As the soil surface dries, a point is reached when the soil cannot supply water to the surface sufficiently fast to maintain the energy-limited rate, and a "soil-limited" rate of evaporation occurs. The latter is less than the energy-limited rate. Sometimes these phases of evaporation are called the constant rate and falling rate periods. Use of these terms assumes that the energy for evaporation is supplied at an essentially constant rate. Due to the diurnal fluctuations of energy exchange at the soil surface the energy available for evaporation of water undergoes corresponding diurnal fluctuations. Because of the time-span of the evaporation events (about 15 days) we decided not to simulate the diurnal fluctuations, and a constant rate was imposed.

The choice of -15,000 cm as the pressure head for switching from a flux to a potential type upper boundary condition is arbitrary. It is felt that the value chosen is reasonable and that another, perhaps more negative choice, would not change the results significantly.

The initial condition chosen for the drainage simulations was that corresponding to saturated downward flow with barely ponded water at the soil surface. In this case, the average hydraulic gradient initially applied to the profile is approximately unity. In a uniform profile of constant conductivity the pressure head would be essentially zero throughout the profile.

Drainage Without Evaporation.

A summary of conditions for the simulations of drainage without evaporation at the surface is given in Table 6. The water content profiles at various times for draining uniform 300 cm profiles of the Coarse and Fine tailings fractions, without evaporation at the top , are shown in Figures 12 and 13. The long time limit ($t \rightarrow \infty$) of these profiles is that corresponding to static equilibrium, with flux Q equal to zero and the pressure head at a given depth equal to the negative of the elevation of that depth above the water table. Water content profiles during drainage of a uniform Medium profile were qualitatively similar to those for the Coarse profile and are not shown. Figures 14 and 15 show the time dependence of water content, θ, at the depths indicated. The equilibrium limits of water content for each depth are shown by the short dashes at the right of the graph.

The water flux across the water table versus time is shown in Figures 16 and 17. Figure 16 shows the flux during the early period of drainage (0-1 day) and Figure 17 during the later period (up to 30 days) of drainage. Also included is the flux versus time for a draining column of Medium tailings. The flux across the water table is downward and since it is in the negative z axis direction, it is negative. At the onset of drainage

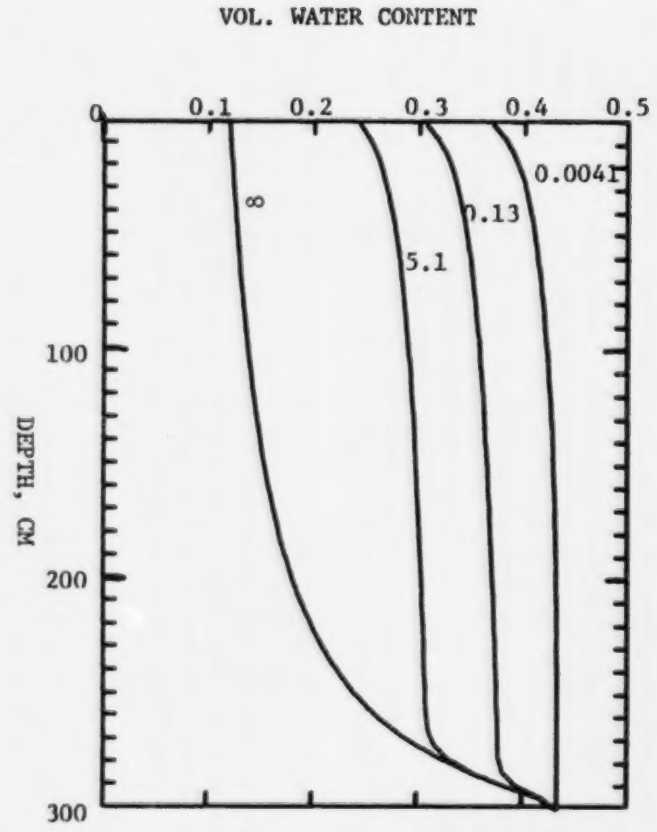

Fig. 12. Water content distributions at several times during the drainage to a water table at 300 cm of a uniform Coarse tailings profile without evaporation at the surface. The numbers on the curves are the time of drainage in days.

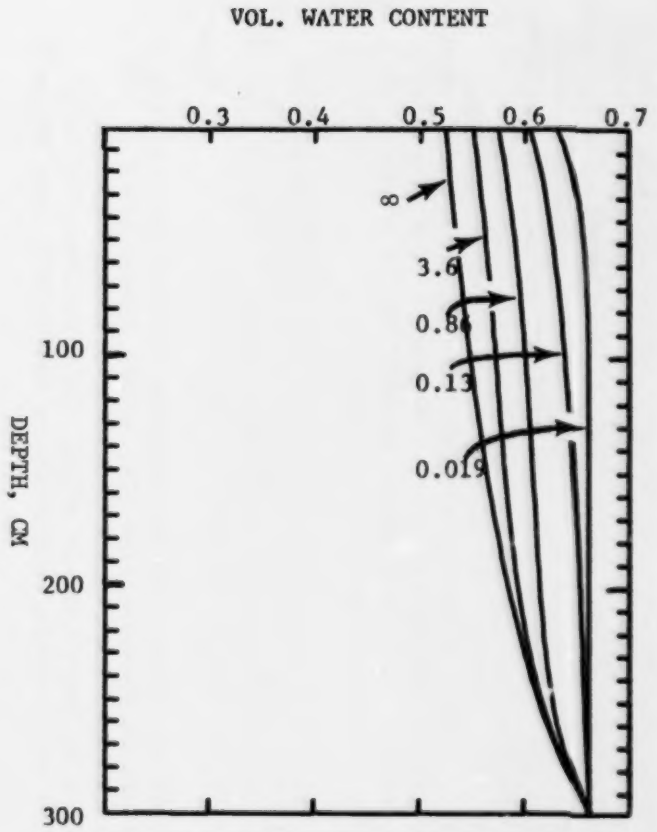

Fig. 13. Water content distributions at several times during the drainage to a water table at 300 cm of a uniform Fine tailings profile without evaporation at the surface. The numbers on the curves are the time of drainage in days.

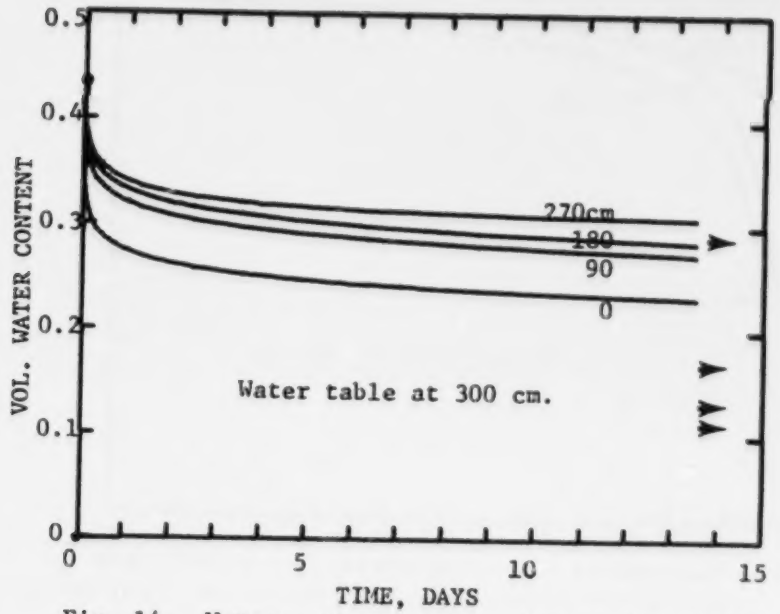

Fig. 14. Water content versus time at the depths indicated in a uniform Coarse profile draining without evaporation at the top.

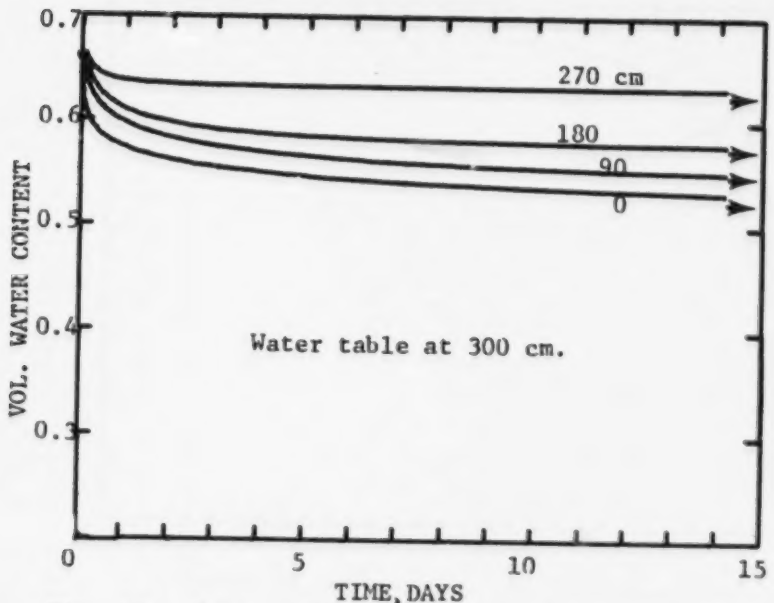

Fig. 15. Same as Fig. 14, except for a uniform Fine tailings profile.

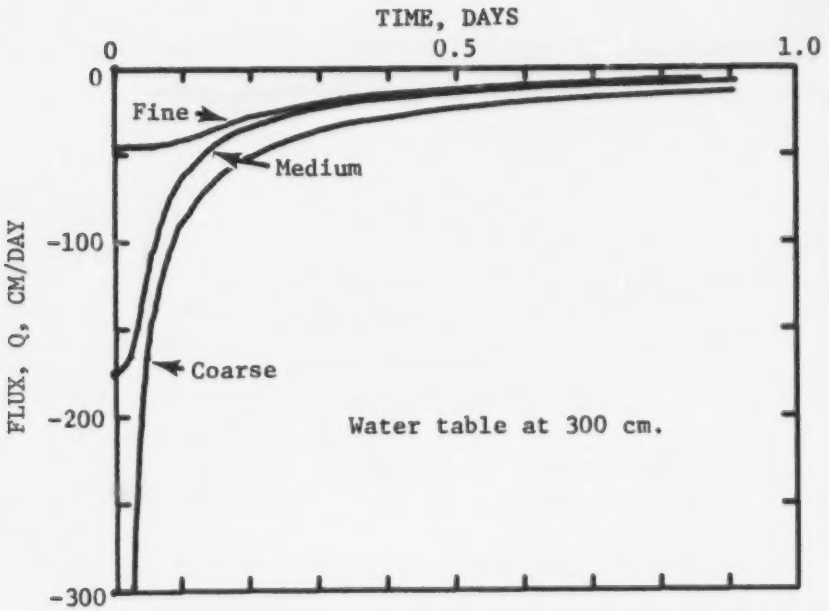

Fig. 16. Flux across the water table (0 - 1 day) from uniform profiles of Coarse, Medium and Fine tailings draining without evaporation at the surface.

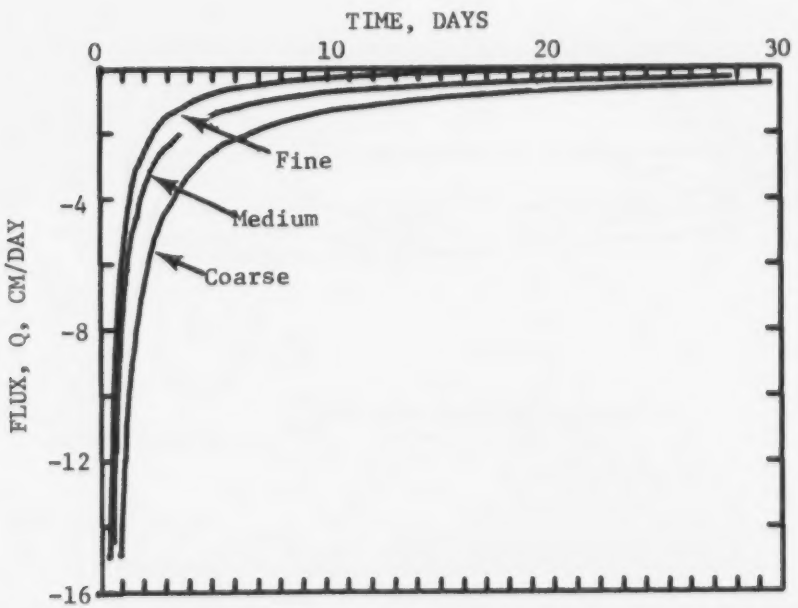

Fig. 17. Same as Fig. 16, except 0 to 30 days.

TABLE 6

SUMMARY OF CONDITIONS FOR SIMULATIONS OF DRAINAGE WITHOUT EVAPORATION

Profile:	Uniform, either Coarse, Medium or Fine tailings.
Upper Boundary Condition:	No evaporation, zero flux for $t > 0$.
Lower Boundary Condition:	Water table, $h = 0$ for $t > 0$ at a depth of 300 cm.
Initial Condition:	Saturated, downward flow with barely ponded water at surface, unit hydraulic gradient; zero pressure head gradient.

the magnitude of the flux is equal to the saturated conductivity of the profile. Thus in the case of the draining Coarse profile, the initial flux was -874 cm/day, in the Medium profile it was -175 cm/day, and in the Fine it was -45.5 cm/day. Within a short time (1 day or less) after the initiation of drainage the flux decreases in magnitude and approaches zero asymptotically.

The simulations of drainage of uniform 300 cm columns of each of the tailings materials without evaporation were continued until the static equilibrium condition was reached. From the results, the time of drainage required to reach equilibrium was estimated. These times were 100-150 days, 1000-2000 days, and 10000 days or more for the Fine, Medium and Coarse fractions, respectively. The times are indefinite because of the asymptotic approach toward equilibrium. The order of time to drainage to equilibrium may seem contrary to what might be expected. However, these results are consistent with experimental observations on draining soil columns. The Coarse fraction does drain very rapidly at first. After a very rapid period of initial drainage the water content in the profile is reduced and consequently the hydraulic conductivity. The latter part of the drainage of the Coarse fraction then must occur at a low level of conductivity, and the drainage rate is very low. Observation of the water content in the profile of Coarse material during this period might lead one to conclude that the profile was at equilibrium due to the slow rate of change. However, in terms of the potential of the water in the profile, equilibrium has not been reached, and will only slowly be approached.

In the Fine profile the initial drainage rate is lower than in the Medium or Coarse profiles. The water content of the Fine material decreases relatively less than it does in the Coarse profile. This means that the decrease in conductivity during drainage of the Fine profile will be less

than the conductivity decrease in the Coarse material. For example, the upper part of the Fine column profile drains to a volumetric water content of about 0.52, which corresponds to a conductivity of about 6×10^{-2} cm/day (See Fig. 9). The water content upper part of the Coarse profile decreases to about 0.12, corresponding to a conductivity of about 2×10^{-5} cm/day. Thus the latter part of the drainage of the Coarse profile functions at a much lower level of conductivity than is found in the drainage Fine profile, and consequently, the Coarse profile is slow to reach equilibrium.

Drainage with Evaporation.

A summary of conditions for the simulations is given in Table 7. Figs. 18 and 19 show the water content profiles at various times during the drainage of uniform profiles at Coarse and Medium tailings when a potential evaporative flux of 1 cm/day was imposed at the soil surface. The most notable difference between these profiles and those for drainage without evaporation is the very pronounced drying in the surface 5 to 10 cm. (Compare Figs. 12 and 18 for the Coarse tailings). The water content versus time at selected depths in these profiles is shown in Figs. 20 and 21. The surface (depth 0 cm) dries quickly until the pressure head at the surface reached the chosen value of -15,000 cm for switching from a constant flux upper boundary condition to a constant potential upper boundary condition. Examination of the water content-depth curves in Figs. 12 and 18, and the water content-time curves in Figs. 14 and 20 shows that the influence of the evaporation at the surface on the θ-profile in the Coarse material, does not extend beyond 90 cm depth and perhaps not that far. The same was true of the Medium profiles. Simulations of

TABLE 7

SUMMARY OF CONDITIONS FOR SIMULATIONS OF DRAINAGE WITH EVAPORATION

Profile:	Uniform, either Coarse, or Medium tailings.
Upper Boundary Condition:	Potential evaporation rate of 1 cm/day until pressure head at the surface decreased to -15,000 cm. Thereafter, a constant pressure head of -15,000 cm.
Lower Boundary Condition:	Water table, $h = 0$ at a depth of 300 cm for $t > 0$.
Initial Condition:	Saturated, downward flow, with barely ponded water at the surface; zero pressure head gradient.

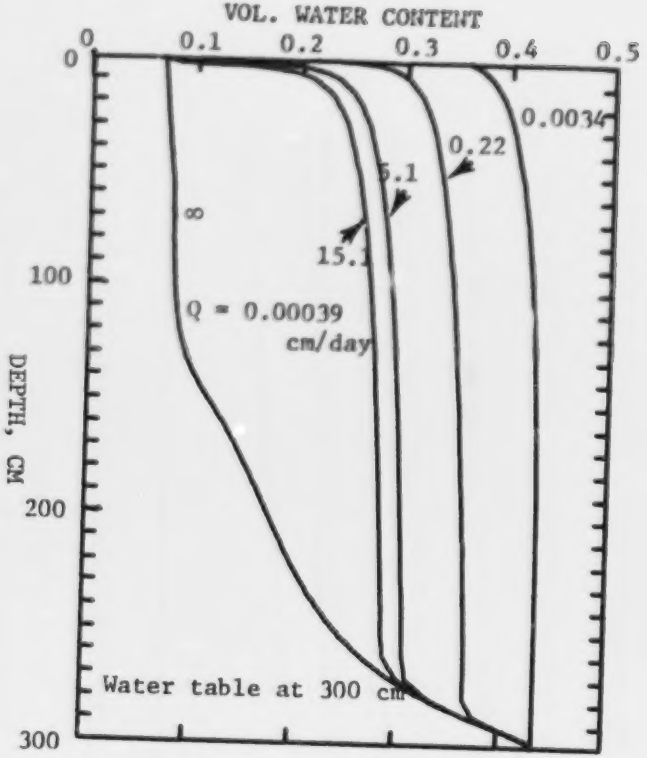

Fig. 18. Water content distributions at several times in a uniform Coarse tailings profile draining to a water table with a 1 cm/day potential evaporation rate at the surface. Numbers on the curves are the time in days. The profile labeled ∞ is the steady state limit of such a flow.

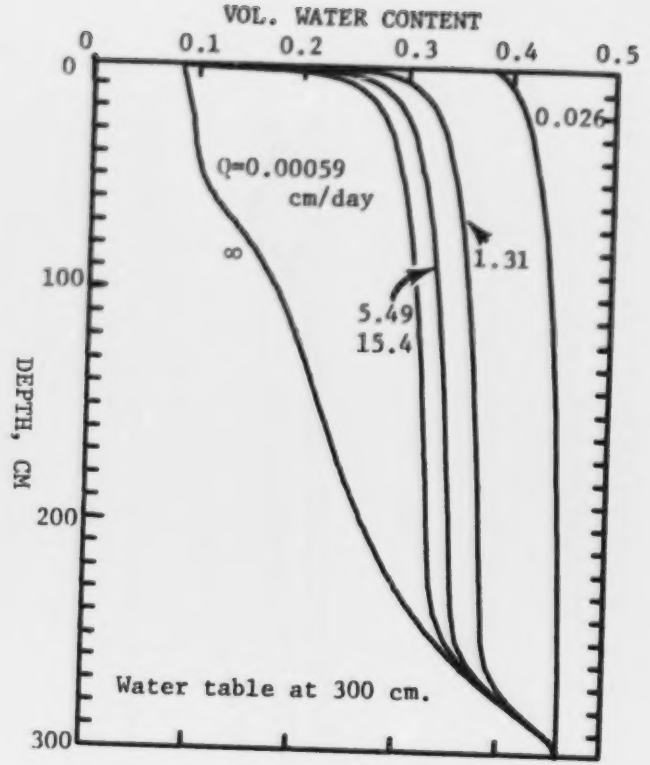

Fig. 19. Same as Fig. 18, except for a uniform Medium tailings profile.

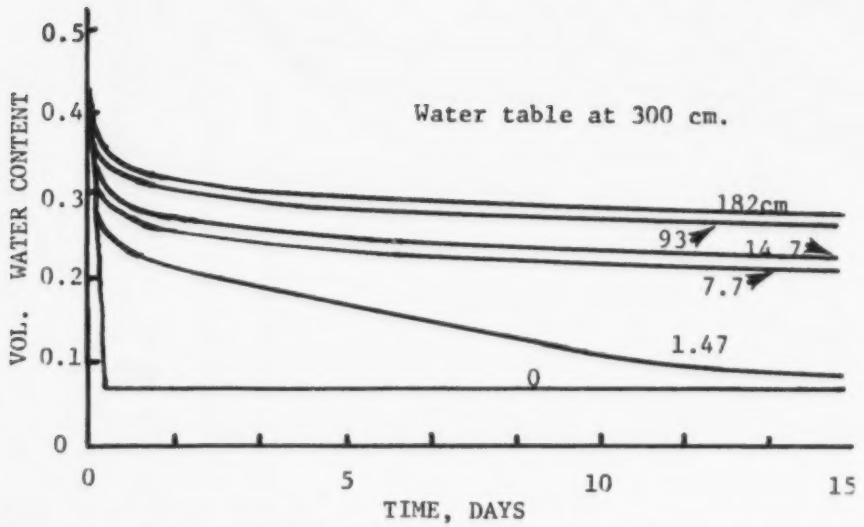

Fig. 20. Water content versus time at the indicated depths in the uniform Coarse tailings profile of Fig. 18.

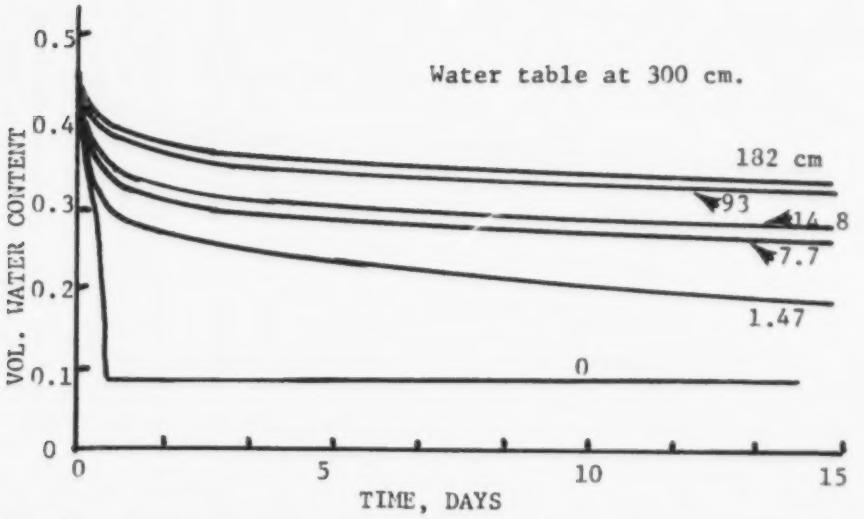

Fig. 21. Water content versus time at the indicated depths in the uniform Medium tailings profile of Fig. 19.

drainage with evaporation at the surface for the Fine material were not done due to the limitations of time for this study. The water content profiles in the Fine material draining with evaporation at the surface would be quite similar to those shown in Fig. 13 below a depth of approximately 70 to 90 cms. At shallower depths the evaporation at the surface would cause a rapid decrease of water content, which would be qualitatively similar to that displayed in the upper portion of the Coarse and Medium profiles. The water content at the surface in the Fine material would become equal to that corresponding to a pressure head of -15,000 cm, which is about 0.34.

If the upper boundary pressure head condition of -15,000 cm were to be imposed for a sufficiently long time (and with a water table at the bottom of the profile), the long-time limit of the flow in these profiles would be a condition of steady state with an upward flow from the water table. The water content profile labled $t \to \infty$ in Figs. 18 and 19 are those corresponding to this steady flow. In this condition the flux Q would be constant and in the upward direction. The values of Q shown in Figs. 18 and 19 are these steady state upward flow values. These water content profiles at $t \to \infty$ represent a lower bound on the water content distribution that might be found in the profile. Steady state upward flow will not be attained, because of the rainfall events that occur at irregular intervals. These infiltration events will keep the upper part of the profile wetter than that labeled $t \to \infty$.

The flux versus depth in the Coarse and Medium profiles draining with evaporation at the surface is shown in Figs. 22 and 23. The plane of zero flux, above which the flow is upward (flux positive) and below which the flow is downward (flux negative), moves downward into the profile as time increases. The position of the plane of zero flux is another measure of the depth of influence of the evaporative condition at the surface. At about 5 days the zero flux plane had moved to a depth of about 10-15 cm, which illustrates that the influence of the evaporation at the surface on the water behavior in the profile is confined to depths less than perhaps 30 cm at drainage times less than 15 to 30 days.

The linearity of flux versus depth over most of the profile shows that the time rate of change of water content is essentially the same at all depths. This follows from the continuity equation for the water, viz.:

$$\frac{\partial \theta}{\partial t} = - \frac{\partial Q}{\partial z}$$

The flux across the upper end of the profiles is shown in Fig. 24. The imposed 1 cm/day evaporation is sustained for only a short time - about 0.3 day for the Coarse profile and 0.6 day for the Medium profile. After this time the flux decreases with time asymptotically toward the very low flux value for a steady upward flow with a low pressure head (e.g., -15,000 cm) at the soil surface. This flux is about 0.00039 cm/day for the Coarse and 0.0059 cm/day for the Medium tailings.

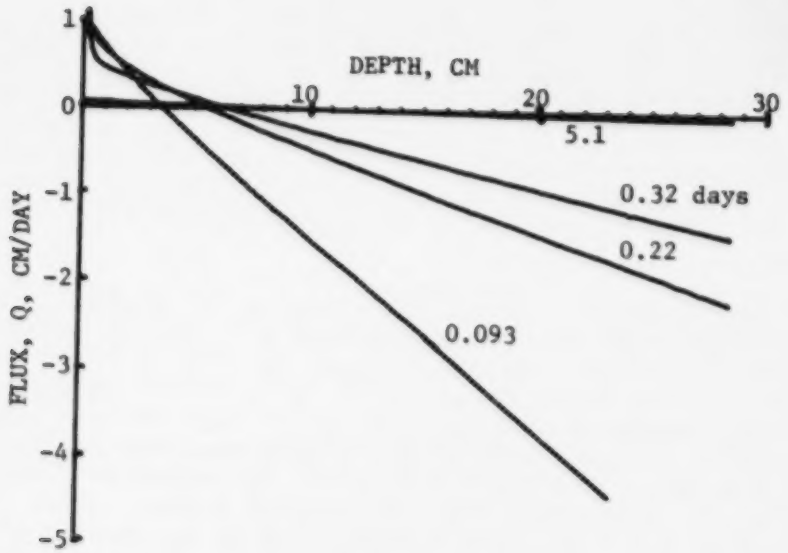

Fig. 22. Flux versus depth in the upper 30 cm of the uniform Coarse profile of Fig. 18.

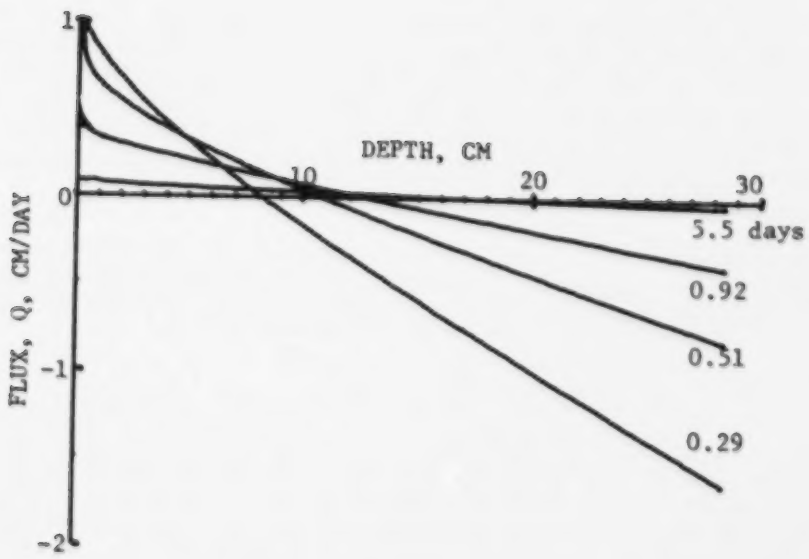

Fig. 23. Flux versus depth in the upper 30 cm of the uniform Medium tailings profile of Fig. 19.

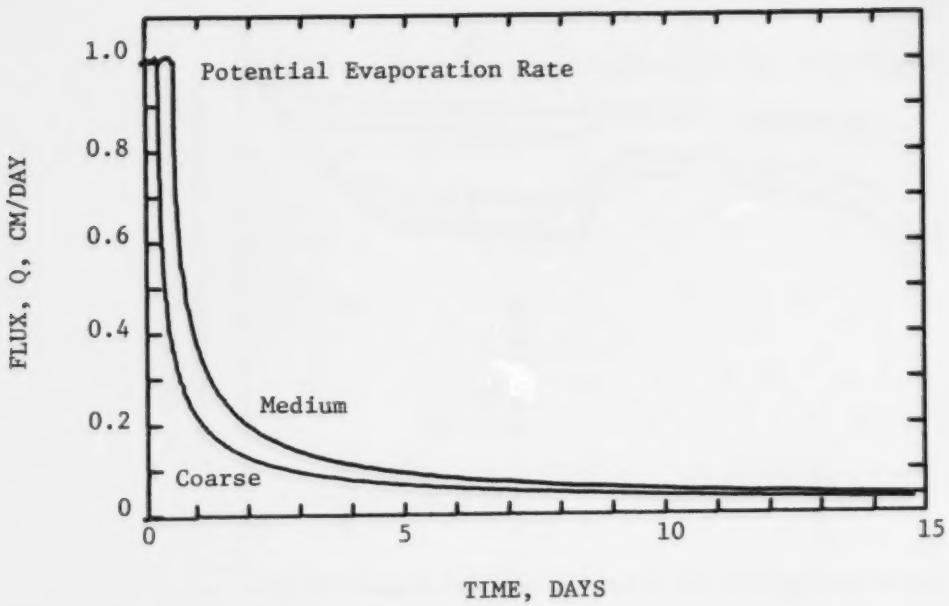

Fig. 24. Flux across the surface (actual evaporation rate) of the uniform Coarse and Medium profiles of Figs. 18 and 19, draining to a water table with a potential evaporation of 1 cm/day imposed at the surface.

During the 15 day drainage and evaporation period the evaporative losses were 1.6 and 2.1 cm for the Coarse and Medium profiles, respectively. During this same period the drainage losses were 51.6 and 37.3 cms for these two profiles. The small evaporative loss compared to the drainage loss indicates further that the evaporation has little effect on the behavior of the water content profiles except at very shallow depths.

Drainage of Layered Profiles with Evaporation.

The drainage of two 300 cm profiles each with two layers of tailings material was simulated. The first, designated C/M, had a 150 cm Coarse layer over a 150 cm Medium layer. The second, designated C/F, had a 150 cm Coarse layer over a 150 cm Fine layer. Each was subjected to a potential evaporation rate of 1 cm/day at the surface.

C/M. Conditions for this simulation are summarized in Table 8. The water content profiles, and pressure head profiles at several times during the drainage are shown in Figs. 25 and 26. Within the Coarse layer above 110 cm depth the water content profile at a given time is the same as that obtained for a uniform Coarse profile, i.e., the Medium layer below 150 cm depth did not significantly affect the drainage of the upper part of the Coarse layer. For example, the profiles at 5.1 days above 100 cm depth in the uniform Coarse profile (Fig. 18) and in the C/M profile

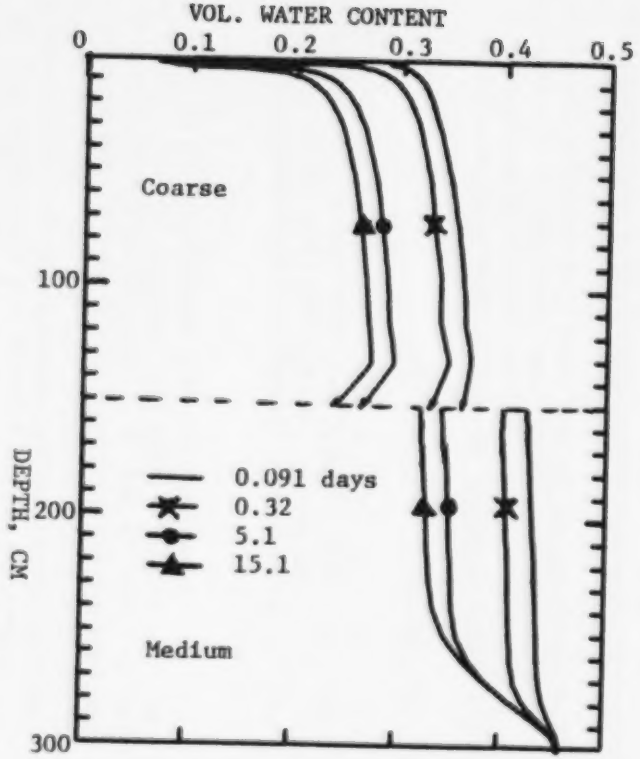

Fig. 25. Water content distributions at various times in a two-layer, Coarse over Medium, profile draining to a water table at 300 cm and with a 1 cm/day potential evaporation rate at the surface.

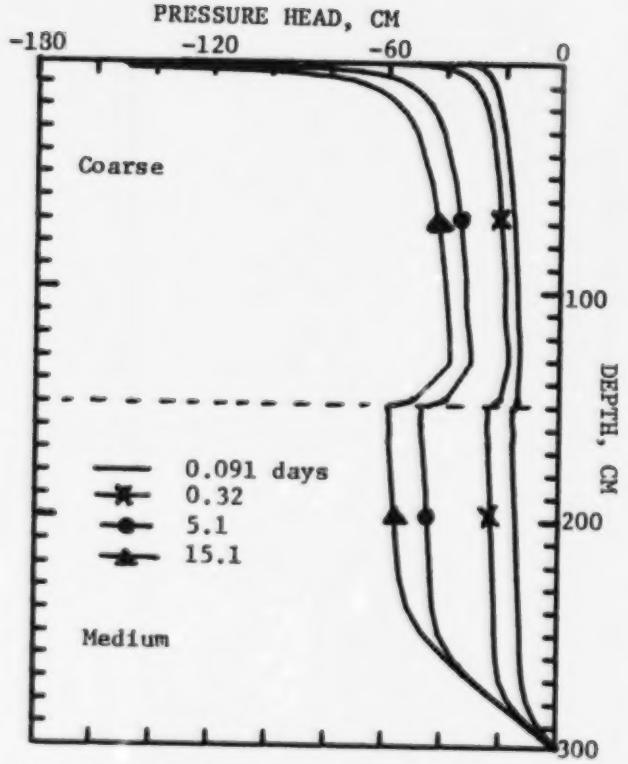

Fig. 26. Pressure head distributions for the profile of Fig. 25.

TABLE 8

SUMMARY OF CONDITIONS FOR SIMULATION
OF DRAINAGE OF A TWO-LAYER, COARSE OVER MEDIUM
(C/M) PROFILE

Profile:	Coarse tailings, 0 to 150 cm depth. Medium tailings, 150 to 300 cm depth.
Upper Boundary Condition:	Potential evaporation rate of 1 cm/day until pressure head at the surface decreased to -15,000 cm. Thereafter, a constant pressure head of -15,000 cm.
Lower Boundary Condition:	Water table, h=0 at a depth of 300 cm, t > 0.
Initial Condition:	Saturated. Downward flow with barely ponded water at the surface.

(Fig. 25) are essentially identical. There was, however, a zone in the Coarse layer between 115 and 150 cm depth just above the Medium material, which drained more than the material above it. This occurs because of the development of pressure heads in this zone which are more negative than those found at somewhat shallower depths in the Coarse material (See Fig. 26).

It is required by the physical laws of soil water flow that the pressure head be continuous across the boundary between layers of differing texture. Since the layers have different water retention properties (different values of θ at a given h) there will be a discontinuity in the water content profile at the boundary between the layers. This is displayed in Fig. 25.

The time dependence of the flux at the surface in the C/M profile was the same as that for the uniform Coarse profile (See Fig. 24). This is to be expected in view of the fact that the water content distributions in the upper part (depth less than 100 cm) for the C/M and uniform Coarse profiles are the same. The cumulative evaporation in 15 days was consequently the same for both columns (1.6 cm).

The flux across the water table in the C/M profile is shown in Figs. 27 and 28. The initial drainage rate of the profile is determined by the conductivity of the lower layer - in this case 175.5 cm/day (See Fig. 27). After a short time the drainage rate from the C/M profile becomes essentially the same as that from a uniform Coarse profile.

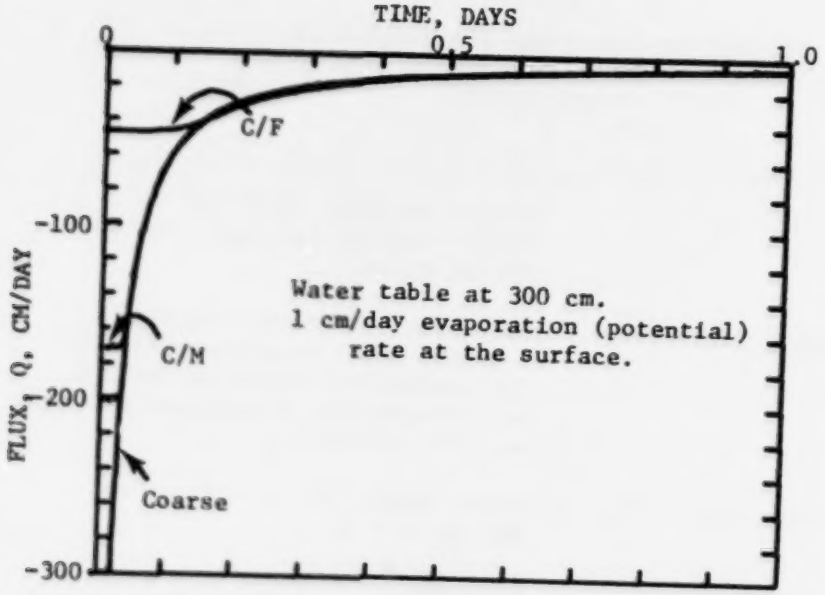

Fig. 27. Flux across the water table (0 - 1 day) for the draining profiles of uniform Coarse tailings (Fig. 18), Coarse over Medium (Fig. 24), and Coarse over Fine tailings (Fig. 29).

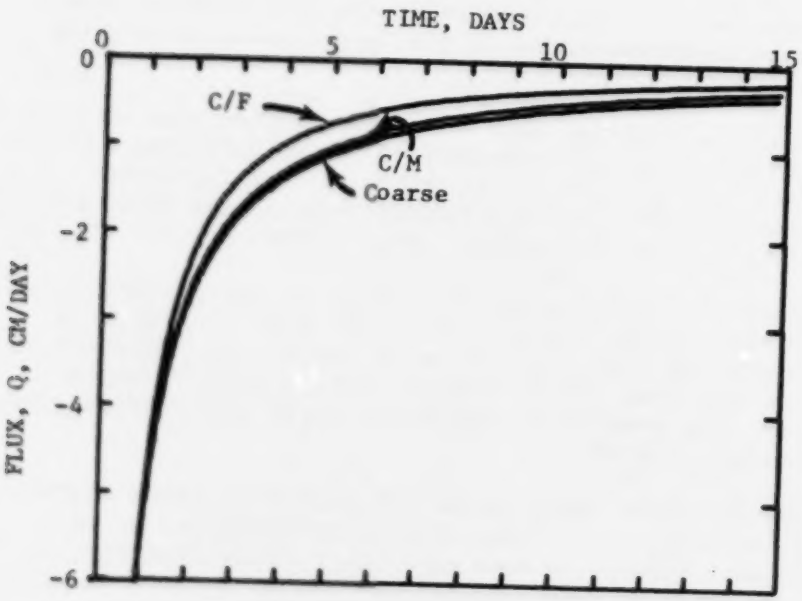

Fig. 28. Same as Fig. 27, except 0 to 15 days.

C/F. Conditions for the simulation are summarized in Table 9. Water content profiles and pressure head profiles for the drainage, with 1 cm/day evaporation at the surface of this profile, are shown in Figs. 29 and 30. As in the C/M profile, the water content profiles above a depth of about 110 cm in the Coarse layer are the same as in a uniform Coarse profile. A zone just above the Fine layer is initially wetter than the same depths in the uniform Coarse profile but at later times drains faster. The discontinuity in the θ-profiles is more pronounced in the C/F profile than in the case of the C/M profile. This is because of the greater disparity between the water retention properties of the Coarse and Fine layers.

The time-dependence of the evaporation rate at the surface was the same as that for the uniform Coarse profile (See Fig. 24), hence the total evaporation in the 15-day period will be the same, viz, about 1.6 cm.

TABLE 9

SUMMARY OF CONDITIONS FOR SIMULATION
OF DRAINAGE OF A TWO-LAYER
COARSE OVER FINE PROFILE

Profile:	Coarse tailings	0 to 150 cm depth
	Fine tailings	150 to 300 cm depth
Upper Boundary Condition:	Potential evaporation rate of 1 cm/day until the pressure head at the surface decreases to -15,000 cm. Thereafter, a pressure head of -15,000 cm.	
Lower Boundary Condition:	Water table, h=0, at 300 cm depth.	
Initial Condition:	Saturated. Downward flow.	

The flux at the water table, shown in Figs. 27 and 28, is initially equal to the negative of the saturated conductivity of the lower Fine layer (- 47 cm/day). After a short time (about 0.2 day) the drainage rate becomes the same as that for a uniform Coarse profile. After about 1 day the drainage rate is somewhat less than that for either the uniform Coarse or C/M profile (Fig. 28).

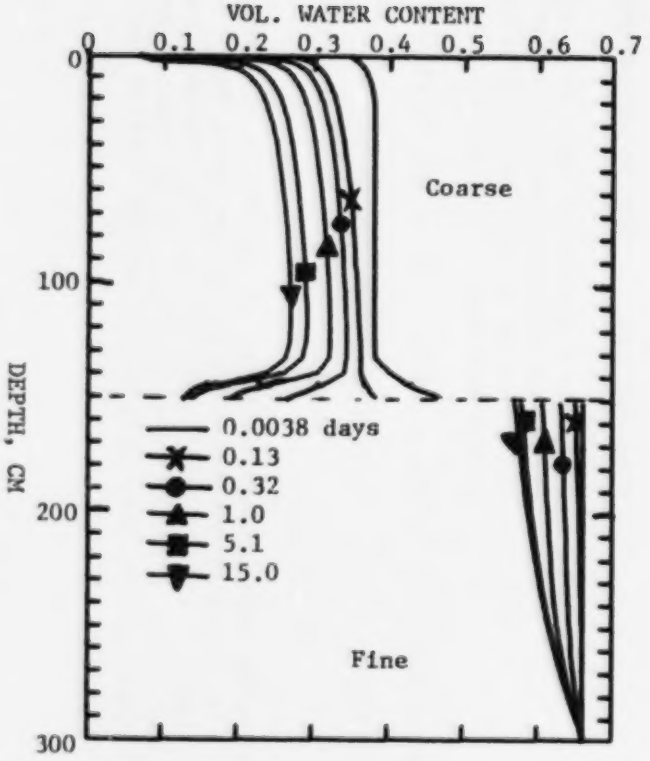

Fig. 29. Water content distributions at various times in a two-layer Coarse over Fine profile draining to a water table at 300 cm and with a potential evaporation rate of 1 cm/day at the surface.

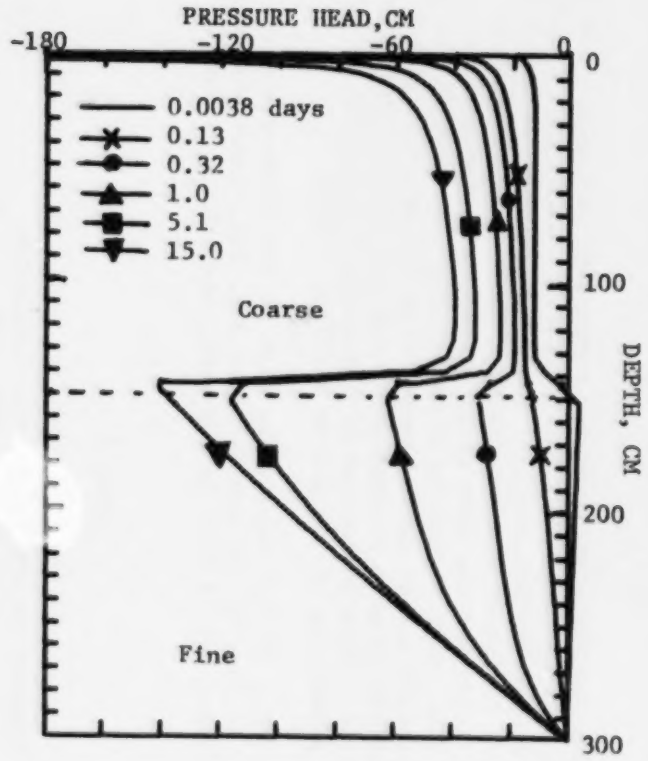

Fig. 30. Pressure head distributions for the profile of Fig. 29.

INFILTRATION EVENTS

The characteristics (duration, intensity, frequency, etc.) of the rains, to which a particular tailings pile is subjected, will depend on its geographic location. With particular reference to the Vitro mill site, hourly rainfall data from the Salt Lake City, Utah weather station were examined in order to develop some idea of the nature of the rainfall in that area, and to provide guidance in the selection of the upper boundary condition for simulation of rainfall infiltration. Examination of the data for the years 1966 through 1970 showed the following characteristics for the rainfall: There were 456 rainfall events in the 5 year period. Thus the average spacing of events was about 4 days. The spacing between events was most often less than two days (273 out of 456 cases). In 10 cases out of the 456 the spacing was 15 or more days. Rains of 2 cm or more occurred 14 times. Most of the rains (322) delivered less than 0.5 cm. The average annual rainfall at the Salt Lake station is about 20 cm. In the 5 year period there was one rainfall that delivered about 6 cm of rain.

Rainfall infiltration events were simulated on two 3 meter profiles, a uniform Coarse profile, and a layered profile, with 30 cm of Medium tailings on 30 cm of Fine tailings which was in turn over Medium tailings from 60 to 300 in depth. This profile will be designated hereafter by M/F/M.

Infiltration into a Uniform Coarse Profile.

The initial condition for this simulation was the θ and h profile resulting from 15 days of drainage with 1 cm/day evaporation at the surface. In the simulation of rainfall infiltration, a specified flux is imposed as the upper boundary condition. This flux is downward, in the negative z-axis direction, and hence is negative, and equal in magnitude to the rainfall rate. The flux may be time dependent. As long as the pressure head at the surface of the profile is less than zero, the flux condition is maintained. If the pressure head at the surface becomes equal to or greater than zero, the upper boundary condition is switched to a potential condition with a pressure head equal to or greater than zero. This procedure simulates the ponding of water on the soil surface that may occur under rainfall. Conditions for the simulation of infiltration into the uniform Coarse tailings profile are summarized in Table 10.

The time dependence of flux at the profile surface, which is the negative of the rainfall rate, is shown in Figure 31. The total amount of rain applied in the event was 2.28 cm with a peak intensity of 11.3 cm/day, and an average intensity of 6.4 cm/day. The intensity during the last half of the event was 7.5 to 8 cm/day.

Figure 32 shows the water content profiles at various times during the rainfall infiltration event. The total depth of penetration of the rain into the tailings profile was less than 20 cm as indicated by the water content profiles. Fig. 33 shows the water content distributions in the top 30 cm. Corresponding to these θ profiles is the set of pressure head profiles shown in Fig. 34. These profiles display the characteristic

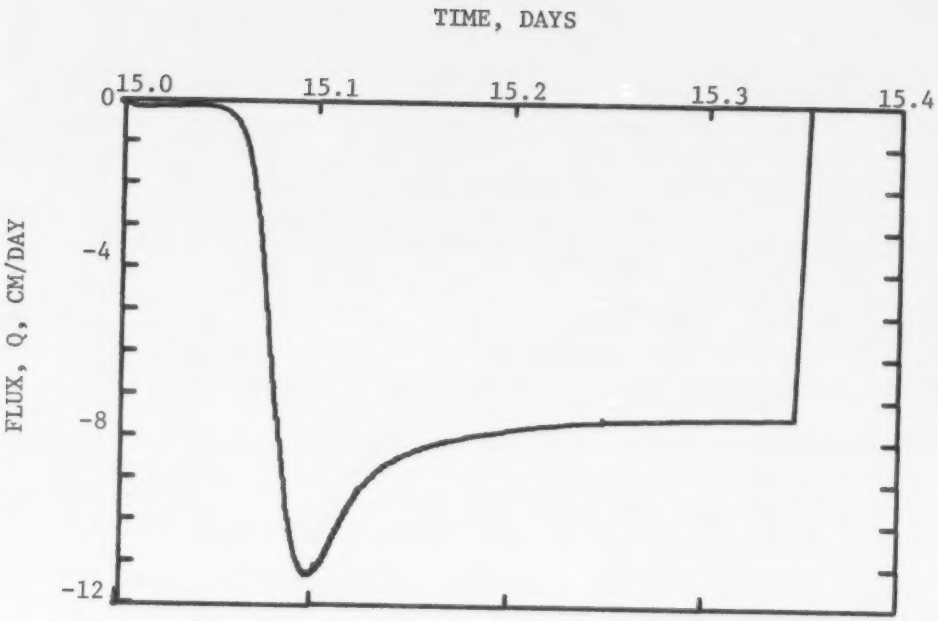

Fig. 31. Flux across the surface (negative of the rainfall rate) of the uniform Coarse profile of Fig. 32.

TABLE 10

SUMMARY OF CONDITIONS FOR SIMULATION
OF INFILTRATION INTO A UNIFORM COARSE PROFILE

Profile:	Uniform coarse tailings.
Upper Boundary Condition:	Time dependent rainfall rate simulated by a time dependent negative flux at the surface (shown in Fig. 31). Total of 2.28 cm of rain applied.
Lower Boundary Condition:	Water table h = 0 at 300 cm depth.
Initial Condition:	Water content and pressure head profiles resulting from 15 days of drainage with a potential evaporation rate of 1 cm/day at the surface. (See Table 7, and Fig. 18).

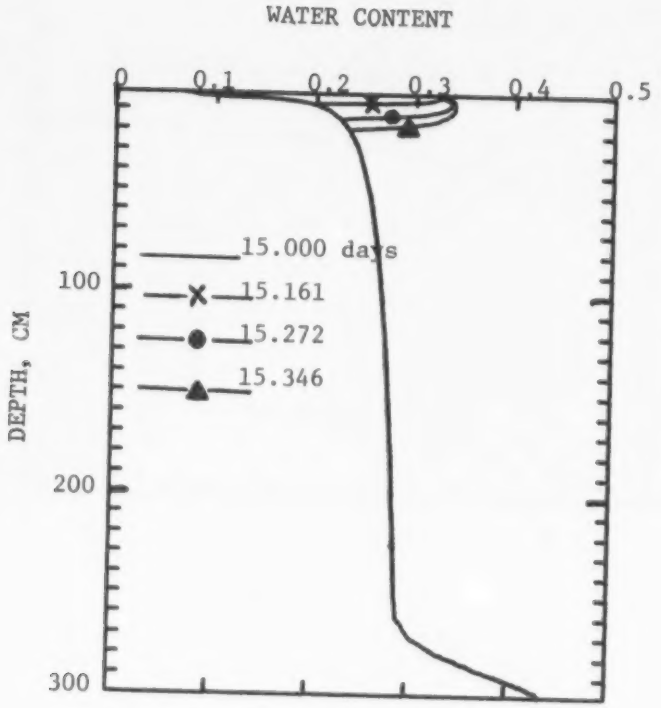

Fig. 32. Water content distributions in the uniform Coarse profile subjected to the upper flux shown in Fig. 31 (2.3 cm rain). Times shown are from the start of the initial drainage of the profile.

infiltration wetting front. The water content and pressure head at the surface approach values corresponding to a hydraulic conductivity equal to the rainfall rate, or the negative of the surface flux. The pressure head and water content decrease slowly with depth until the wetting front is reached.

Figure 35 shows the soil water flux versus depth at various times, some of which correspond to the water content profiles of Fig. 33. The flux profile at 15.1 days corresponds closely to the peak in the rainfall rate (See Fig. 31). Since the lower part of the profile is still draining, below the position of the wetting front the flux is downward, and hence negative, and essentially zero in magnitude. As the rainfall rate decreased from its peak value to the general level of 7.5 cm/day the flux at the surface shifted accordingly.

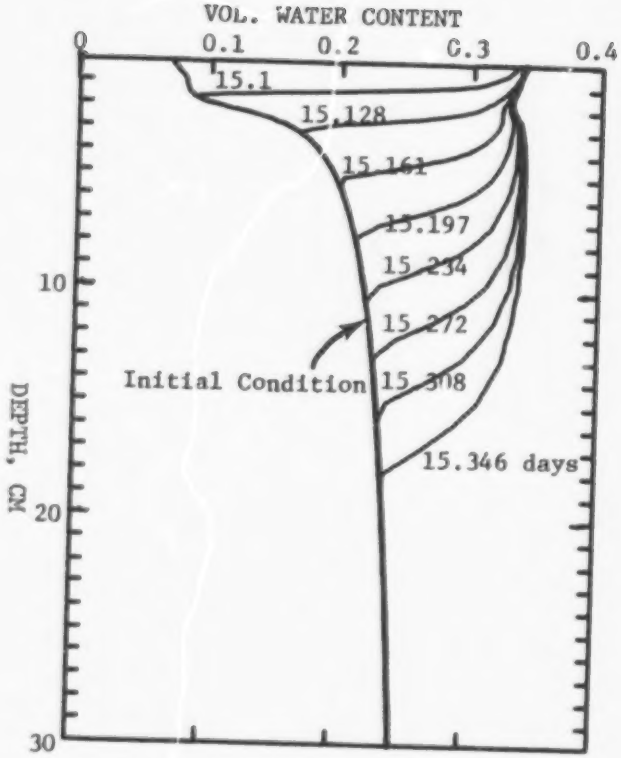

Fig. 33. Detail of water content distributions in the upper 30 cm of the uniform Coarse tailings profile of Fig. 32.

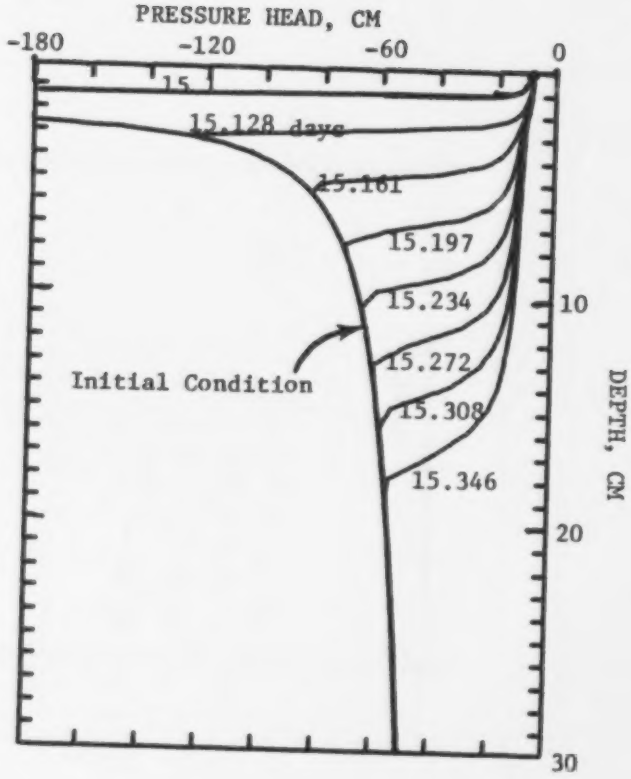

Fig. 34. Pressure head distributions corresponding to the water content distributions of Fig. 33.

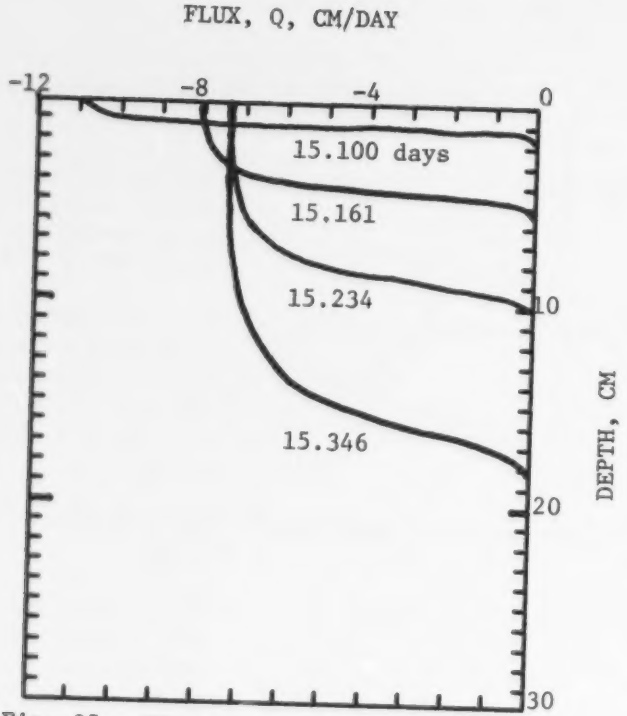

Fig. 35. Flux versus depth in the upper 30 cm of the profile of Fig. 32 at several times during the 2.3 cm rainfall event.

Infiltration into the M/F/M Profile.

The initial condition for this simulation was the steady state pressure head profile corresponding to upward flow from a water table at a depth of 300 cm and a surface pressure head of - 15,000 cm. Two rainfall-infiltration events were considered, one in which 6 cm of rain was applied and another in which 12 cm was applied. The conditions for these simulations are summarized in Table 11.

The flux conditions imposed at the surface for these events are shown in Fig. 36. Both rain events had the same intensity-time characteristic, with the 6 cm rain terminating sooner than the 12 cm rain. The peak rainfall intensity was about 47 cm/day, at 0.09 day after the initiation of the rain. In the latter part of each rain the intensity was approximately 13-14 cm/day. These rains represent extreme events when considered in relation to the Salt Lake precipitation data. In the rainfall data for Salt Lake City there were no single events in which as much as 12 cm of rain was obtained. There was one event in which about 6 cm was obtained.

TABLE 11

SUMMARY OF CONDITIONS FOR SIMULATION OF INFILTRATION OF 6 AND 12 CM RAINFALL INTO THE M/F/M PROFILE

Profile:	Medium tailings, 0 to 30 cm depth. Fine tailings, 30 to 60 cm depth. Medium tailings, 60 to 300 cm depth.
Upper Boundary Condition:	Time-dependent rainfall rate simulated by a time-dependent flux at the surface (shown in Fig. 35). Two rainfall events, a 6 cm rain, and a 12 cm rain.
Lower Boundary Condition:	Water table, h = 0, at 300 cm depth.
Initial Condition:	The steady state water content and pressure head profiles corresponding to upward flow from a water table at 300 cm depth and a surface pressure head of -15,000 cm.

Water content profiles at a sequence of times during the infiltration are shown in Fig. 37. The detail of the top 90 cm of the profile is shown in Fig. 39. The wetting front advances through the 0-30 cm Medium layer, until at some point between 0.497 and 0.606 days the front enters the Fine layer. Note the discontinuity in the θ-profiles due to the layering. The front penetrated to slightly more than 50 cm by the time the rain was ended at 0.803 days. In Fig. 39 the number in parenthesis on each profile is the depth in cm of infiltrated water at the time corresponding to that profile. Thus, e.g., at 0.301 days, 5.5 cm of water had infiltrated and the penetration into the profile was about 20 cm. Flux profiles corresponding to the water content profiles for this case are shown in Fig. 38. These flux profiles are qualitatively similar to those shown in Fig. 35 for infiltration into a uniform Coarse profile.

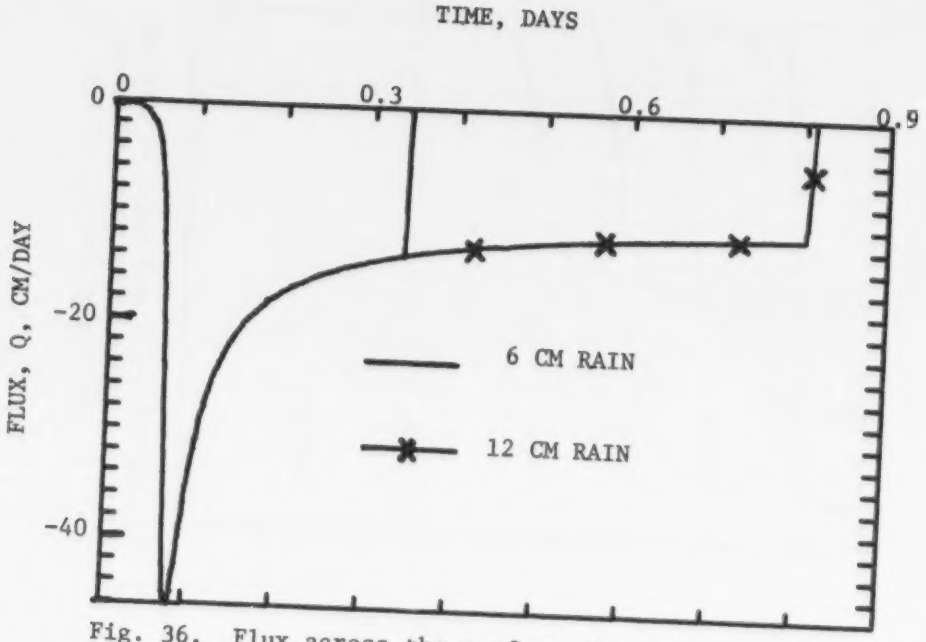

Fig. 36. Flux across the surface (negative of the rainfall rate) of the layered (M/F/M) profile.

The depth of penetration of a given rainfall infiltration event will depend on the amount of water infiltrated and the initial water content in the profile. For a given amount of rain the greater the initial profile water content, the greater the depth of penetration. The initial condition for the infiltration simulation on the uniform Coarse profile is probably somewhat wetter than would on the average be found at a long time (>2-3 hrs.) after the initial drainage of the profile. In that simulation about 2.3 cm of rain penetrated 20 cm. If the initial water content profile had been drier, the depth of penetration would be correspondingly less. The initial condition for the rainfall infiltration into the M/F/M profile is probably somewhat drier than the average initial condition that would be found in situ. In the M/F/M case, 2.75 cm of water penetrated about 10 cm (See Fig. 39) compared to the 20 cm of penetration for 2.3 cm of water in the uniform Coarse profile with its higher initial level of water content.

The depth of wetting front penetration, d, of a given amount of rain, r, may be estimated if we assume that the initial water content θ_i is constant with depth, and that the water content above the wetting front θ_u is also constant with depth. Then the depth of the wetting front is given by:

$$d = r / (\theta_u - \theta_i)$$

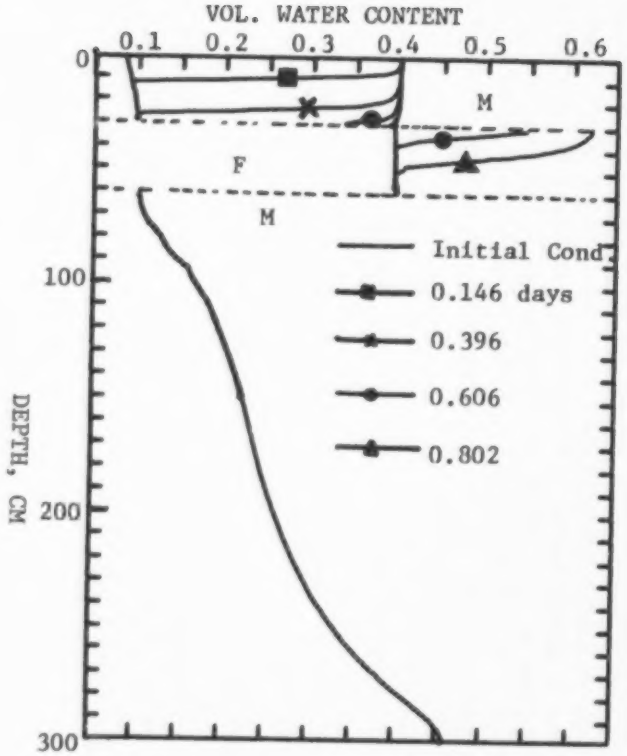

Fig. 37. Water content distributions in a layered (M/F/M) profile at several times during a 12 cm rain.

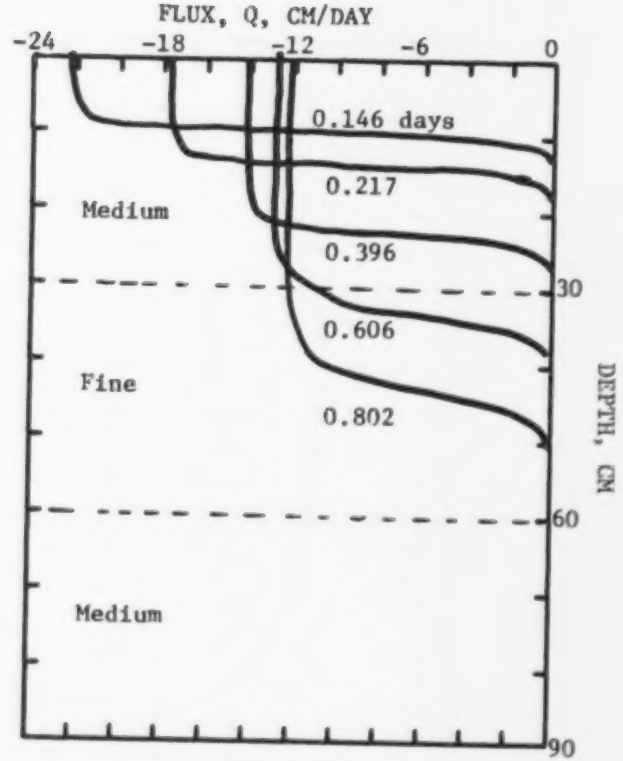

Fig. 38. Flux versus depth at various times in the upper 90 cm of the M/F/M profile of Fig. 37.

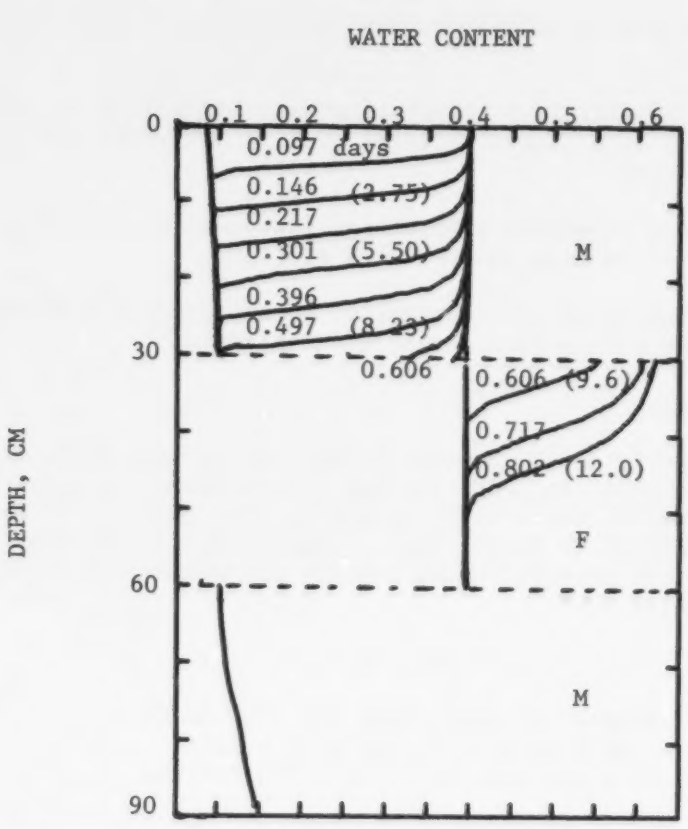

Fig. 39. Detail of water content profiles in the upper 90 cm of the M/F/M profile of Fig. 37. Numbers in parentheses are the depths of infiltrated water at the times corresponding to each profile.

From the characteristics of the rainfall events at Salt Lake City, it appears that most of the rain events would not penetrate more than 5 to 10 cm, and only infrequently to depths of 15 to 20 cm. Penetration in this context is measured in terms of the water content profile. Layers of Fine material, if present below these depths, would not affect the penetration of the rain during the event. However they may have an influence on the redistribution within the profile following the rain.

EVAPORATION FOLLOWING A RAIN

Three simulations of an evaporation period after a rain event were made:

(1) 0.5 cm/day potential evaporation rate imposed for 15 days on the uniform Coarse railings profile following the 2.28 cm rain event.

(2) 0.5 cm/day potential evaporation rate imposed for 15 days following the 12 cm rain on the M/F/M profile.

(3) 0.5 cm/day potential evaporation rate imposed for 60 days following a 6 cm rain on the M/F/M profile.

Uniform Coarse Profile.

The θ and h-profiles at the end of the 2.28 cm rain event (t = 15.357 days) were the initial condition for the subsequent evaporation. The approximate nature of these profiles may be seen in Figs. 33 and 34, by observing the profiles at 15.346 days. Conditions for the simulation of evaporation from the uniform Coarse profile are summarized in Table 12.

TABLE 12

SUMMARY OF CONDITIONS FOR SIMULATION
OF EVAPORATION FOLLOWING A RAIN
ON A UNIFORM COARSE TAILINGS PROFILE

Profile:	Uniform coarse tailings, 0 to 300 cm depth.
Upper Boundary Condition:	Potential evaporation rate of 0.5 cm/day simulated by a flux boundary condition, initial pressure head the surface decreased to -15,000 cm. Thereafter, a constant pressure head of -15,000 cm. Total period of evaporation, 15 days.
Lower Boundary Condition:	Water table, h=0, at 300 cm depth.
Initial Condition:	Water content and pressure head distributions resulting from the infiltration of 2.28 cm of rain (See Figs. 33 and 34).

Water content profiles during the evaporation are shown in Figs. 40 and 41. While the surface was being dried by evaporation the wetting front continued to penetrate the column. Eventually the wetted zone at the top of the profile was removed by a combination of upward flow to the surface and downward flow toward the water table. Over the 15 day period there was a further slight drainage of the lower part of the column at depths to about 270 cm. (See Fig. 40). The profile at 20.8 days shows that the water content at depths between 35 and 70 cm increased slightly above that found in this region at the end of the rain (15.357 days), and then decreased again at later times.

Flux profiles for the 0-30 cm depth are shown in Fig. 42. Immediately at the end of the rain the plane of zero flux, above which flow is upward and below which flow is downward, is at the soil surface. At later times there is a negative peak of flux (downward flow) in the range 15-20 cm, within the zone wetted by infiltration and below the plane of zero flux. This peak becomes smaller with the passage of time as the infiltrated water moves downward.

The flux at the surface as a function of time from the end of the rain is shown in Fig. 43. The 0.5 cm/day potential evaporation rate was maintained for only a short time - a little more than a day - at which time the surface dried to a pressure head of -15,000 cm and the boundary condition was switched from a flux condition of 0.5 cm/day to a potential condition of h = -15,000 cm. Subsequent to the switch of boundary condition the flux at the surface decreases. This behavior of the surface flux is a display of the classical constant rate and falling rate periods. The total evaporation during the 15.8 day period following the rain was 1.14 cm. In the same time period the change in storage in the profile calculated from the water content profiles above a depth of 26.8 cm was 2.41 cm. Since the change in storage is the sum of the evaporation loss and the total flow across the depth of 26.8 cm, the latter was 1.27 cm. Since the profile at 31.1 days shows continued drainage at all depths, all of the 1.30 cm of water - and more - has flowed down through the profile to the water table. The general level of water content in this drainage profile at times of 15 to 30 days after the initiation of drainage from saturation is still high enough so that the conductivity will allow a sufficient flow rate to dissipate more than half of the infiltrated water to the water table. The flow of this fraction of the infiltrated water to the water table took place with only a very minor increase in water content at depths of 30 to 60 cms (e.g., see the θ-profile in Fig. 40 at 20.8 days). Below 100 cm depth the water content always decreased with time, while the infiltrated water was flowing to the water table.

Evaporation from the M/F/M Profile.

Two simulations were made with a 0.5 cm/day potential evaporation rate imposed on the layered profile M/F/M. In the first, the θ and h-profiles at the end of the 12 cm rain event (t = 0.809 days) were the initial condition for the subsequent evaporation. In the second, a 0.5 cm/day potential evaporation rate was imposed on the profile after it had

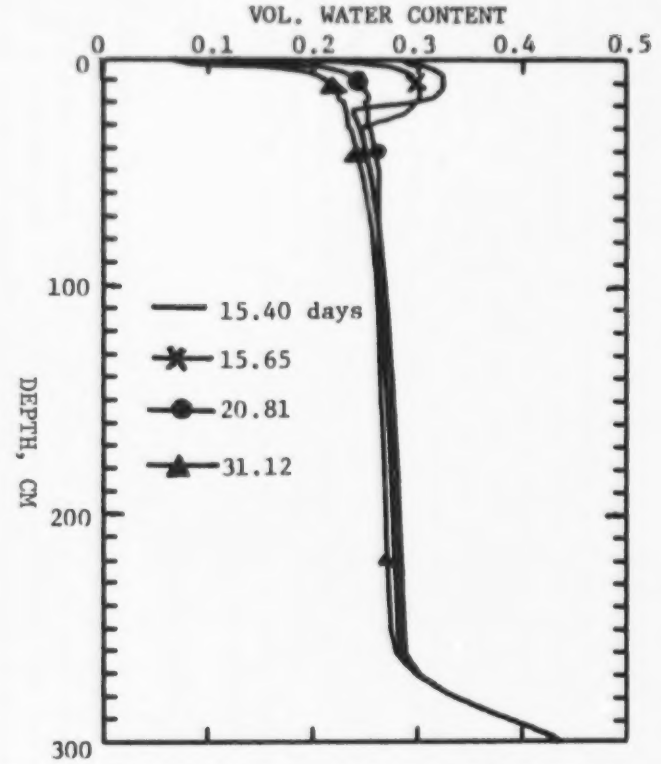

Fig. 40. Water content distributions in a uniform Coarse tailings profile subjected to a potential evaporation rate of 0.5 cm/day after a 2.3 cm rain.

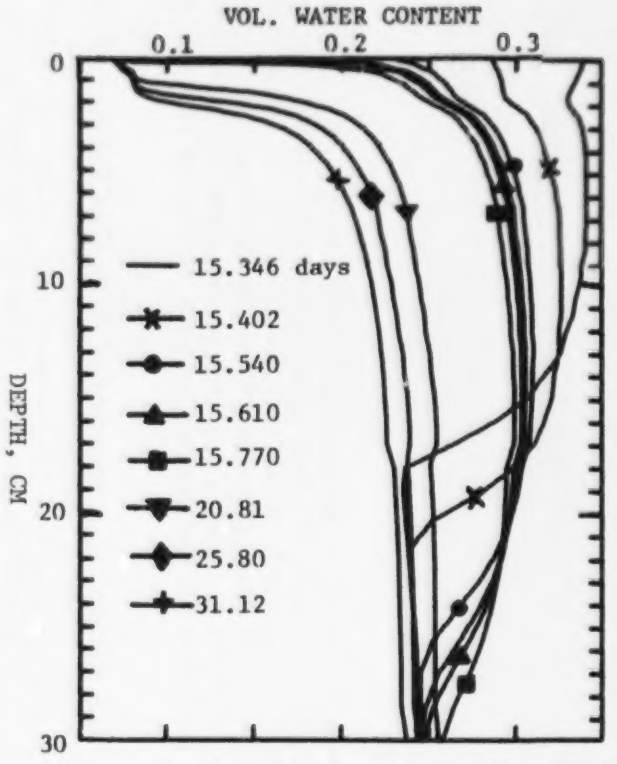

Fig. 41. Detail of water content distributions in the upper 30 cm of the uniform Coarse profile of Fig. 40.

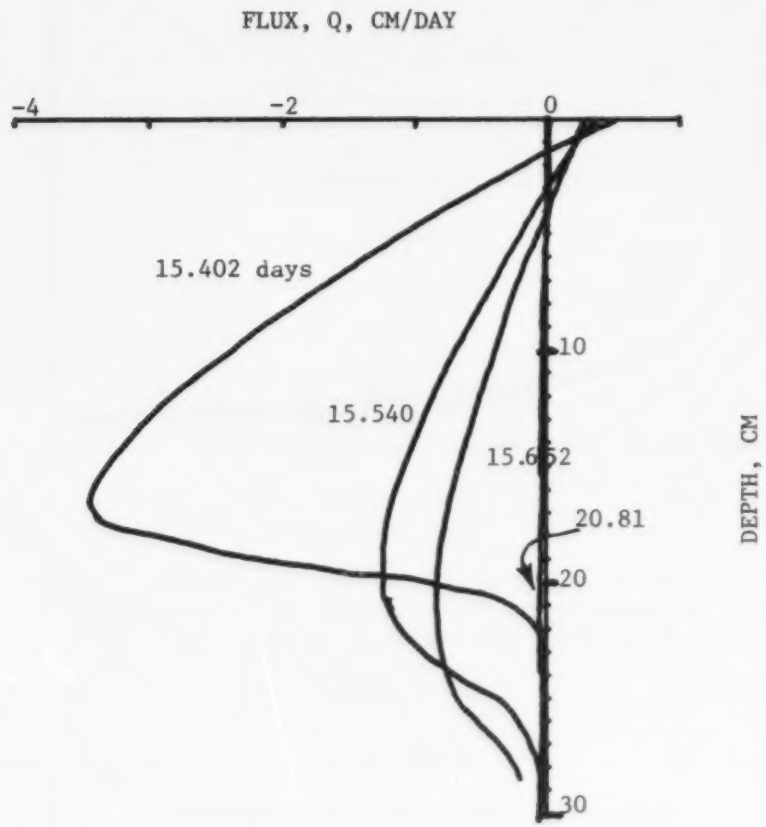

Fig. 42. Flux versus depth at various times during the evaporation from the profile of Fig. 40.

received 6 cm of infiltrated water. The θ and h profiles at that time (t = 0.337 days) were used as the initial condition for this evaporation event.

Evaporation following a 12 cm Rain on the M/F/M Profile. The conditions for this simulation are summarized in Table 13. The water content profiles during a 15 day period of evaporation following a 12 cm rain are shown in Figs. 44 and 45. The profile at 0.82 days is just shortly after the end of the rain. During the course of the evaporation there was water movement to greater depths, i.e., redistribution occurred. There was penetration of the wetting front into the Medium material underlying the Fine layer, with a general decrease of water content throughout the upper Medium layer. The evaporation caused the water content to be

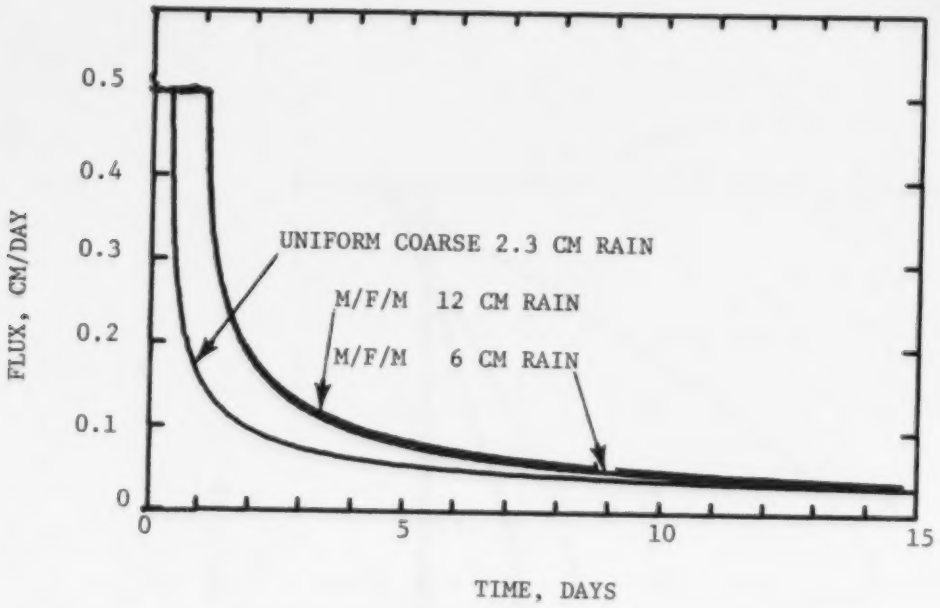

Fig. 43. Flux across the surface during the evaporation from the uniform Coarse profile (Fig. 40), M/F/M profile 12 cm rain (Fig. 44), amd M/F/M, 6 cm rain (Fig. 47).

TABLE 13

SUMMARY OF CONDITIONS FOR SIMULATION OF EVAPORATION FOLLOWING A 12 CM RAIN ON THE M/F/M PROFILE

Profile:	Medium tailings, 0-30 cm depth Fine tailings, 30-60 cm depth Medium tailings, 60-300 cm depth
Upper Boundary Condition	Potential evaporation rate of 0.5 cm/day until pressure head at surface decreased to -15,000 cm. Thereafter, a constant pressure head of -15,000 cm. Total evaporation period, 15 days.
Lower Boundary Condition:	Water table, h=0, at 300 cm depth.
Initial Condition:	Water content and pressure head profiles at the end of a 12 cm rainfall (see Fig. 39).

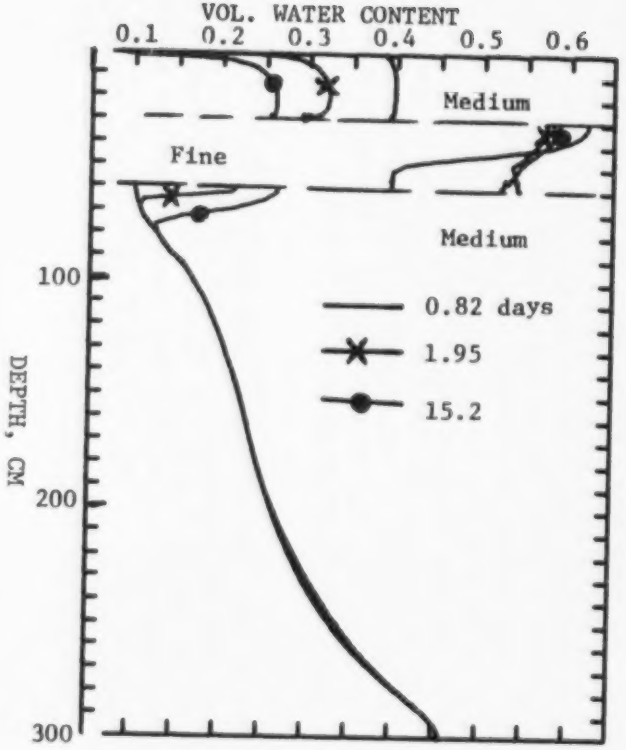

Fig. 44. Water content distributions in the M/F/M profile subjected to a 0.5 cm/day potential evaporation rate after a 12 cm rain.

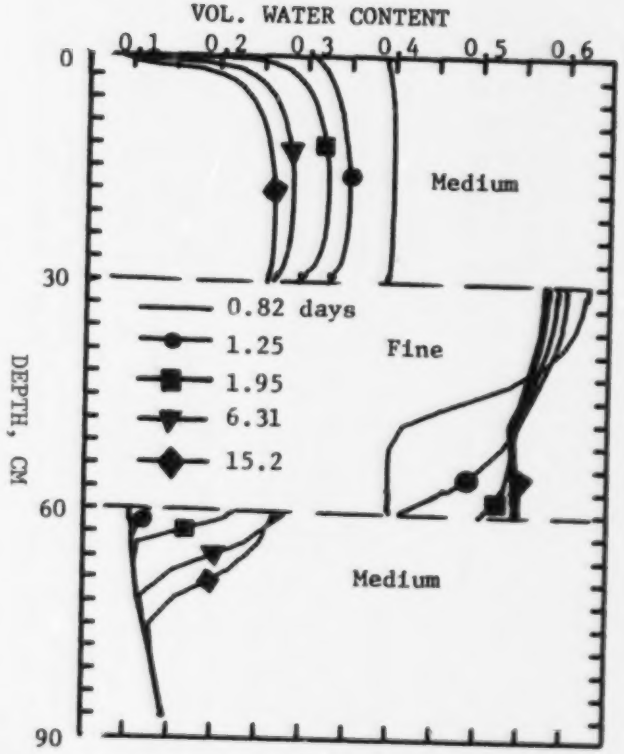

Fig. 45. Detail of water content distributions in the upper 90 cm of the M/F/M profile of Fig. 44, showing the redistribution of water during the evaporation period.

reduced most in the upper 3-4 cm. Also, the zone in the Medium layer a few centimeters deep just above the Fine layer tended to dry faster than depths in the middle of the Medium layer, because at these depths just above the Fine layer, the pressure head is more negative than it is in the mid-part of the Medium layer. Within the Fine layer, the water content decreased in the upper 9-10 cm of the layer. Due to the downward redistribution there was an increase in the water content in the lower 2/3 of the Fine layer. There was also an increase of water content in the 60-75 cm zone of the underlying Medium layer.

Flux profiles are shown in Fig. 46 at times corresponding to some of the θ profiles of Fig. 45. At early times during the evaporation, there is a negative "peak" of flux in the general zone of the profile wetted by the previous rain. This peak is gradually dissipated by downward flow, and the plane of zero flux moves downward into the profile from the surface.

The net change in storage in the depth interval 0 to 80 cm, as evaluated from the water content profiles at the end of the rain (t = .809 days) and at the end of the evaporation period (t = 15.22 days), was -1.54 cm i.e., there was a net decrease of water in this part of the profile. During this same time period the total evaporation calculated from the time integral of the evaporation rate was 1.53 cm. Thus the evaporation accounts for all the decrease in storage and no flow of significance is occurring across the 80 cm depth.

The flux at a depth of 82 cm, calculated from the pressure head profiles at various times during the 15 day evaporation and redistribution period, were all in the range 0.00057 cm/day to 0.00062 cm/day i.e., a small upward flow was indicated. This flow is probably a "residual" effect from the initial condition for the rain event which was a steady state profile with a constant upward flux and with a pressure head of -15,000 cm at the top of the profile. Assuming that there is an average upward flux of 6×10^{-4} cm/day for 15 days, only 9×10^{-3} cm of water would have flowed upward across the 82 cm depth. This amount is too small to be reliably detected by a mass balance on the profile above that depth. The reason these flow rates are small is due to the low level of water content and consequent low conductivity at these depths. These low levels of θ are due to the initial condition chosen for the infiltration, viz. a steady state upward flow profile with h = -15,000 cm at the top of the profile. As was pointed out earlier, this initial condition is drier than would probably be found in profiles in situ.

Within the 0-30 cm upper Medium layer there was a net loss of 4.69 cm of water. Since the evaporation amounted to 1.53 cm there was a total downward flow of 3.16 cm in the 15 day period across the upper surface of the Fine layer. In the upper 10.5 cm of the Fine layer there was a loss of 0.38 cm of water. The lower part of the Fine layer gained 2.04 cm for a net gain in the entire Fine layer of 1.66 cm. The lower Medium layer in the zone 60 to 80 cm depth gained 1.49 cm of water.

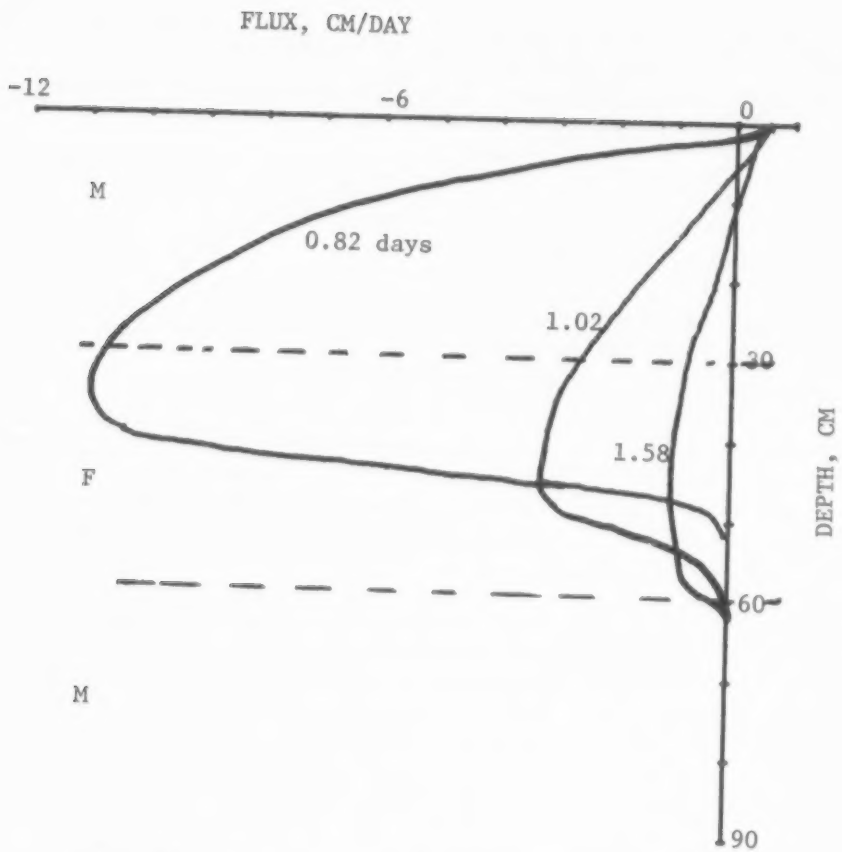

Fig. 46. Flux versus depth at several times during the evaporation and redistribution within the M/F/M profile of Fig. 44.

Since 12.1 cm of water entered the profile during the preceeding rain event, and only 1.53 cm have been lost by evaporation, there has been a net gain of 10.06 cm of water within the upper 90 cm of the profile. If the evaporative condition were maintained for a longer time the evaporative loss would occur at a rate which is about .035 cm/day at 15 days and will decrease asymptotically toward essentially zero as time increased. (See Fig. 43). Another 15 days of evaporation would probably account for about 0.5 cm of evaporation. This amount is small compared to the 10.6 cm net gain of water by the profile at 15 days. It is most likely then that the 10 cm of water will remain within the profile and move slowly toward the water table. Within a time period of up to 30 days after a rain event it is fairly likely that there would be another rain event of sufficient magnitude to cause another net gain of water in the upper part of the

profile, thus contributing further to the tendency toward a downward flow.

Evaporation from the M/F/M Profile after a 6 cm rain. A potential evaporation rate of 0.5 cm/day was imposed on the layered profile after approximately 6 cm of rain had infiltrated (t = 0.337 days). The evaporation lasted about 60 days. Conditions for the simulation are summarized in Table 14.

TABLE 14

SUMMARY OF CONDITIONS FOR THE SIMULATION OF EVAPORATION FOLLOWING A 6 CM RAIN ON THE M/F/M PROFILE

Profile:	Medium tailings, 0-30 cm depth Fine tailings, 30-60 cm depth Medium tailings, 60-300 cm depth
Upper Boundary Condition:	Potential evaporation rate of 0.5 cm/day until pressure head at surface decreased to -15,000 cm. Thereafter, a constant pressure head of -15,000 cm. Total evaporation period, 60 days.
Lower Boundary Condition:	Water table, h=0, at 300 cm depth.
Initial Condition:	Water content and pressure head distributions resulting from infiltration of 6 cm of rain on the M/F/M profile.

Water content profiles at selected times during the evaporation period are shown in Figs. 47 and 48. At the end of the preceeding rain 6.06 cm of water had infiltrated. Fifteen days after the rain, 1.66 cm of water had been lost by evaporation. There was no significant change of water content in the Medium layer at 60 cm depth. The 0-30 cm Medium layer had a net loss of 2.22 cm and the Fine layer a net gain of 0.56 cm, resulting in a net loss for the profile of 1.66 cm, which matches the evaporative loss. At this time (15 days) 4.4 cm of the 6.06 cm of infiltrated water are still within the profile.

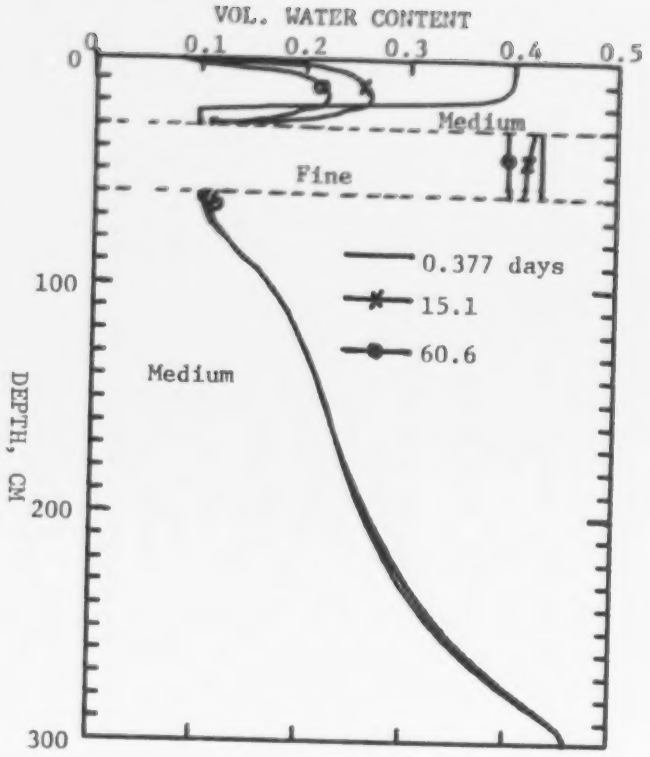

Fig. 47. Water content distributions in the M/F/M profile with a 0.5 cm/day potential evaporation rate after a 6 cm rain.

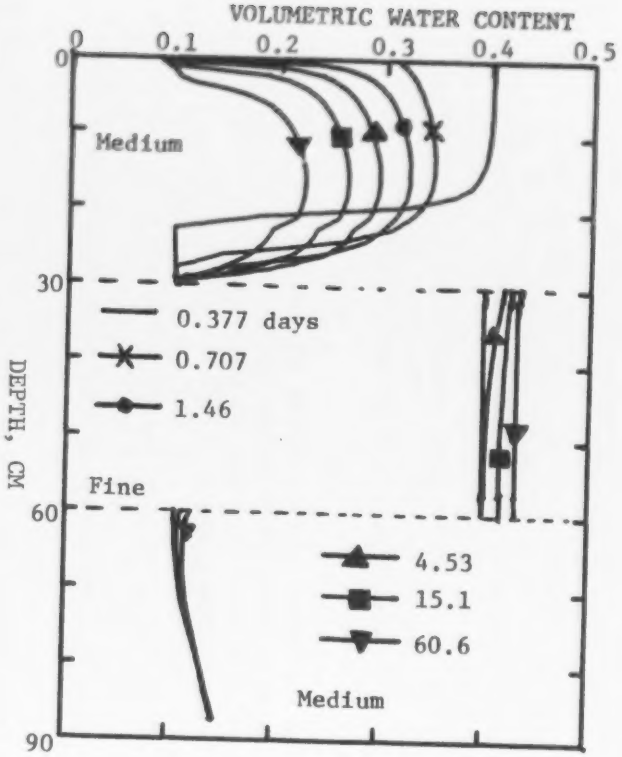

Fig. 48. Detail of the water content distributions in the upper 90 cm of the M/F/M profile of Fig. 47.

In the period 15 to 60 days an additional 0.87 of water was lost by evaporation, for a total evaporative loss (0-60 days) of 2.53 cm. At 60 days there was a slight increase in water content in the 60 to 80 cm zone. At 60 days, 3.53 cm of the 6.06 cm of infiltrated water were still in the profile. The 0-30 cm Medium layer contained 2.97 cm of the 3.53 cm. At 82 cm depth the flux was about 0.00069 cm/day (upward). The effect of this flux on storage above 82 cm in the 60 day period is negligible (less than .04 cm). It is unlikely that evaporation uninterrupted by a rain would occur for as long as 60 days in the Salt Lake City environment. Thus 3.5 to 4 cm of the 6 cm of infiltrated water would continue to flow downward to the water table.

Flux profiles at times corresponding to some of the θ-profiles of Fig. 47 are shown in Fig. 49. Immediately after the end of the infiltration the flux in the upper profile decreases in magnitude and an upward flow (the evaporation) begins from a region close to the surface. A negative peak of flux occurs at a depth near the bottom of the zone that was wetted by infiltration. This peak gradually becomes smaller with increasing time. The plane of zero flux is above a depth of 20 cm even at 60 days, showing that the evaporation loss that occurs during this period comes from the upper 20 cm of the profile.

In the two evaporation simulations from the M/F/M profile, there was no downward flow of any part of the infiltrated water to the water table. This is because of the low level of water content at depths of about 90 - 100 cm which was consistent with the initial condition for the 6 and 12 cm rains. At the low water contents found at these depths the conductivity is low, and also the hydraulic gradient is acting in a direction to cause a small upward flow. Consequently there is no drainage to the water table and the net gain of water to the profile is "trapped" in the upper part of the profile. Additional rain events will each cause an additional net gain of water to the profile which will slowly force the water deeper into the profile.

DISCUSSION OF THE FLOW IN THE TAILINGS PROFILE

After the initial drainage of the saturated pile, the general nature of the water content behavior in the profile would seem to be as follows: Each rain event causes an increase in water content in the upper part of the profile. The level of water content at the surface reached during the rain depend on the intensity and duration of the rain. If the rain is very short in duration and of low intensity there will be only a small increase in water content at the surface and only a small depth of penetration of the wetted zone. If the rain lasts for more than perhaps 30 minutes or an hour the water content at the surface tends toward the value of θ associated with a hydraulic conductivity equal to the rainfall rate. This is because the hydraulic gradient at the surface tends toward unity, and thus according to Darcy's law the flow rate at the surface is numerically equal to the hydraulic conductivity. Examples of this condition are shown in Figs. 32 and 33 for infiltration into the uniform Coarse profile and

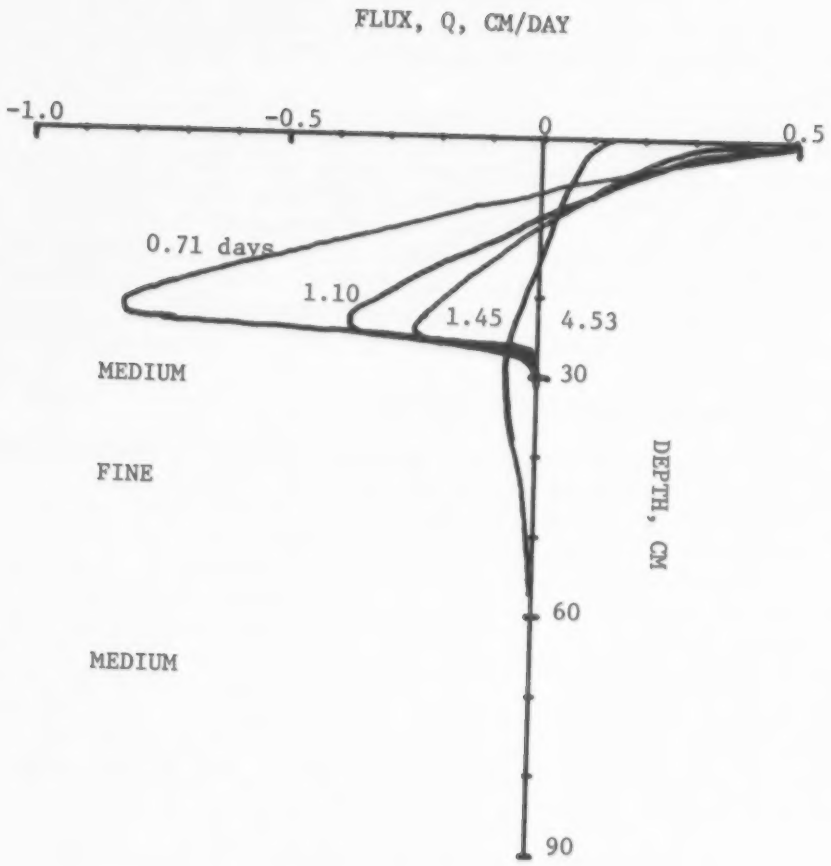

Fig. 49. Flux versus depth in the upper 90 cm of the M/F/M profile of Fig. 47.

Fig. 37 for the infiltration into the M/F/M profile. The higher the rainfall rate, the higher the water content at the surface of the profile. If the rainfall rate exceeds the conductivity at the rewet water content 1/ of the tailings at the surface, ponded water will develop on the surface. This will accumulate until runoff occurs. In view of the high hydraulic conductivities at rewet water content and zero pressure head of the Coarse

---

1/ See definition in Glossary.

and Medium fractions (874 and 175 cm/day, respectively) it is unlikely that ponding will occur if either of these materials is on the surface in depths greater than 20-25 cm. If the Fine fraction were at or near the surface (at depths of less than 10-15 cm) it is possible that ponding could occur. A rainfall rate greater than 45 cm/day would theoretically produce ponding on the Fine material.

The increase of water content in the upper part of the profile produced by the rain is transient, and does not last more than a day or so after the end of the rain. Evaporation removes water from the upper part of the profile, perhaps the top 10-15 cm and over a period of 15-30 days following a rain. Downward flow will occur below this depth and reduce the level of water content in the wetted zone. Examples of this kind of behavior are shown in Fig. 40 for evaporation from a uniform Coarse profile, in Fig. 44 for evaporation from the M/F/M profile following a rain.

The Development of the Quasi-Steady State Profile

Some fraction of each of the rainfall amounts applied to the tailings profile is retained in the profile and does not evaporate during the evaporation period following the rain. If the amount of applied rain is very small (a few tenths of a centimeter or less) probably all of it is soon returned to the atmosphere by evaporation. Larger amounts of rain will have a larger fraction of the water retained in the profile, which is then available to move slowly downward to the water table. For example, of the 2.3 cm of infiltrated water on the uniform Coarse profile (See Figs. 32, 33, 34, and 35), about 1.1 cm evaporated in a 15 day evaporation period following the rain. The rest drained to lower depths in the profile. In the case of the 12 cm rain on the M/F/M profile, about 10 cm of water were still in the profile after a 15 day period of evaporation. This water is available to move slowly downward in the profile.

Each rain and evaporation event produces fluctuations in the water content and flux in the upper part of the profile. The amplitude of these fluctuations decreases with depth (Klute and Heermann, 1974). At a sufficiently great depth - perhaps 1 meter - the flow condition approaches a quasi-steady state downward flow. The flow rate associated with this condition averaged over time periods longer than a few days - perhaps over a month or a year - could be estimated if we knew the fraction of each rain event that was retained in the profile during the time period taken for averaging. If the amount of rain in a given period Δt is R, and if f is the fraction of this amount retained in the profile, the magnitude of the average downward flux $|Q_d|$ in the lower part of the quasi-steady state profile would be

$$|Q_d| = \frac{fR}{\Delta t}$$

Since the wetting front associated with most rain infiltration events does not penetrate below 20-30 cms, layering in the profile below this depth would not seem to have any effect on the fraction of the rains "trapped" in the profile. Consequently, the value of $|Q_d|$ would not be affected by such layering.

The water content distribution in the lower part of a profile in quasi-steady flow can be estimated from a steady state flow analysis based on Darcy's law. This process requires a knowledge of the value of $|Q_d|$, the distribution of layers of the various materials in the profile and their hydraulic conductivity functions. In order to place an upper bound on the water content profile, we can assume that all the annual rain flows to the water table. Under this assumption for an annual rainfall of 20 cm, the value of $|Q_d|$ is 0.054 cm/day. Since this flow is downward, the flux is -0.054 cm/day. Figs. 50, 51 and 52 show the water content distributions for steady state flow in a uniform Medium profile, and two layered profiles. The first layered profile is the M/F/M profile used in the previously described infiltration and evaporation simulations. The second layered profile (Fig. 52) is made up of an alternating sequence of 30 cm layers of Medium and Fine tailings. These water content distributions in the depth range below 100 cm will be indicative of the water content distribution to be found in the lower part of the profiles in the quasi-steady state flow condition described above.

In the uniform Medium profile (Fig. 50) the level of water content (about 0.3) is essentially constant in the depth interval from 100 to 200 cm. This value of θ is that associated with a conductivity of 0.054 cm/day in the Medium tailings, and the flow in this region occurs at unit hydraulic gradient. If $|Q_d|$, the average downward flow rate, were to increase, the water content in this region of the profile would increase to a value associated with a conductivity equal to $|Q_d|$. Also shown in Fig. 50 is the water content distribution for zero flux. These two distributions of θ represent upper and lower limits on the fluctuations of water content to be expected in the quasi-steady flow identified above, in the depth range below perhaps 80-100 cm. At shallower depths rainfall and evaporation events will cause perturbations in θ that will fall outside these curves.

Fig. 51 shows steady state water content distribution for the M/F/M profile for the same two fluxes, viz., $Q = 0$ and $Q = -0.054$ cm/day. Again we may regard the θ distributions below 90-100 cm as indicative of those to be found in such a profile in the quasi-steady flow. The pressure of the Fine layer at 30-60 cm depth has negligible effect on the distribution below 100 cm.

Water content distribution in a profile consisting of alternating 30 cm layers of Medium and Fine tailings with steady state flow at $Q = 0$ and at $Q = -0.054$ cm/day are shown in Fig. 52. Comparing the θ levels in the Medium material at corresponding depths in Figs. 51 and 52, it can be seen that the Fine layers tend to somewhat reduce the water content of the lower part of each Medium layer. Of course the water content of the Fine

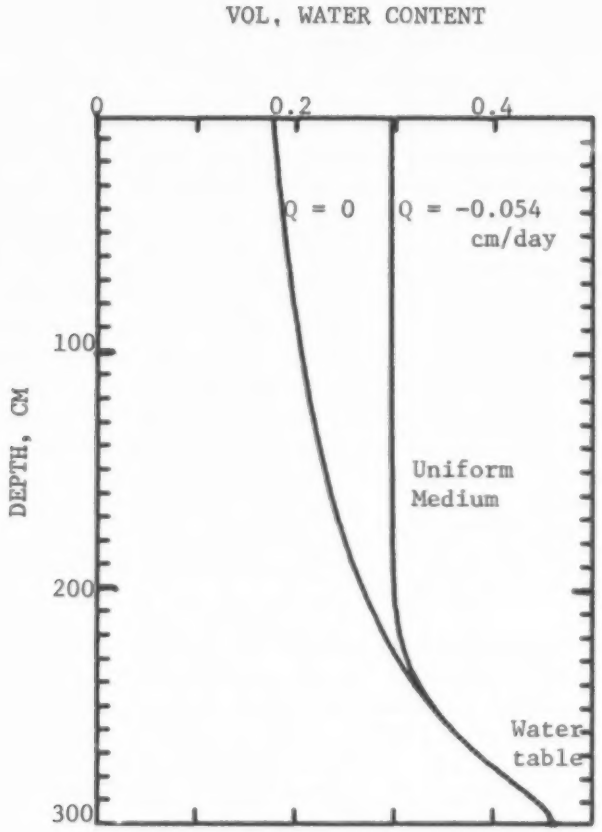

Fig. 50. Water content distributions for two states of steady flow in a uniform Medium tailings profile.

layers is much higher than that of the Medium layers due to the water retention capability of the Fine fraction, and the presence of these Fine layers will cause the average level of water content in the profile to be increased.

The effect of water extraction by vegetation on the profile distribution of water was not simulated in this study due to the lack of sufficient time to do so. However, several comments about the probable effect of extraction of water by roots of vegetation may be made. In a low rainfall environment such as the Vitro site, the vegetation will use all the water that falls as precipitation. This means that transpiration losses added to soil surface evaporation losses will usually return all the infiltrated water to the atmosphere, and little water will flow to the water table.

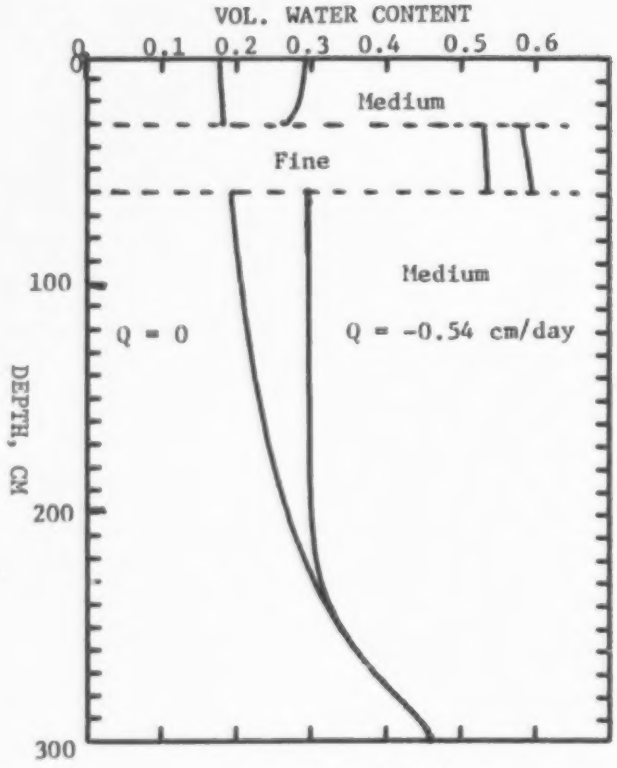

Fig. 51. Water content distributions for two states of steady flow in a profile of Medium tailings with a Fine layer at 30 to 60 cm depth.

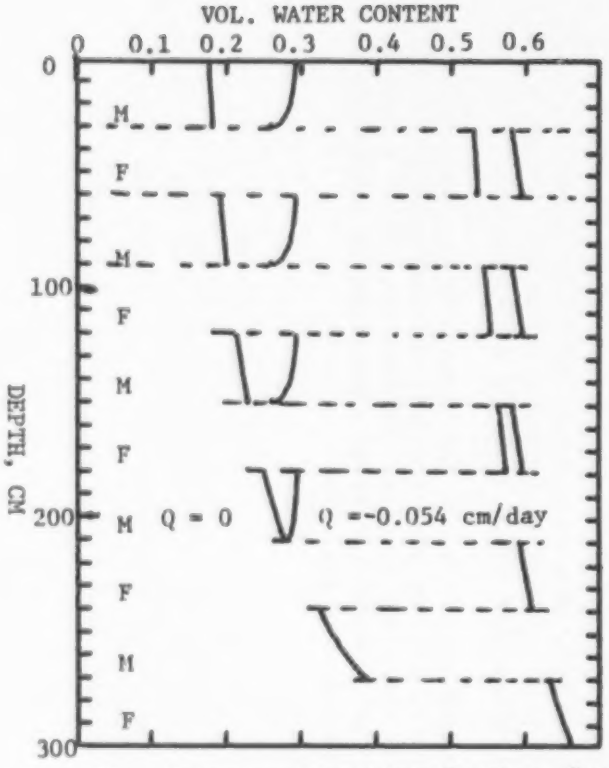

Fig. 52. Water content distributions for two states of steady flow in a profile composed of alternating 30 cm thick layers of Medium and Fine tailings.

Some rain events may be of sufficient magnitude to allow a portion of the rain to flow to the water table simply because evapotranspiration at its prevailing rate cannot intercept all the infiltrated water before some of its gets below the root zone to a water table. It appears that, generally, vegetation would tend to keep the upper part of the profile at a lower water content than would be found without vegetation.

Within the time available for the present study, the simulations and analysis conducted did not show the full development of the quasi-steady condition in the lower profile. Neither were we able to fully examine the effect of layering and water extraction by vegetation on the water regime in the tailings profiles.

REFERENCES

Blake, G. R. 1965. Particle density. In Methods of Soil Analysis, Part I., Monograph No. 9, Am. Soc. of Agron., C. A. Black, et al. (Eds.), Ch. 43, pp. 371-373, Madison, Wisconsin.

Childs, E. C. 1969. The Physical Basis of Soil Water Phenomena. John Wiley and Sons., New York, N. Y.

Croney, D., Coleman, J. D. and Bridge, P. M. 1952. The suction of moisture held in soil and other porous materials. Road Research Technical Paper No. 24, Road Research Laboratory, Dept. of Sci. and Industrial Research, London.

Day, P. R. 1965. Particle fractionation and particle-size analysis. *In* Methods of Soil Analysis, Part I., Monograph No. 9, Am. Soc. of Agron., C. A. Black, et al. (Eds.), Ch. 43, pp. 545-566, Madison, Wisconsin.

Gardner, W. H. 1965. Water content. In Methods of Soil Analysis, Part I, Monograph No. 9, Ch. 7, pp. 82-125, C. A. Black, et al. (Eds.), Am. Soc. of Agron., Madison, Wisconsin.

Gillham, R. W., Klute, A., and Heermann, D. F. 1976. Hydraulic properties of a porous medium: measurement and empirical representation. Soil Sci. Soc. Am. J. 40:203-207.

Jackson, R. D., Reginato, R. J. and von Bavel, C. H. M. 1965. Comparison of measured and calculated hydraulic conductivities of unsaturated soils. Water Resources Res. 1:375-380.

Klute, A. 1973. Soil water flow theory and its application in field situations. *In* Field Soil Water Regime, R. R. Bruce et al. (Eds.), Special Publication No. 5, Soil Sci. Soc. Am., Madison, Wisconsin.

Klute, A. 1972. The determination of the hydraulic conductivity and diffusivity of unsaturated soils. Soil Sci. 113:264-276.

Klute, A. and Heermann, D. F. 1974. Soil water profile development under a periodic boundary condition. Soil Sci. 117:265-271.

Kunze, R. J., Uehara, G. and Graham, K. 1968. Factors important in the calculation of hydraulic conductivity. Soil Sci. Soc. Am. Proc., 32:760-765.

Laliberte, G. E., Brooks, Royal H., and Corey, Arthur T. 1968. Permeability calculated from desaturation data. J. Irrig. and Drainage Div., ASCE 94:57-71.

Mualem, Y. 1974. A conceptual model of hysteresis. Water Resources Research 10:514-420.

Nielsen, D. R., Biggar, J. W., and Erh, K. T. 1973. Spatial variability of field-measured soil-water properties. Hilgardia 42:215-260.

Rose, C. W. 1966. Agricultural Physics. Pergammon Press, N. Y., N. Y.

Swartzendruber, Dale. 1969. The Flow of Water in Unsaturated Soils in Flow in Porous Media. Roger J. M. DeWiest, (Ed.), Academic Press, New York.

Taylor, S. A. and Ashcroft, G. L. 1972. Physical Edaphology. W. H. Freeman, San Francisco.

Von Rosenberg, Dale V. 1969. Methods for the Numerical Solution of Partial Differential Equations. American Elsevier Publication Co., N. Y., N. Y.

GLOSSARY

Evaporative flux, potential: The water flux across the soil surface under conditions such that the rate of evaporation is determined by the energy available to evaporate water.

Flux: The volumetric flux density: The volume of soil water transported through unit cross sectional area of soil per unit time.
Symbol: Q
Dimensions: $\frac{\text{Volume of soil water}}{\text{Area soil x time}}$ or $\frac{L^3}{L^2T}$ or $\frac{L}{T}$

Gravitational head: The energy per unit weight of the soil water due to its elevation above a reference level. A component of the hydraulic head. Symbol: Z
Dimensions: Length.

Hydraulic conductivity: The ratio between the soil water flux and the negative of the hydraulic gradient. A measure of the ability of soil or porous medium to transmit water by mechanically driven flow. A maxmium for a given soil at saturation of that soil. In unsaturated soil is a function of the water content. Decreases strongly with decreasing water content. Symbol: K
Dimensions: same as those for flux, $\frac{L}{T}$.

Hydraulic gradient: The rate of increase of hydraulic head with position. In one dimension, the vertical, the gradient is $\partial H/\partial Z$ where H is the hydraulic head. Dimensionless. A measure of the driving force for Darcy flow.

Hydraulic head: The energy per unit weight of the soil water due to the combined effects of gravity and pressure. The elevation of the free water surface in the open arm of a manometer connected to the point in the soil at which the hydraulic head is to be measured (see Figure 1).
Symbol: H. Dimensions: Length.

Hydraulic properties: The water retention function, $\theta(h)$ and the hydraulic conductivity function, either $K(\theta)$ or $K(h)$.

Hysteresis: In the context of soil water, the term refers to the fact that the hydraulic functions, in particular $\theta(h)$, are not single valued, i.e., the relation between θ and h depends on the past sequence of pressure heads which have prevailed, or whether the soil is wetting or drying. See Figure 2.

Mass balance: A mathematical statement of the conservation of mass principle. Considering a volume element of a medium in which mass transport of a substance is occurring, the partial time derivative of the concentration increases because of (1) an excess of flow into the element over flow out of the element, and/or (2) the production of the substance by some reaction or process within the element. For the soil water and one dimensional flow in the Z direction, a mass balance may be written as:

$$\frac{\partial \rho L}{\partial t} = - \frac{\partial (d_L Q)}{\partial Z} + G$$

where ρ_L - the mass of water per unit bulk volume of soil

G - the mass of water produced per unit soil volume and per unit time by reactions

d_L - the density of the soil water.

Since $\rho_L = d_L \theta$, where θ is the volumetric water content, and assuming that d_L is constant, the density may be factored out of the time and space derivative terms to yield a volume balance

$$\frac{\partial \theta}{\partial t} = - \frac{\partial Q}{\partial Z} + S$$

where $S = G/d_L$ in the volume of soil water produced by reactions or processes per unit soil volume per unit time.

Pressure head: The energy per unit weight of the soil water due to the combined effects of pressure and solid-liquid interactive forces. A component of the hydraulic head. Symbol: h.
Dimensions: Length of fluid column, quite commonly that of a water column. See also Figure 1 for the evaluation of pressure head from piezometer and tensiometer measurements. The pressure head is negative in unsaturated soil.

Profile: (1) The vertical distribution of a substance in a soil column or soil profile, e.g., the "water content profile."

(2) Also used to refer to the vertical array of layers the matrix of a soil, as, e.g., a "soil profile."

Rewet water content: The water content attained by wetting a relatively dry soil to zero pressure head. Due to entrapment of air the soil will not be completely saturated, i.e., the rewet volumetic water content is less than the total porosity. The water content attained by wetting the soil along the M W C to zero pressure head. See Figure 2.

Source term: A term in a mass or volume balance equation for a substance which describes the time rate of production of the substance per unit volume of medium. See, e.g., S in Equation (2). Production may be positive or negative, i.e., consumption is negative production.

Steady state: Refers to a state of flow, e.g., of water, which is time-invariant, i.e., all pertinent physical variables such as water content, flux, hydraulic head, etc., are constant with time. In the volume balance equation for the soil water, Eq.(2), steady state flow is described by $\partial\theta/\partial t = 0$.

Suction: Soil water suction. The negative of the soil water pressure head. A measure of the combined effect of soil water pressure and solid-liquid interactive forces on the energy per unit weight of the soil water.

Water capacity: The rate of increase of volumetric water content with soil water pressure head, $d\theta/dh$. Symbol: C. Dimensions: L^{-1}. The slope or derivative of the water retention function, $\theta(h)$ (See Figure 2).

Water content, volumetric: The volume of soil water per unit bulk volume of soil. Symbol: θ. Dimensions: None, but on occasion it maybe useful to identify it as the ratio of soil water volume to bulk soil volume.

Water content, weight basis: The ratio of the mass of soil water to the over-dry mass of soil solids.

Water retention function: The relation between water content and soil water pressure head. In this report, the function $\theta(h)$ (See Figure 2).

Water table: The locus of points in the soil water system at which the soil water pressure is atmospheric, or the pressure head is zero.

Wetting front: A region of relatively steep rate of change of water content with distance which is characteristically found when water is imbibed or infiltrated into a dry soil.

*U.S. GOVERNMENT PRINTING OFFICE: 1978--684-041/2035